AN ABSTRACT OF THE THESIS OF

Robert Wayne Crews for the Ph.D. in Physics

Date thesis is presented: June 1952

Title: CHARGED PARTICLE OBSERVATIONS OF Li + T REACTIONS

Abstract approved_ Redacted for privacy

A triton beam from the Los Alamos 2.5 Mev electrostatic accelerator has been used in bombarding lithium-6 and lithium-7 target nuclei. Charged particles which result from the interactions were detected with a proportional counter and recorded by an 18-channel pulse height analyzer.

The accelerator, target chamber, and proportional counter are described.

Six interactions have been observed.

(1) $Li^6 + T \rightarrow He^5 + He^4 + 15.27$ Mev

(2) $He^{5*} + He^4 + 12.6$ Mev

(3) $2He^4 + n + 16.10$ Mev

(4) $Li^7 + D + 0.99$ Mev

(5) $Li^7 + T \rightarrow He^6 + He^4 + 10.12$ Mev

(6) $He^{6*} + He^4 + 8.01$ Mev

Reactions (2) and (6) indicate levels in He^5 and He^6 of approximately 2.7 Mev and 2.11 Mev, respectively.

Energy dependence of alpha-particle yields representing reactions (1), (5), and (6) have been measured at 90° and at 165° for triton energies varying by increments of 0.10 Mev from 0.62 to 2.29 Mev. For reactions (5) and (6) values for differential cross section have been calculated. At 90°, reactions (5) and (6) have maximum values of 2.6 and 8.1 millibarns, respectively. At 165°, the two reactions have nearly the same maximum of about 4.1 millibarns. The bombarding energy at which all four of these maxima occur is about 1.85 Mev.

During bombardment of metallic lithium targets, oxygen and nitrogen contaminants in lithium were detected. As a consequence, targets of lithium-6 fluoride and lithium-7 fluoride were used in observing the above reactions. The resulting incidental triton bombardment of oxygen, nitrogen, and fluorine gave evidence for levels in C^{13}, N^{15}, O^{18}, F^{19}, and Ne^{22}. These are discussed.

CHARGED PARTICLE OBSERVATIONS OF Li + T REACTIONS

by

ROBERT WAYNE CREWS

A THESIS

submitted to

OREGON STATE COLLEGE

in partial fulfillment of
the requirements for the
degree of

DOCTOR OF PHILOSOPHY

June 1952

APPROVED:

Redacted for privacy

Professor of Physics

In Charge of Major

Redacted for privacy

Head of Department of Physics

Redacted for privacy

Chairman of School Graduate Committee

Redacted for privacy

Dean of Graduate School

Date thesis is presented: June 1952

Typed by Rita F. Langhorst

ACKNOWLEDGMENT

Work performed at the Los Alamos Scientific Laboratory of the University of California is the basis for this dissertation. The author was permitted to undertake this work through a joint arrangement of the Laboratory, the Atomic Energy Commission, and Oregon State College.

The subject discussed herein was suggested by Dr. R. F. Taschek, whose friendly guidance has been invaluable.

TABLE OF CONTENTS

TABLE OF CONTENTS

(Continued)

CHARGED PARTICLE OBSERVATIONS OF Li + T REACTIONS

INTRODUCTION

Knowledge, which, in the long run, leads to an understanding of nuclear structure and forces, is enhanced by information gained from observing interactions of light nuclei. Occasionally, monoenergetic sources of charged particles or neutrons are discovered (in the form of high cross-section-resonances) in the course of such studies. These are often of immediate practical importance.

The observations to be described were planned as a preliminary survey of a relatively unexplored region of experimentation -- the interactions of tritons with Li^6 and Li^7 nuclei. The Los Alamos 2.5 Mev electrostatic accelerator has been used to accelerate tritons to various energies between 0.62 and 2.28 Mev. Charged particles resulting from interactions of these tritons with the Li^6 and Li^7 nuclei have been observed at two angles: 90° and 165° to the incident triton beam.

Exoergic reactions which may occur with the residual nuclei in the ground state:

(1) $Li^6 + T \rightarrow Be^9 + 17.67$ Mev

(2) $2He^4 + n + 16.10$

(3) $Be^8 + n + 16.00$

(4) $He^5 + He^4 + 15.27$

(5) $Li^7 + H^2 + 0.99$

(6) $Li^8 + H^1 + 0.80$

(7) $Li^7 + T \rightarrow Be^{10} + 17.23$ Mev

(8) $Be^9 + n + 10.42$

(9) $He^6 + He^4 + 10.12$

(10) $2He^4 + 2n + 8.86$

(11) $Be^8 + 2n + 8.76$

(12) $He^5 + He^4 + n + 8.01$

(13) $2He^5 + 7.26$

(masses and method used in determining these Q-values are discussed in APPENDIX III.)

Of these, the reactions actually observed were (2), (4), (5), and (9). In (4) and (9), excited states were also observed for He^5 and He^6.

Incidental to these observations, reactions resulting from triton bombardment of nitrogen, oxygen, and fluorine were also observed. They give evidence for excited states in C^{13}, N^{15}, O^{18}, F^{19}, and Ne^{22} and will be discussed in the chapter concerned with analysis of results.

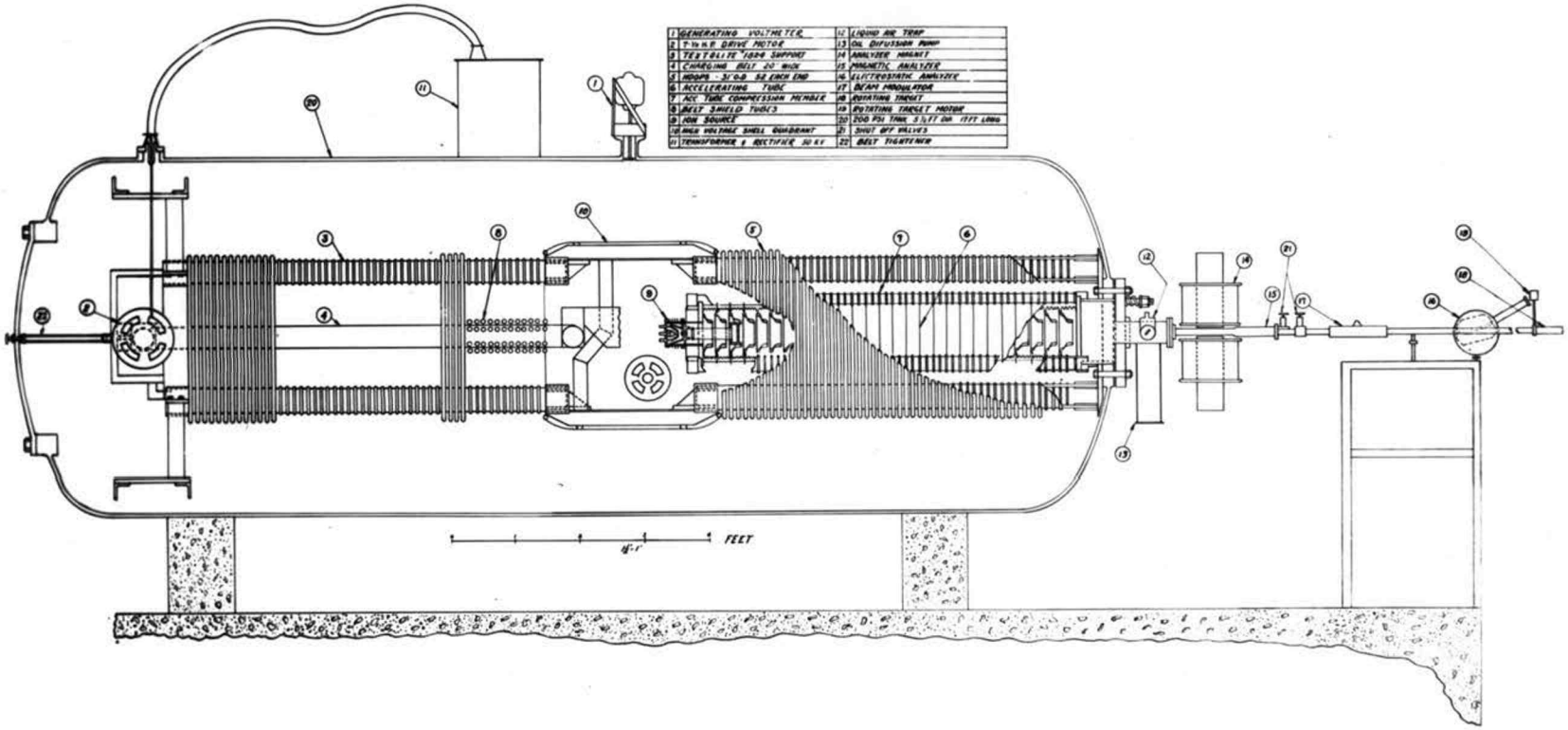

Figure 1. Diagram of the Los Alamos 2.5 Mev Electrostatic Accelerator

EQUIPMENT

I. Description of the Electrostatic Accelerator

The Van de Graaff accelerator which was used for this study has been described briefly by McKibben (20, pp.1-5). The schematic elevation is shown in Figure 1. (Numbers appearing in parentheses, in the following description of the accelerator, refer to Figure 1.)

This machine is one of a type described by Herb, Parkinson, and Kerst (12, pp.75-83) in 1937. The external envelope (20) is a cylindrical tank of 3/4 inch boiler plate 5 1/2 feet in diameter and 15 feet long. This contains the high potential shell, charging belt assembly, and accelerating tube. During operation, the tank is filled with dry nitrogen gas at pressures ranging from 100 to 135 p.s.i., depending upon the voltages desired.

A positive potential of from 0.4 to 2.7 Mev may be maintained on the cylindrical shell (10) by spraying electrons from it upon a continuous woven cotton belt (4) (20 inches wide and about 14 feet in perimeter) which passes over a grounded drive pulley at one end of the pressure vessel and a driven pulley inside and at the potential of the shell. A 7 1/2 horsepower electric motor (2) drives the belt such that in 1/10 second, the charge sprayed on it at one pulley is carried a distance of about 6 1/2 feet to the other pulley to be removed. A full-wave rectifier consisting of two kenotrons and an x-ray transformer (11), whose primary voltage is controlled with a variac, provides a positive charging current of $\sim$0.5 milliamperes

at 30 to 50 kv.

The accelerating tube (6) extends from the high potential shell to ground potential at the other end of the tank. It consists of 29 cylindrical sections of porcelain 2 1/2 inches long, 10 1/2 inches in diameter (outside) and about 7 1/8 inches in diameter (inside). These are cemented together having steel electrodes, 12 inches in diameter (outside) with 2 1/2 inch holes in their centers, placed between successive sections. The steel electrodes provide focussing for ions passing through the tube. The tube is held in compression against the end of the tank by two textolite tubes (7).

Independent of the accelerating tube, the shell is supported from each end of the tank by two textolite tubes (3). A system of closely spaced hoops of steel tubing (5), which extend from the shell to each end of the tank, enclose the supporting textolites, the charging belt, and the accelerating tube. A system of corona points along the textolites and between the hoops produces a uniform potential gradient from the shell to ground at each end of the tank.

External parts attached to the accelerating tube include the magnet box (15), the electrostatic analyzer (16) and the target tube (18). These are all a part of the same vacuum system which is maintained at a pressure of about 10^{-6} millimeters of mercury when the machine is not in operation and at pressures of three to eight times this amount when triton or proton beams are produced. The

vacuum is produced by a DPI MCF-700 oil diffusion pump (13), two diffusion-type booster pumps (MB-100 and VMB-7) and a forepump arranged in series. When triton-enriched hydrogen gas flows down the tube, the forepump is excluded from the system and replaced by a pair of mercury-in-glass Toepler pumps operating in push-pull. These pump the gas into a collection tank from which it may be reclaimed and used again.

When tritium-enriched hydrogen gas is allowed to flow into the Zinn-type ion source (9) (14, pp.28-30), which terminates the accelerating tube at the high potential end, some of the gas is ionized as it passes through the arc maintained within the ion source while the machine is in operation. Positive ions are drawn through a small aperture in the probe (an electrode maintained at about 5 kv negative). These are repelled by the charge on the shell and forced to move along the accelerating tube. As they pass the ground end of the tube and enter the magnet box, they are separated by the magnetic field ($\sim$4 kilogauss) which is in the vertical plane. Ions in the mass-3 component (T^+ , HD^+, or HHH^+) are deflected about 20° and move on to the target. Ions having a mass of 6 (TT^+ or DDD^+) are deflected 14° and pass through the electrostatic analyzer. Actually, the amount of deuterium known to be present in the gases used and in the walls of the ion source and accelerating tube is so small that it will not be present in measurable amounts. Thus, one may observe as many as eight beams coming from the accelerating tube when tritium gas flows through the ion source. These beams are: masses-1 (H^+), 2 (HH^+), 3 (T^+ and

HHH^+), 4 (HT^+), 5 (HHT^+), 6 (TT^+), 7 (HTT^+), and 9 (TTT^+). They are observed as fluorescent spots on a quartz plate at the outer edge of the magnet box. Reversing the current in the magnet coils (14) deflects the beams onto the quartz plate. Relative strengths of these beams vary with the composition of the gases used and with the varying conditions existing in the arc from time to time. Generally, with the gas mixture described above, the most intense beams are those containing masses 1, 2, 3, 4, and 6. The mass-6 beam is used to control the machine energy.

The machine control system is described elsewhere (1, pp. 1-5). It makes use of the mass-6 beam, mentioned above, by taking signals produced when the beam strikes two slightly overlapped plates placed beyond the electrostatic analyzer. These signals are relayed to a difference amplifier and the resulting signal is fed to the grid of a gammatron tube located just outside the tank opposite the high voltage shell. The plate of this gammatron is attached to a corona needle bar which projects through the tank wall and is aimed at the shell. Fluctuations in the energy of ions in the mass-6 beam are immediately reflected by a change in the grid potential of the gammatron. The latter changes the corona current flow, altering the shell potential to correct for the energy variation which was indicated. The machine energy desired is obtained by placing a specified potential difference on the plates of the electrostatic analyzer, which deflects the beam through a fixed angle only when the energy of the beam is correct.

Proton beam currents up to 50 microamperes have been

obtained with this machine as measured on 3/16 inch diameter targets located about nine feet from the grounded end of the accelerating tube. Energy fluctuations are less than $\pm$ 1.5 kev (20, p.2). Beam currents are measured with a current integrator which has been described elsewhere (9, p.325-326).

II. Description of the Target Chamber and the Proportional Counter

In making the initial plans for a study of the charged particles resulting from the interactions of tritons and lithium nuclei, several requirements for the target and detection apparatus were evolved. These may be outlined as follows:

A. The target system must permit:
   1. Use of solid targets which can be adequately cooled
   2. Rapid interchange of different target materials
   3. Keeping targets in a vacuum or in an inert atmosphere
   4. Rotation of target surface to known angles with the collimated beam of bombarding particles
   5. Beam current measurements
      a. For targets which are opaque to the beam
      b. For targets which allow most of the beam to pass through
   6. Detection to be made at continuously variable angles (or at several fixed angles) to the incident triton beam

B. The detection apparatus must be capable of:
   1. Recording pulses produced by protons, deuterons, and alpha particles
   2. Supplying information from which the energy, and possibly the nature, of a particle can be deduced.
   3. Detecting alpha particles ranging in energy from about 1 to 13 Mev

4. Having relatively low background counting rates.

A scattering or target chamber and a proportional counter were designed and built to satisfy these requirements. These are described and illustrated in IIA and IIB.

IIA. The Target Chamber

Effort which went into the design and construction of the target chamber proved to be well worthwhile when it was put into operation. It was found to be reasonably versatile and quite dependable. Numbers in parentheses, which are used in describing the chamber, refer to Figures 9, 10, and 11.

The main framework of the chamber, shown in Figure 9, is the cylindrical pill box of dural (1), around the edge of which are located the fixed-angle counter ports (2). In Figure 10, are indicated the target holder (3) in the bottom plate and the liquid air trap (4) in the top plate. The beam collimating tube and the Faraday cage are also placed on the periphery at 180° and 0° positions, respectively.

The target holder is shown in Figure 10. It has three major parts, a disk-topped cylinder (7), an aluminum rod (8) which slides within the cylinder and contains the target disk clamped vertically at its upper end, and an offset valve (9) which may be used to seal the upper end of the cylinder (after the target has been pulled down into the latter). The bottom end of the aluminum rod is provided with a finned flange and taper pin key (10). This makes

possible adequate cooling and positioning of the target with respect to the target holder. Throughout the target chamber and the counter, sliding, rotating, and most static vacuum seals are produced by extensive use of neoprene "O"-rings which have been lubricated with silicone stop-cock grease.

The target holder receptacle, shown in Figure 11, is built into the bottom plate of the chamber. It contains an offset valve (12) for the opening into the chamber proper (13), an intermediate pump-out space (14) between the target holder and the chamber, and indices marked in degrees for positioning the target holder so that the target may be placed with its face at any known angle to the beam (up to 90° each way from normal). A radially-compressed "O"-ring seal (15), indicated in Figure 10, is made when the target holder is "plugged into" its receptacle. Rotation while in place and rapid interchange of target holders are made possible with this arrangement. The target can be kept in a vacuum at all times, whether it be in the chamber or out.

The target receptacle, shown in detail in Figure 11, is made in two parts, insulated from each other by a resistance greater than 200 megohms. The inner part (16) is in contact with the chamber while that containing the target holder (17) is insulated from ground. Within the chamber volume, a dural cylinder (18) is placed concentric to the rod supporting the target. It extends to within about 1/8 inch of top and bottom plates of the chamber and is supported on insulated plugs (19) which are cemented to the inner face

of the target receptacle. Where this cylinder is intersected by the horizontal plane in which the collimated beam lies, apertures (20) are provided at angles corresponding to those for the ports located on the chamber periphery. A lead wire (21) brought out through a kovar seal in the target receptacle permits placing this cylinder negative to ground ($\sim$300 volts) so that it may serve as an electron barrier surrounding the target. An accurate beam current measurement may thus be made directly between the target holder and ground, when the target is opaque to the beam.

The Faraday cage (6), shown in detail in Figure 9, which is placed on the periphery of the chamber at 0° was provided to permit one to make beam current measurements while targets not opaque to the beam were used. It consists of an insulated brass cup (22) in which the beam could be collected. An electron barrier electrode (23) is located just forward of the cup and insulated from it. The back of the cup (24) is made of nickel gauze. The position of the beam terminating in the Faraday cage is indicated by the fluorescence it produces in the quartz disk (25) which serves as a back plate to the cage. Preliminary alignment of the chamber in the target beam was a simple procedure when a target blank having a centrally-drilled 1/8 inch hole through it (26) was placed normal to the beam and its image observed on the quartz window.

In Figure 10 is shown the collimating tube (5), which is located diametrically opposite to the Faraday cage. It is a small dural tube into each end of which a beam-defining diaphragm is

placed. At that end, located within a cup-shaped connector (for attaching the chamber to the target tube of the electrostatic accelerator) is a large tantalum disk (27) which stops most of the beam. The fraction of the beam which passes through the small aperture in this diaphragm is further reduced by a similar aperture in the tantalum plug (28) at the rear of the tube. The dural cap (29) over the target-end of the tube contains an aperture just slightly larger than those in the tantalum plugs. This is known as the scraping aperture and serves to remove from the collimated beam most of those particles which were scattered from the edges of the previous tantalum diaphragms. The result of this collimating arrangement is to define a beam spot 1/8 inch in diameter on the target disk.

Incidental to the collimating process, the forward tantalum aperture is heated by the large fraction of the beam energy dissipated in it. Circulating water is forced through the water jacket (30) which is placed around the dural tube and immediately behind the cup-shaped connector to carry heat away from this region.

The counter ports (2), shown in Figures 9 and 10, are eleven assemblies. Each consists of a protruding nozzle, the inner end of which may be closed by an offset valve (31). The ports are located 30° apart from 15° to 165° on one side of the chamber and from 30° to 150° on the other side.

A defining aperture is located in an aluminum plug forced into the outer end of each nozzle. Each of these apertures was milled 1/4 inch long (vertically) with a 1/8 inch end mill. As the

counter window lies next to this opening when the counter is placed on the nozzle, the solid angle (Figure 13) defined for the counter is approximately the same at each port. The difference in solid angle for the 90° and 165° ports is not measurable with the counter when a standard source is placed at the target position, facing normal to the port in each case. As calculated from the measurable geometry, the solid angle is $4.36 \pm 0.25 \times 10^{-4}$ steradians.

The offset valves (31) at the ports permit each one to be closed and opened independently. A two stepped spacing collar (33) is placed around the shaft of each valve to allow it to be opened (and rotated out of the opening) or pulled closed and held closed against atmospheric pressure. The counter window valve assembly which is mounted on the end of the counter is provided with a pump-out line. Thus, one may move the counter from one angle to another without disrupting the vacuum in the chamber by closing the valve within the nozzle (and one which seals off the counter window), letting air into the intermediate region, removing the counter, placing it on the nozzle at the next desired angle, pumping out the intermediate region, and opening valves in the nozzle and in front of the counter window. This can be done within one minute. A description of the valve to the counter window will be given along with that for the counter itself in IIB.

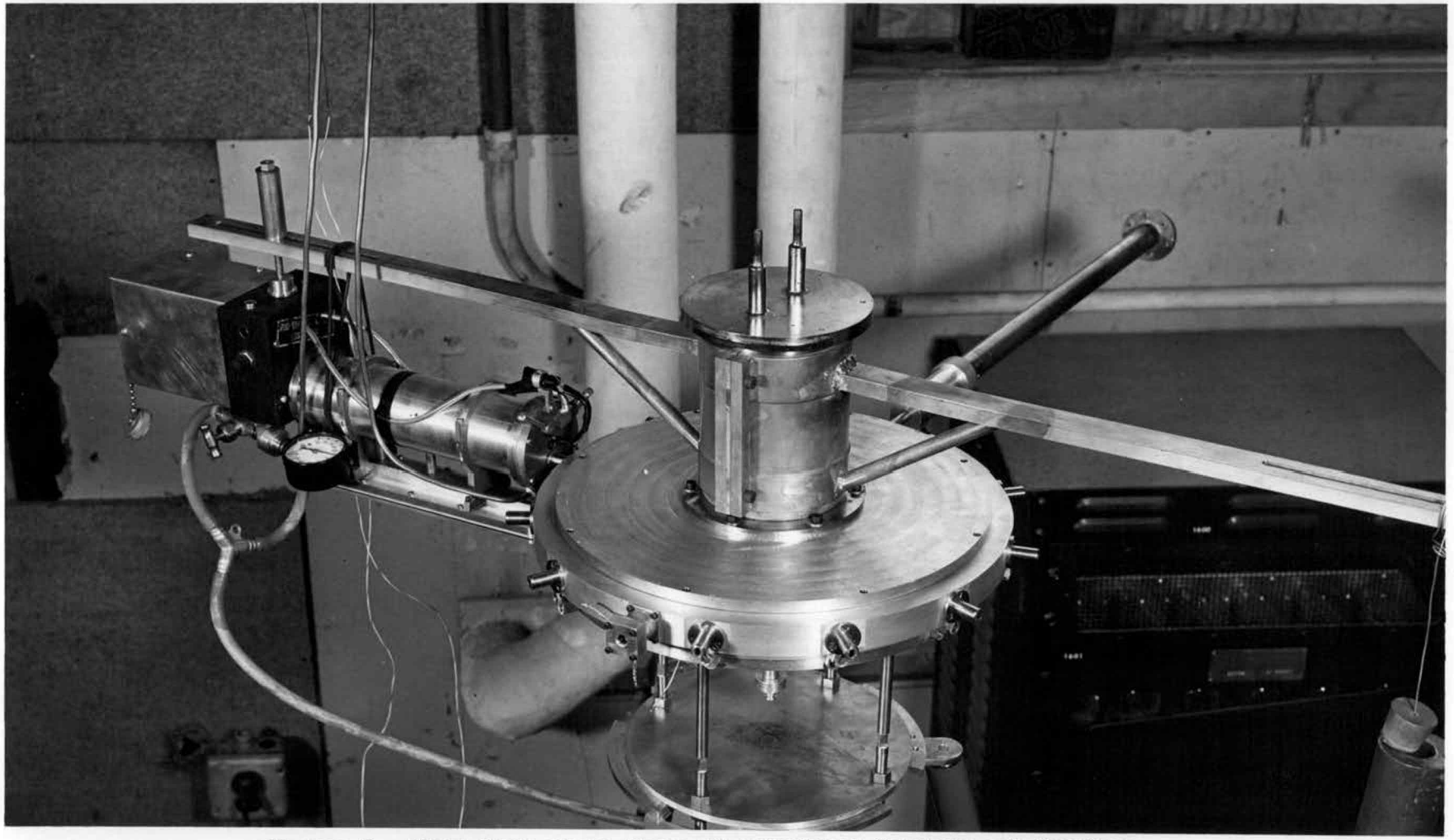

Figure 2. View from above Rear of Assembled Counter and Chamber

Chamber is shown removed from the accelerator with the counter in position at 90°.

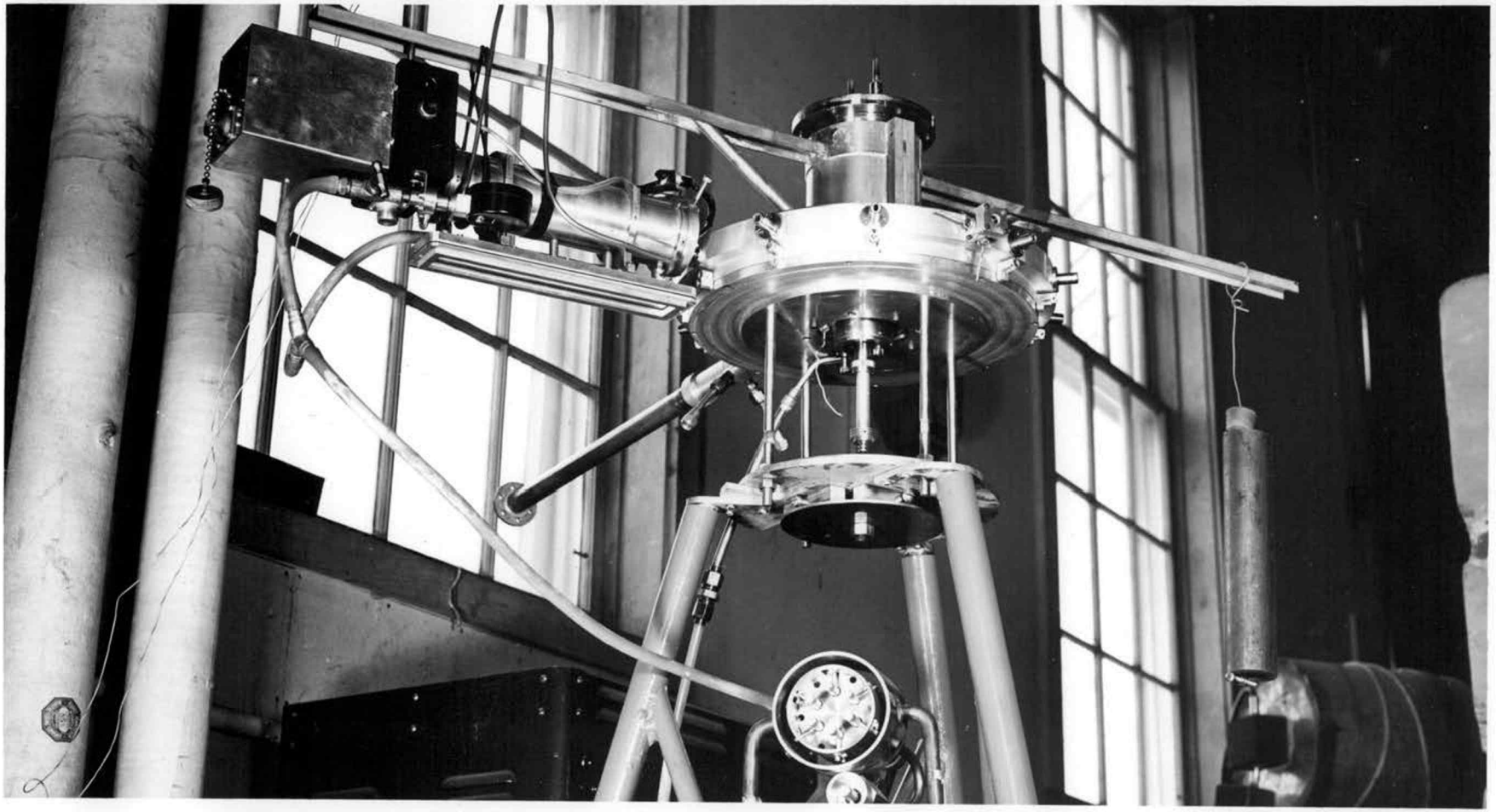

Figure 3. Assembly of Counter and Chamber as Viewed from Below at 30°

Counter is at 90°. Target holder rod is shown in down position. The 7-valve manifold for the pump-out system is shown in the upper part of the tripod support below the chamber.

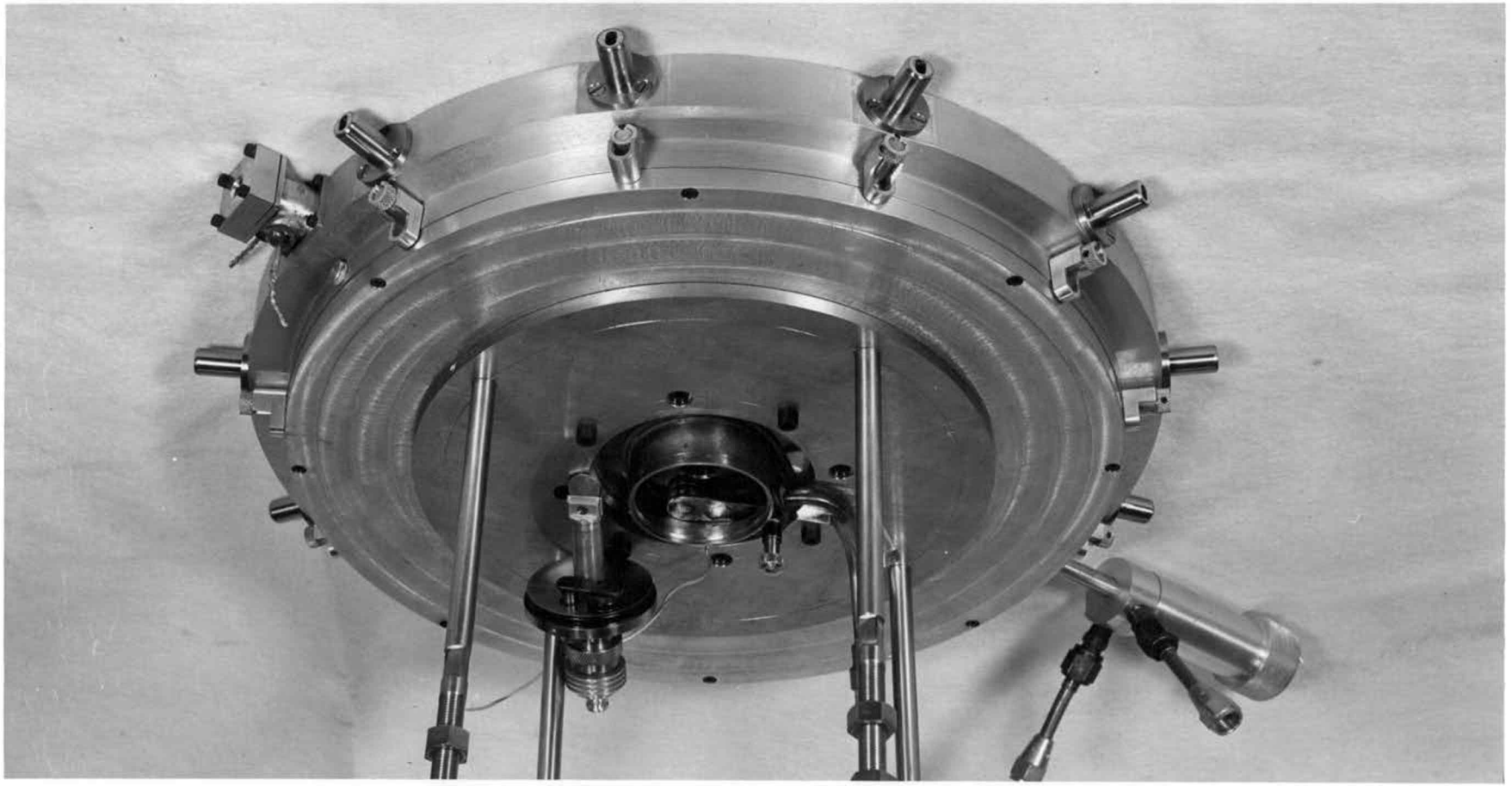

Figure 4. A View of the Chamber from 45° Below

The Faraday cage is at left, the target tube connector and water cooling jacket at right, and the target holder receptacle in the center. The target holder is shown near the receptacle with the target clamped in place at the upper end of the rod, which is in the up position. The offset valves for holder and receptacle are shown opened.

Figure 5. The Chamber with Top Plate Removed

The chamber is shown on a ring stand as viewed from above at 150°. The electron barrier sleeve surrounding the target is seen in the center of the chamber. The offset valve is open for the 45° port. Other ports are closed.

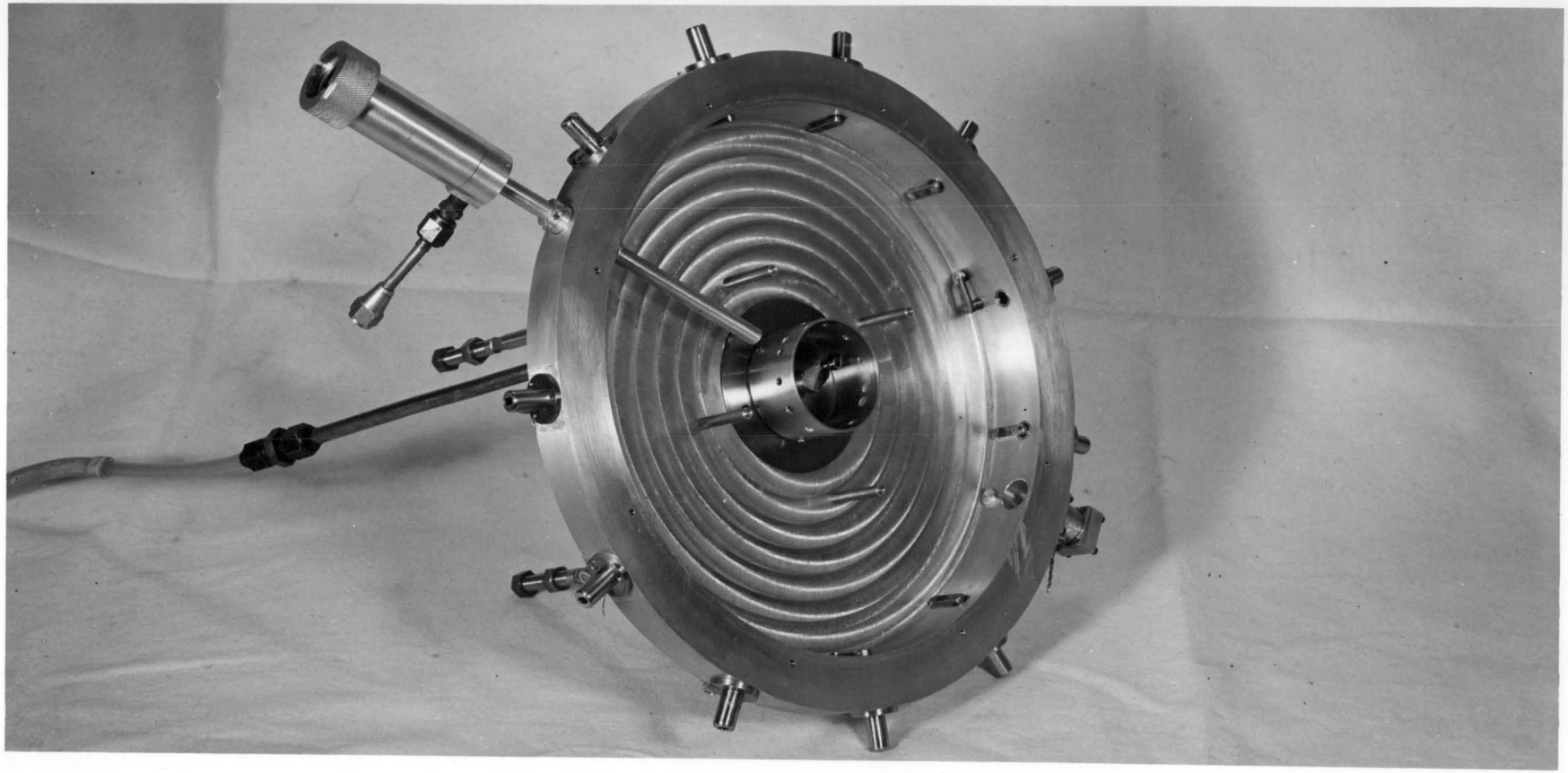

Figure 6. The Inside of the Chamber as Viewed from the Top

The collimator extends inward from upper left. The target is shown in position. Carbon which was deposited where the beam struck the target can be seen. For observations of reactions at 90°, the target was placed at an angle of 45° to the beam, hence the elliptical appearance of the carbon spot. Four spacing rods can be seen which serve to support the centers of the top and bottom plates while the chamber is evacuated.

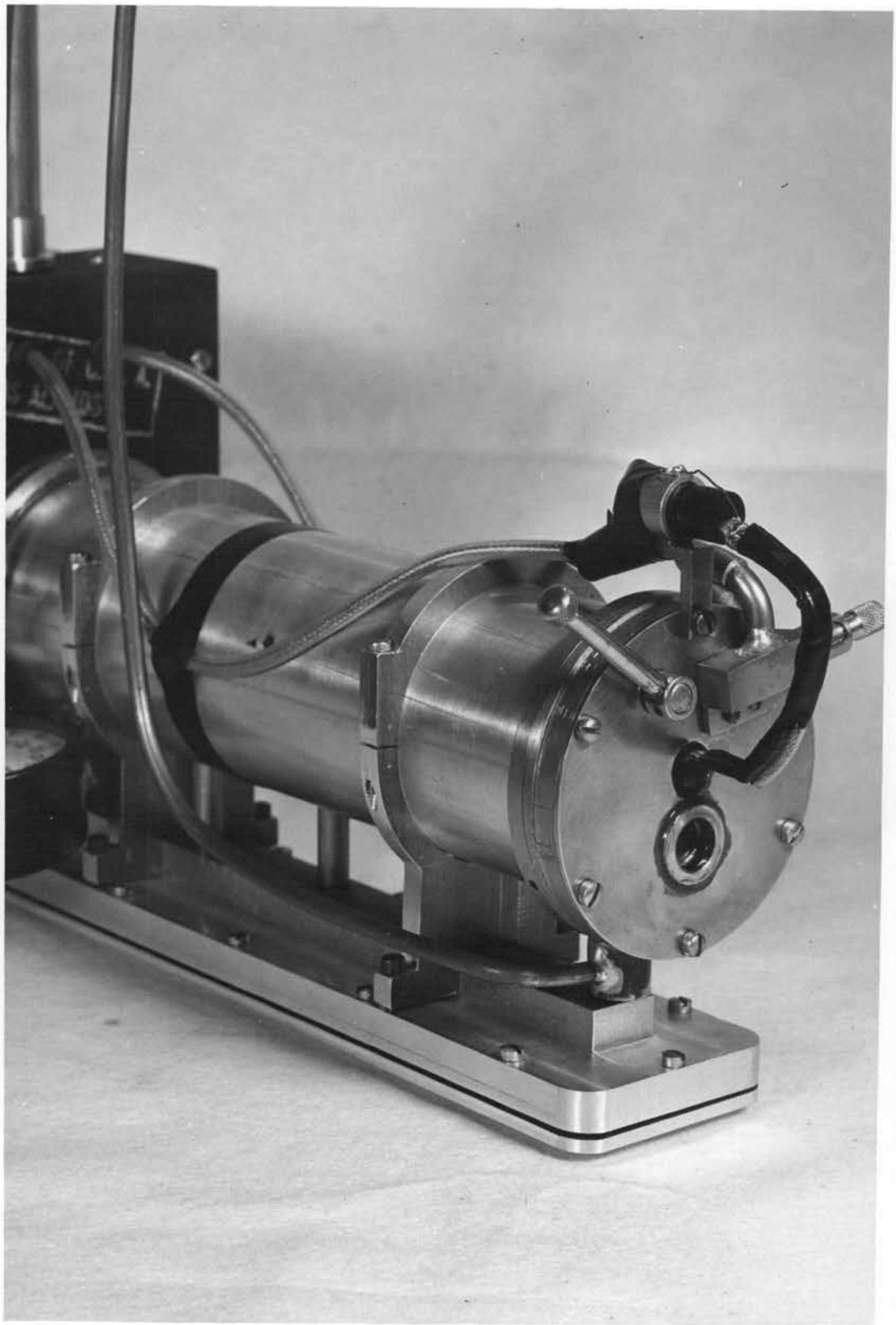

Figure 7. The Counter as Viewed from the Window-End

The window valve is shown in place on the counter. It is closed. At the bottom is the built-in source holder.

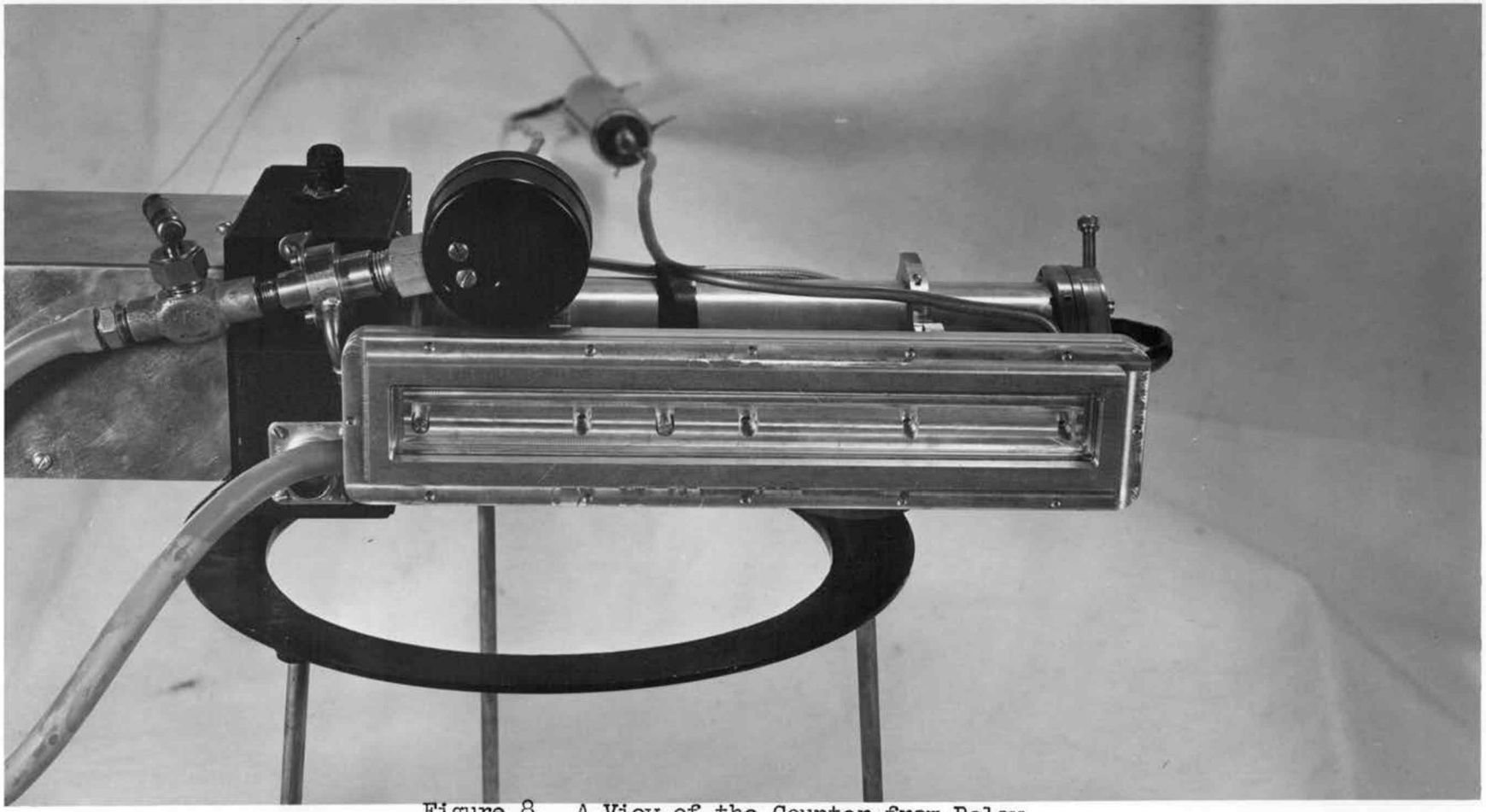

Figure 8. A View of the Counter from Below

Two sources are shown in the source holder. One is in place at the rear position recess, the other is in the dummy recess. Filling lead, valve and pressure gauge can be seen. The purifier is partially visible at the top of the photograph.

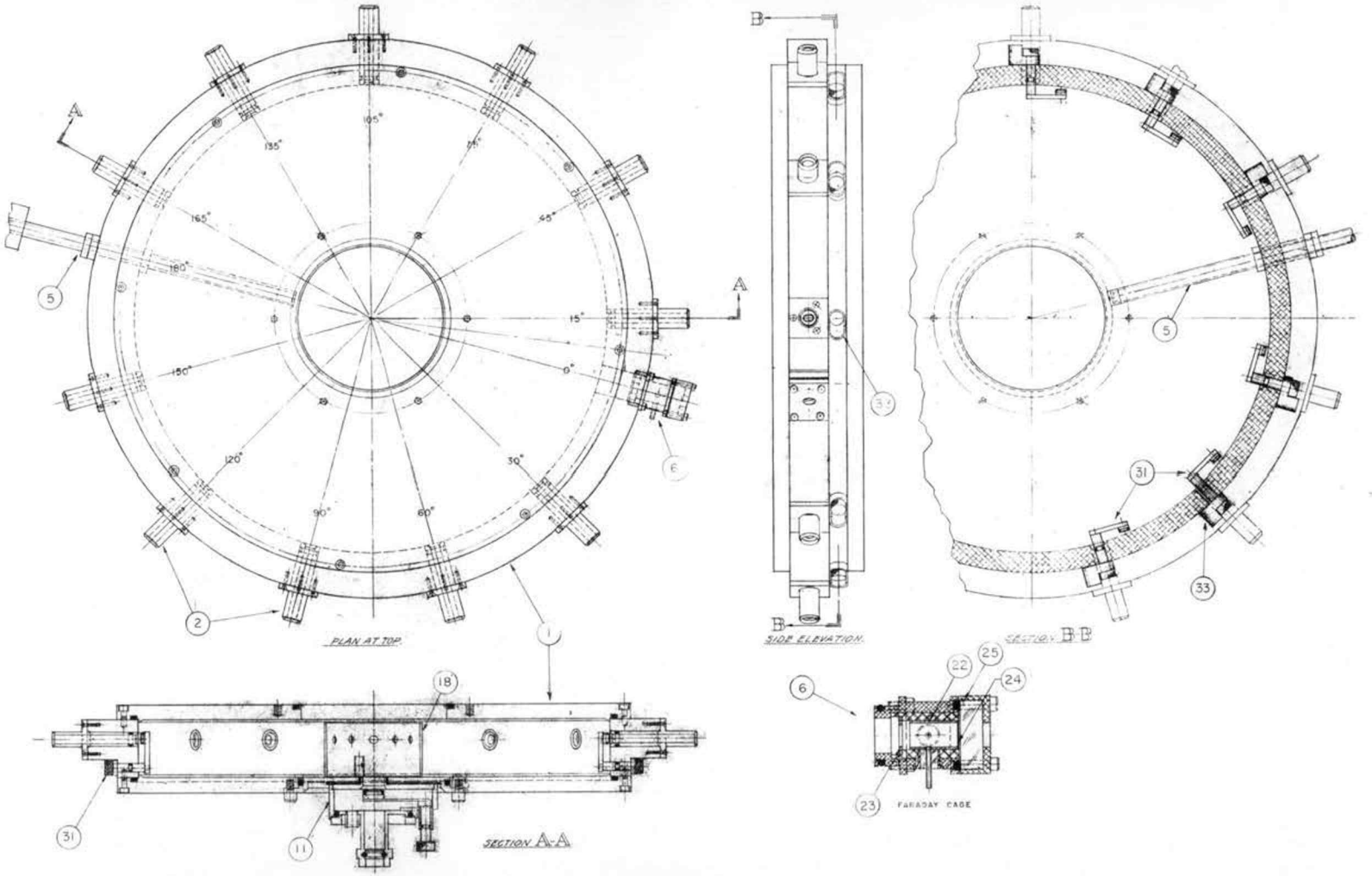

Figure 9. Drawing of the Target Chamber

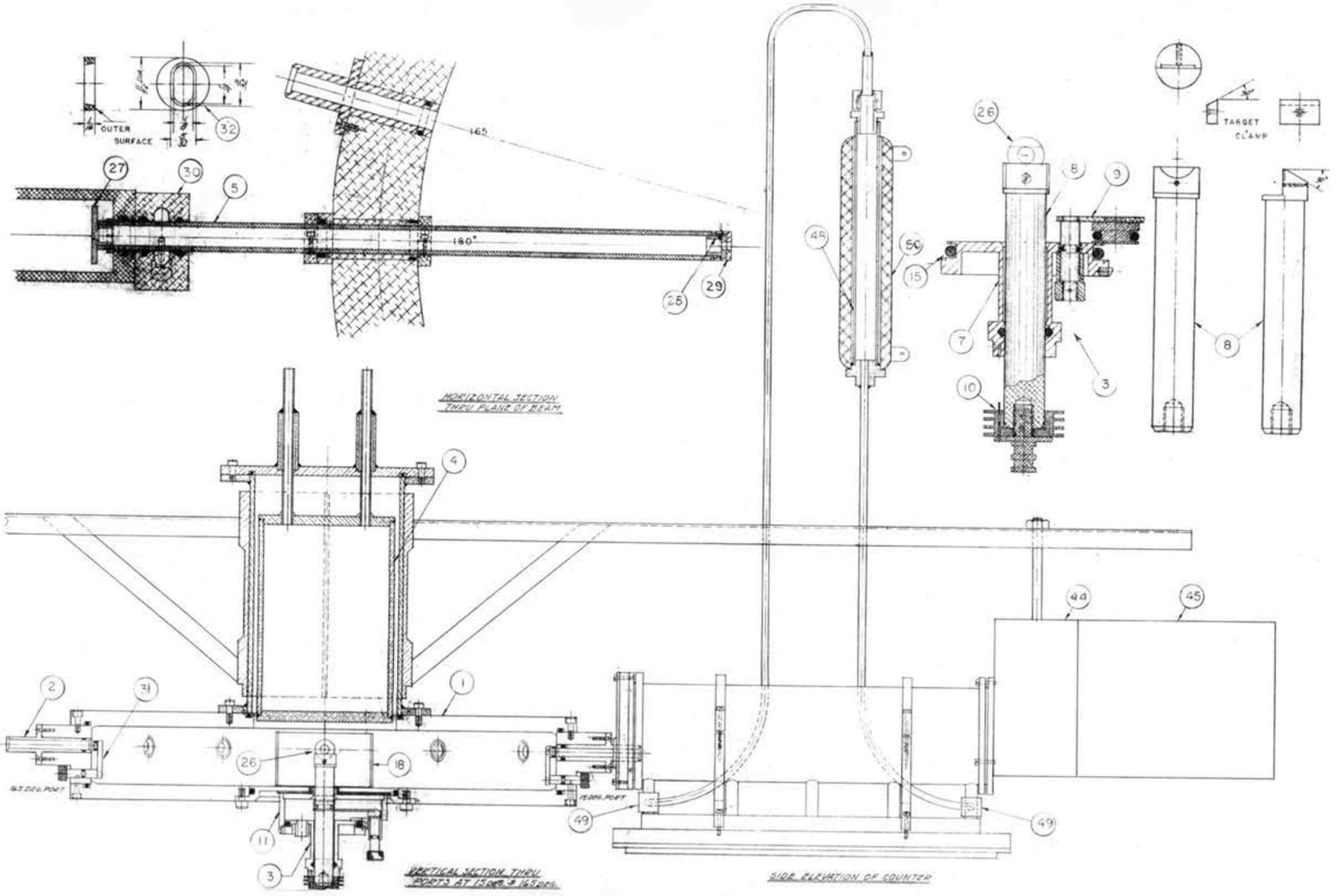

Figure 10. Drawing of Assembly of Chamber and Counter

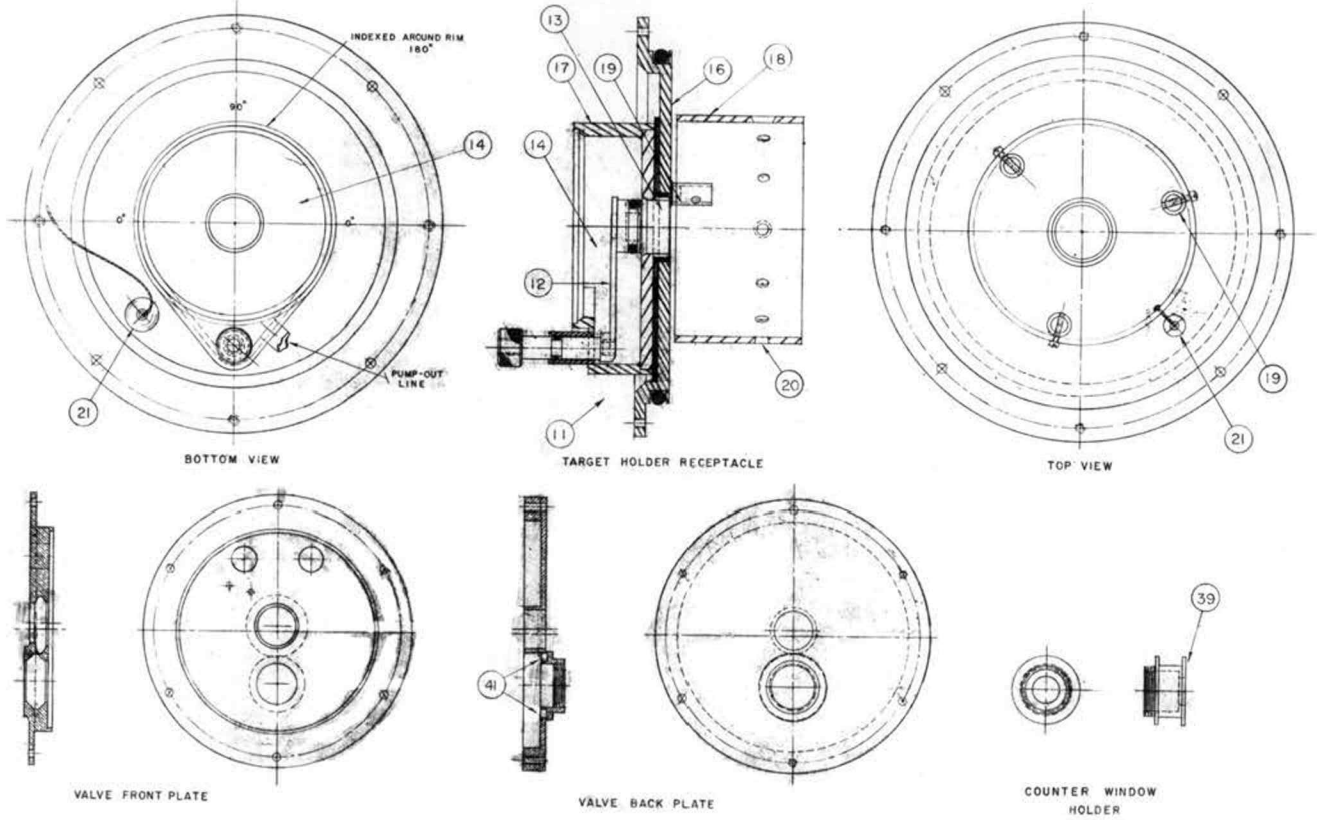

Figure 11. Details of Target Holder Receptacle and Counter Window Valve

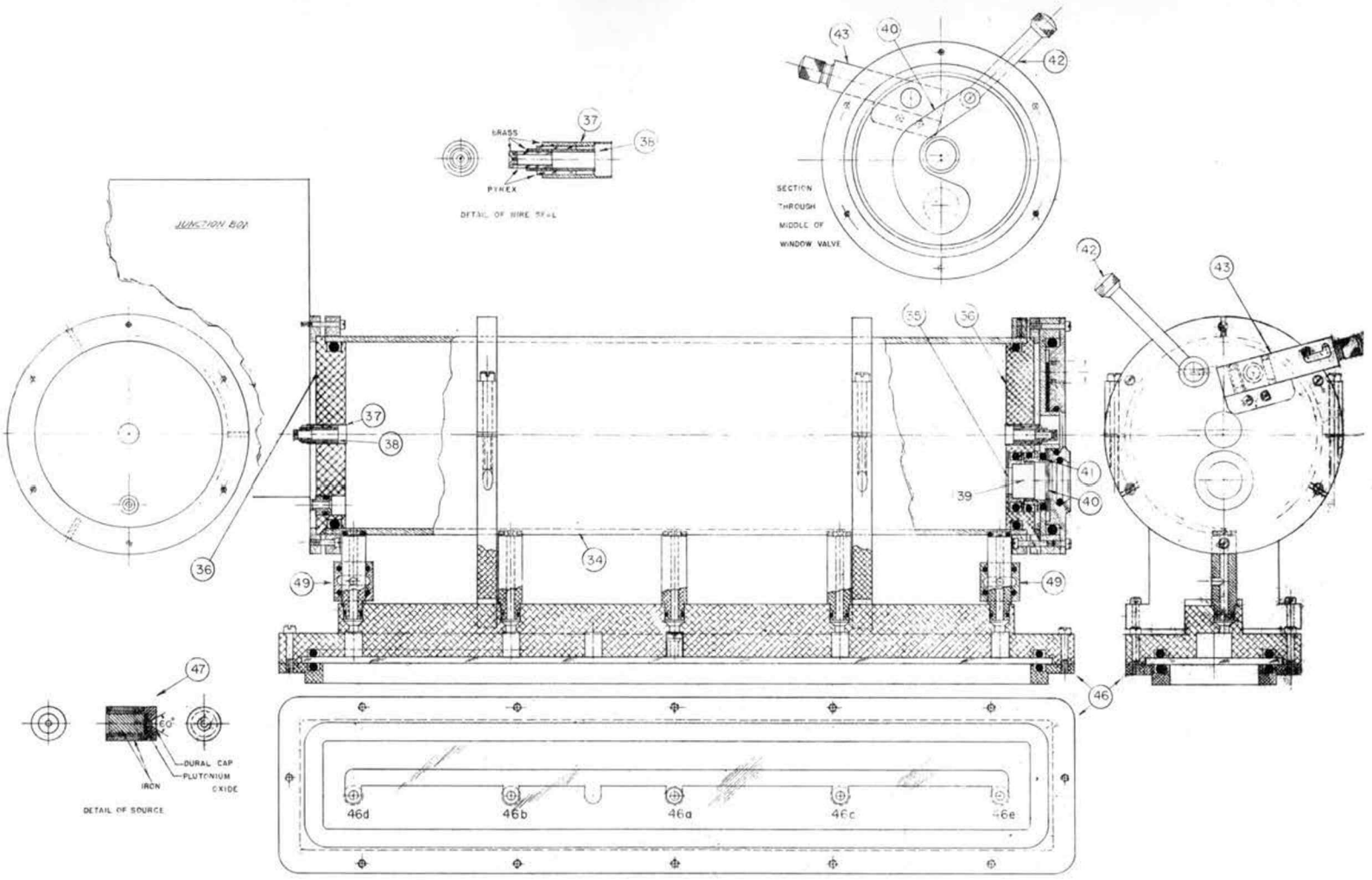

Figure 12. Details of the Proportional Counter

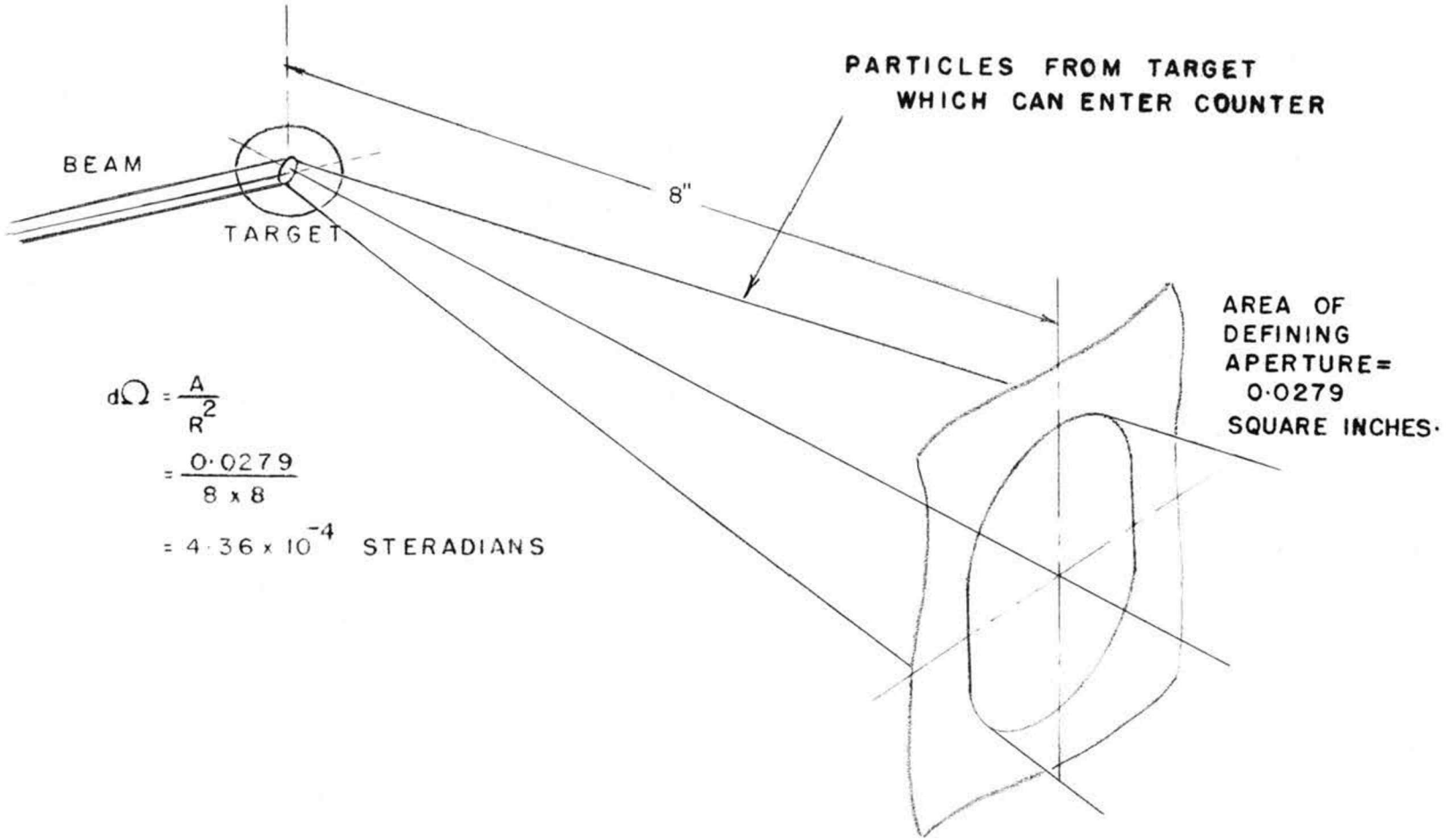

Figure 13. Solid Angle of the Counter Ports

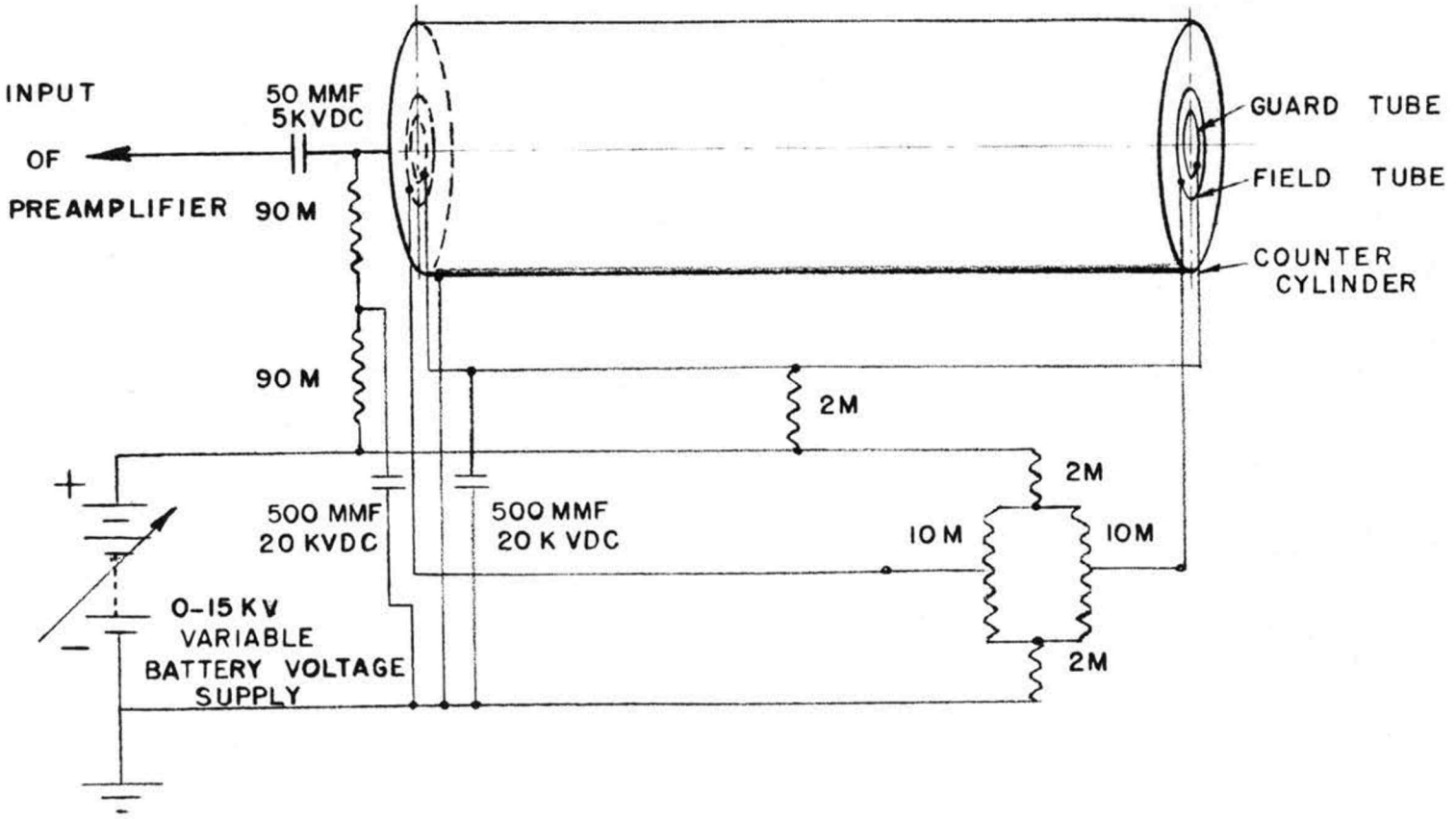

Figure 14. The Counter Circuit

The liquid-air trap (4), shown in Figure 10, is placed directly over the target to minimize the presence of pump oil vapor in the region of the target. This precaution was made in the attempt to eliminate formation of carbon on the targets. However, a thin layer of carbon was found on each of the targets following bombardment for several days. The trap is made of brass, except for the filling tubes which are stainless steel. The whole assembly has been nickel plated to minimize effects of heat radiation.

A manifold of seven valves was constructed for the pump-out vacuum system. Valves were made of "O"-rings on rods which could be pushed into or removed from holes in the back plate of the manifold. Six of these were built into a common cylindrical manifold. The seventh was made similarly but independent of the other six to provide a by-pass for a roughing pump. Operation of this system is quite satisfactory. With it, pump-out cycles have been effected quickly and with a minimum of hand motion. The manifold, which is equipped with a thermocouple vacuum gauge, is visible below the target chamber in Figures 2 and 3.

IIB. The Proportional Counter

A gas-filled proportional counter (26, pp.72-100), (16, pp. 34-50) was designed which can be used to indicate energies of alpha particles between 1.75 and 13.0 Mev. These limits are imposed by properties of the counter window, the length of the counting volume and the nature and pressure of the filling gas, which was fixed during the present experiment. Numbers in parentheses, which are used in

describing the counter, refer to Figures 10, 11, and 12.

As indicated in Figure 12, the counter envelope (34) is made of a 9 inch length of 1/16 inch wall dural tubing, 2 3/8 inches inside diameter. The axial wire is 0.003 inch diameter stainless steel. A mica window (35), 1.06 mg/cm^2 over a 5/16 inch diameter aperture is located 9/16 inch below the wire in one end of the counter. The counter is filled to a pressure of 50 centimeters of mercury with a mixture of commercial argon and carbon dioxide in the proportions 95% and 5%, respectively. Taking into account the stopping power of the window and of the gas, a 1.75 Mev alpha particle will just enter the counter and a 13 Mev alpha particle will just be stopped within the counting volume. Protons with energies in excess of 3 Mev will lose only part of their energy in the counter. Since the design provided for particles to enter at one end of the counter and pass through it parallel to the wire, it was desirable to attempt to minimize any pulse-height distortion near the ends of the counter. Following recommendations of Cockroft and Curran (6, pp.41-42), and those resulting from some experience acquired by others working at Los Alamos Laboratory, the ends of the counters (36) are made of semi-conducting disks of phenolic #942 having small field tubes (37), concentric with the wire, cemented in at their centers. The field tubes are maintained at potentials intermediate to those of the wire and cathode. The purpose of modifying the end of the counter in this way is to permit one to establish a potential gradient in the end which is very nearly the same as that found throughout the counting volume, thus eliminating

the cause for distortion of the radial counter field near the ends of the central wire.

Immediately around the wire and concentric with it, guard tubes (38) are placed. These are maintained at the same potential as the wire but are by-passed to ground. Their purpose is to restrict the number of spurious pulses by minimizing the flow of leakage currents from the wire. A diagram of the counter circuit is shown in Figure 14.

The mica window holder (39), Figure 11, is a detachable cylindrical piece which projects from the back side of the window valve assembly. It is sealed into the window recess in the phenolic end of the counter with "O"-rings. On the inside of the valve case, a steel vane (40) slides across an "O"-ring (41) to seal the window against pressures outside the counter. The vane is operable with the external lever (42) shown in the illustrations. A small plunger valve (43) mounted on the case of the window valve is used when it is desired to pump out the case of the window valve after placing the counter on a port nozzle of the chamber--before opening the window valve and the offset valve in the chamber port.

In constructing the counter components, two adhesive substances were used in making seals not formed by "O"-rings or solder. These are Gelva V-7[1] and Armstrong's adhesive[2], grade A-1, mixed with

---

1. Gelva V-7 is obtainable from Shawnigan Products Corporation, Empire State Building, New York 1, New York.

2. Armstrong Products Co., Argonne Road, Warsaw, Indiana.

activator A. Gelva was used to cement the mica window in place. In assembling electrodes surrounding the wire and sealing them into the phenolic disks, Armstrong's adhesive was used. (The latter was used, also, to assemble the two parts of the target holder receptacle which was described earlier.)

Attached to the rear of the counter (the end opposite that containing the mica window) is a small junction box (44), indicated in Figure 10, which contains the resistors and condensers shown in Figure 14. The junction box has a Los Alamos Model 101 preamplifier (45) attached to its rear face and a cable-connector, through which the counter voltage is supplied, mounted on its bottom edge.

In order to make a test of the effectiveness of the field tubes, a source holder (46), shown in Figure 12, was built into the counter in such a way that a collimated source of plutonium alpha particles could be placed at each of five positions along the length of the counter. The positions are located (a) in the middle of the counter length, (b) and (c) 2 1/8 inches each way from (a), and (d) and (e) about 0.080 inches in from each end of the counter volume. The source (47) is contained in a small iron plug which can be manipulated from outside the source holder with the aid of a small permanent magnet. The bottom face of the source holder is a glass plate which permits one to observe the source in any of the five positions.

Preliminary operation of the counter indicated a continuous degradation, with time, of the counter resolution. It was assumed that the counter gas was being denatured from materials used in making the

counter. Consequently, a purifier (48), Figure 10, was added. This consists of a copper tube containing about 10 grams of calcium metal turnings, surrounded by a heating element and connected to the counter near each end (49) by small, flexible copper tubing. The temperature of the purifier was measured by a small thermocouple junction which was silver-soldered to the purifier wall near the middle of its length. A 100-watt, 50 ohm power resistor (50) was used for the heating element. During the month in which the experimental work was completed, the purifier temperature was maintained continuously at 225° to 230° C. Apparently, this removed water but no CO_2.

The counter was supplied with voltage from a battery supply which can provide continuously variable voltage from 260 to 1500 volts. A meter across this supply permits one to maintain it at a constant potential and to know its value within 5%.

The negative charge collected by the wire when an ionizing event occurs within the counting volume results in a pulse with magnitude proportional to the number of ions produced in the counter gas. This pulse is amplified 100 times in the preamplifier before entering the Los Alamos Model 101A amplifier. In the latter, gain is set at any value from about 50 to 11,800. Pulses in the output of the amplifier enter the Los Alamos Model 180 18-channel pulse height analyzer, described in section III, where they are sorted as to pulse heights and recorded on appropriate scalers. Undistorted output pulses from the amplifier have a maximum of 146 volts.

Three minor experiments were conducted to determine

conditions for best counter operation. Characteristics determined are:

1. Gas amplification as a function of counter voltage
2. Field tube potentials at which a minimum of pulse height distortion occurs near the ends of the counter
3. Pulse height resolution of the counter.

A semi-log plot of pulse height as a function of counter voltage (using a plutonium alpha source in front of the counter window) was obtained (Figure 15). From this curve one can estimate the voltage at which the multiplication is unity by locating the position of the region in which one observes a minimum change in pulse height per unit voltage change. This appears at approximately 270 volts on the counter and at a pulse height of 26 volts. Thus, on the curve, the pulse height corresponding to 670 volts on the counter is ~675 volts. This value is $\sim(26)^2$. Squaring the pulse height amounts to doubling the multiplication. The counter potential used throughout the experiment was 670 to 680 volts, giving a multiplication of two.

Intermediate cylinder potentials are calculated as follows:

Assume a radial field from the inner of two concentric cylindrical conductors. The electric intensity on a concentric cylindrical surface having intermediate radius r is given by Gauss' Law as $E = 4\pi q/2\pi r = 2q/r$, where q is the charge per unit length.

From this expression, one obtains the potential, since $E = -dV/dr = 2q/r$. This integrates to give $V = -2q \log r + k$. The constant is evaluated by assuming the cathode to be at zero potential. Then $V_c = 0 = -2q \log r_c + k$, and $k = 2q \log r_c$. Using the additional

subscripts w and p to refer to wire and field tube, respectively, the ratio, R, of the potential of the field tube to that of the wire is given by

$$R = V_p/V_w = (-2q \log r_p + 2q \log r_c)/(-2q \log r_w + 2q \log r_c)$$
$$= \log (r_c/r_p)/\log (r_c/r_w).$$

The counter has the following dimensions, in inches:

$r_c = 1.185$, $r_w = 0.0015$, and $r_p = 0.110$. For the counter, $R = 0.356$.

To obtain R experimentally, the plutonium source built into the counter was placed at the two end positions and at the middle position. The field tube potential at each end was varied, by the corresponding potentiometer indicated in Figure 14, until the average pulse height at that end was the same as the average pulse height at the middle position. Following these adjustments, voltages applied to the field tubes were measured. At the forward, or window end of the counter, R was found to equal 0.734 while at the back end of the counter, the value obtained for R was 0.355.

This disparity between experimental and calculated values at the forward end is not understood but may be the result of (a) distortions resulting from actual configurations of the counter components at the end and (b) inaccurate determinations of the average pulse height for the source particles which enter the counter very close to the end plate, and may have been inadequately collimated.

Resolution of the counter was measured at the three intermediate positions for the source and the counter when a source was

used in place of the target, in the target chamber. As indicated in Figures 16 and 17, the resolution in the central half of the counter is about 4.4% while that for the counter as a whole, if particles enter parallel to the wire, is about 4.1%. (Since different sources and collimation were used, for particles entering the counter parallel or normal to the wire, a rigid comparison of the values for resolution in the two cases is not justified.)

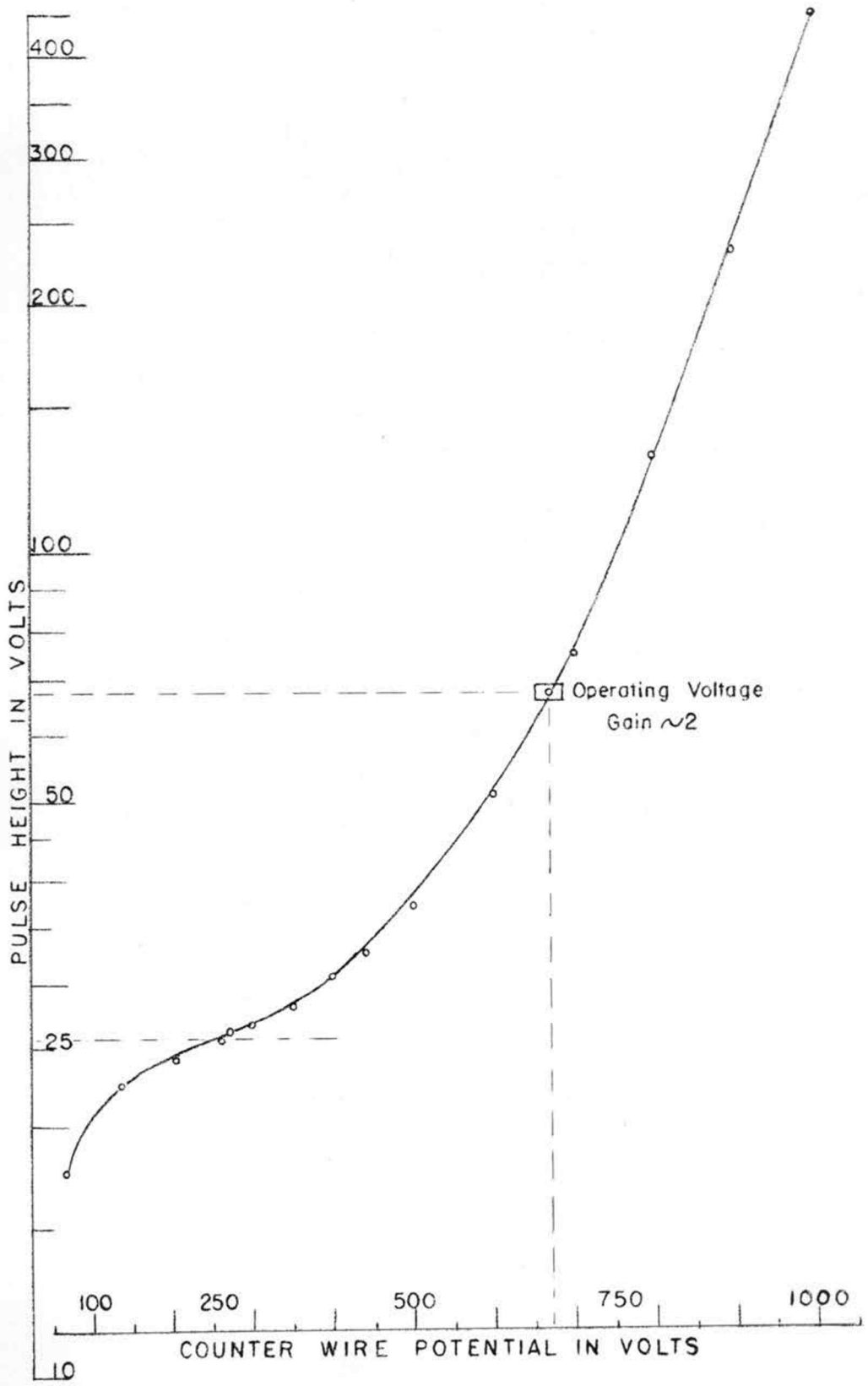

Figure 15. Counter Pulse Height As A Function of Counter Voltage

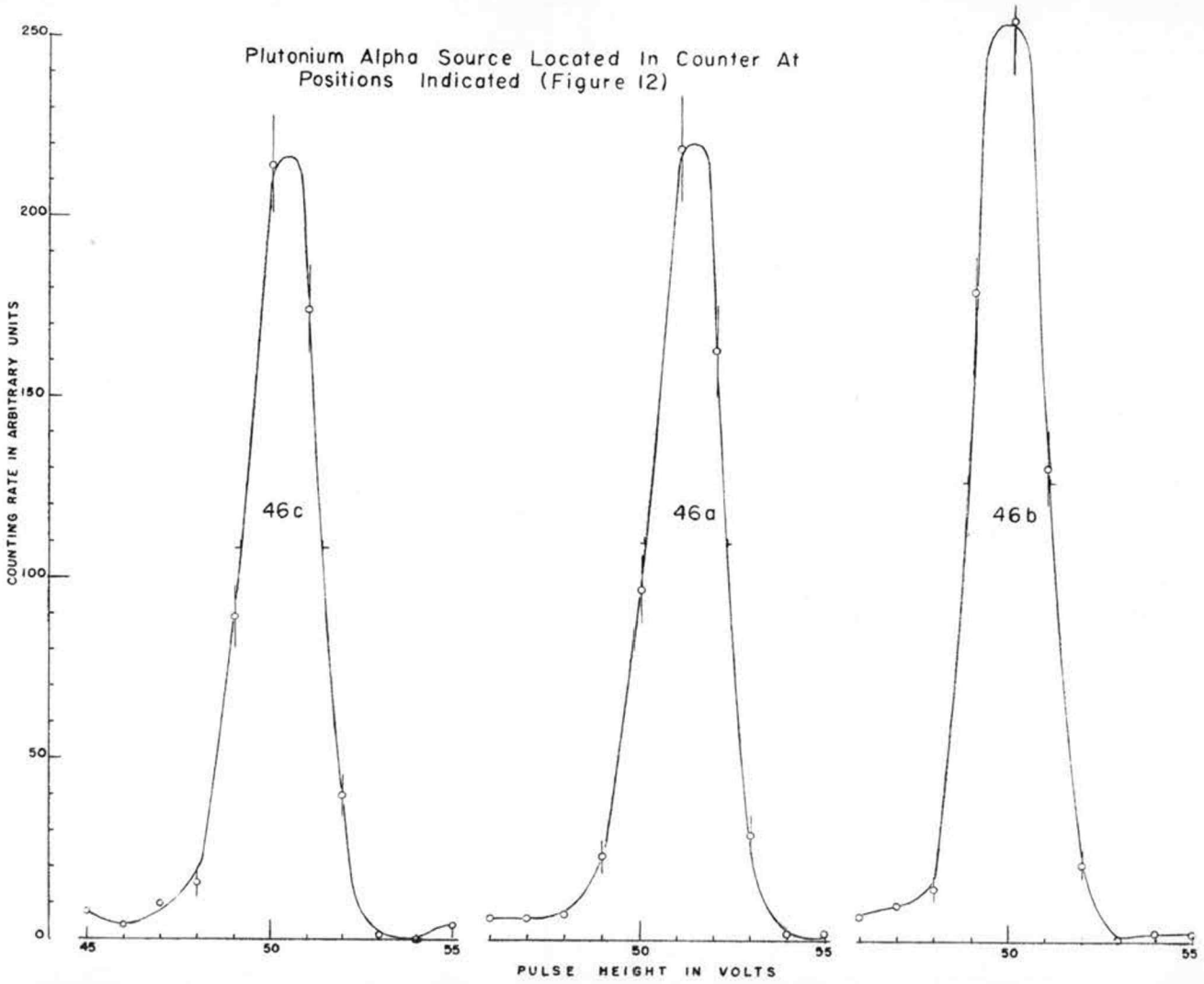

Figure 16. Resolution of Plutonium Alphas--Source in Side of Counter

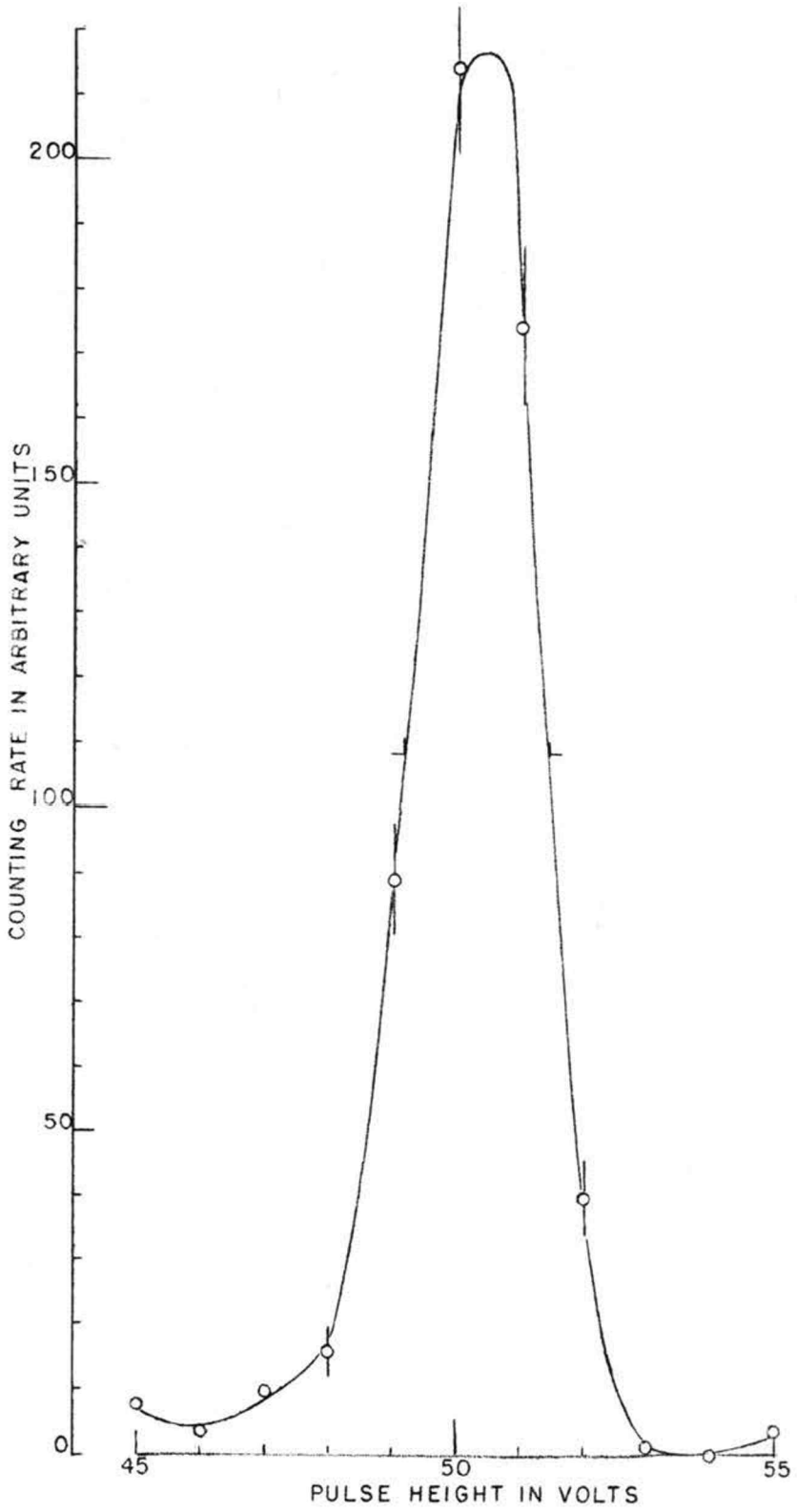

Figure 17. Resolution of Plutonium Alphas From External Source

III. Description of the 18-Channel Pulse Height Analyzer

The Model 180 pulse height analyzer used in this experiment was built at the Los Alamos Laboratory by Mr. C. W. Johnstone. A simplified diagram is shown in Figure 18. The analyzer receives a pulse (1) from the amplifier, sorts it as to relative pulse height (2) and produces a pulse (3) at the input to the appropriate decade scaler, where it is recorded. A gating circuit (4) is shown in the diagram. It was used by placing the position switch to the coincidence position. At this setting, it serves to prevent a pulse which registers in the surplus from registering also as a pulse in one of the lower channels. The appearance of the pulses at various stages in the circuitry are indicated at the top of the diagram. Many of the adjustments provided in the analyzer are not indicated.

The shape of the pulse appearing between the condenser and resistor coupling successive univibrator circuits is shown for the two cases where (5) the following stage does not trigger and (6) the following stage triggers. The final pulse which is fed to a scaler results when a following stage does not trigger.

Channel widths of 1 volt, 2 volts, and 5 volts may be set with the channel width selector (7) which changes the window amplifier gain and makes corresponding adjustments in the resistance network. Widths are calibrated to 1% and stable to better than 2% over periods of several days. Channels are moved up or down the range of pulse amplitude by means of a helipot bias control (8) on the input to the window amplifier.

The shape of the pulses entering the window amplifier may vary such that rise times from 0.1 to 15.0 microseconds can be tolerated, provided that the top of the pulse is flat to 1% with a duration of at least 0.25 microsecond. A 2 microsecond RC clipper was used in the input of the Model 101A amplifier.

The analyzer permits one to make very rapid measurement of pulse heights. As used in this experiment, for most of the data obtained, 2-volt channels were set on the analyzer and the bias was set as low as 13 volts and as high as 103 volts, covering a pulse height range between 13 and 139 volts. A change of gain in the Model 101A amplifier causes a similar change in resolution and range of the pulse heights covered by the analyzer. Channels 1-volt wide were used in making resolution studies of the counter and in determining the pulse heights of the standard source alphas, from time to time.

Linearity checks on the amplifier and pulse height analyzer were periodically made by members of the electronics group who maintained this equipment.

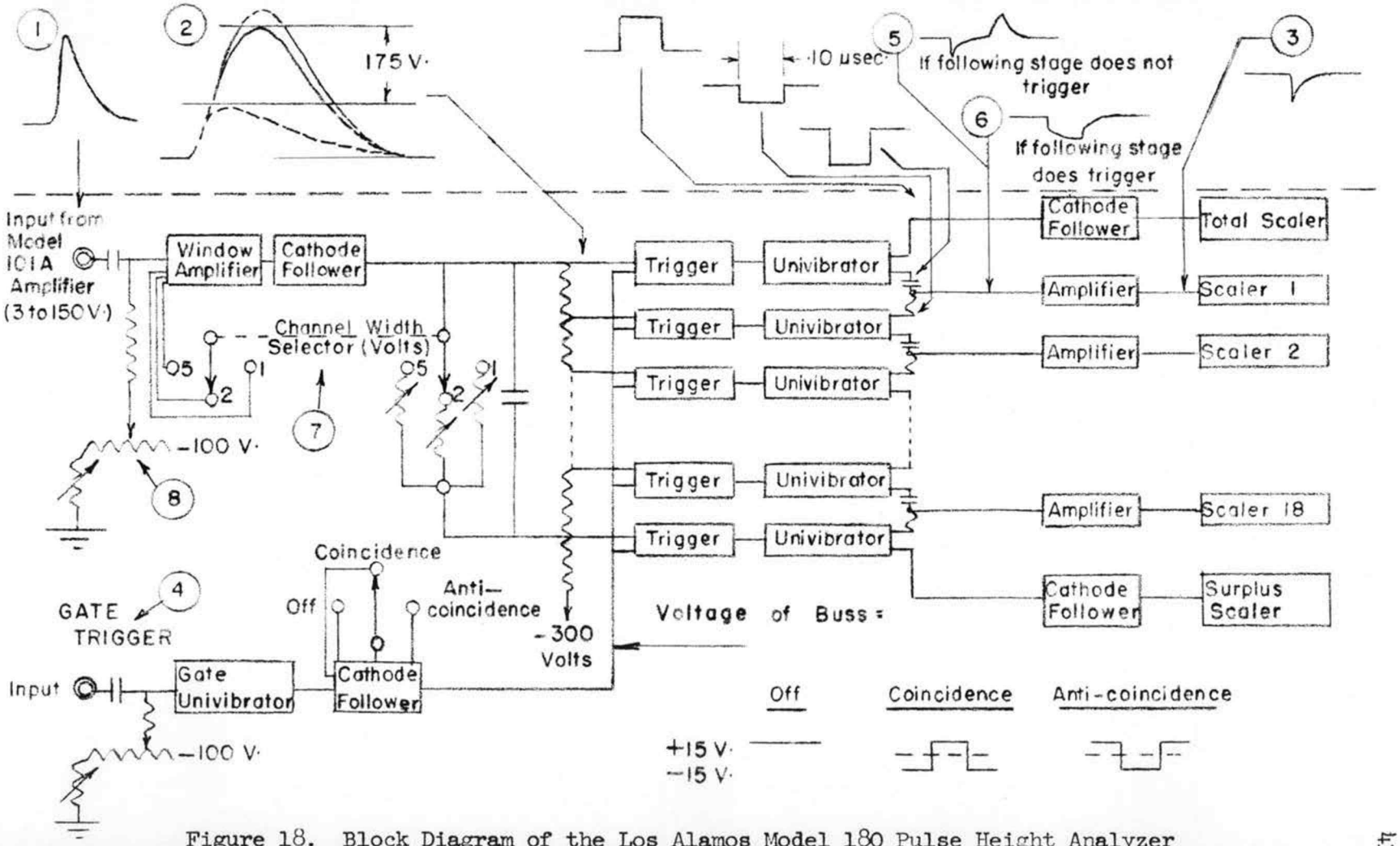

Figure 18. Block Diagram of the Los Alamos Model 180 Pulse Height Analyzer

IV. Description of the Evaporator and the Targets

When it was decided to use metallic lithium or lithium fluoride for targets, it was likewise decided that the target material should be evaporated upon some good-conducting light metal, such as aluminum. Evaporated targets can be made with a quite uniform target thickness and with a good knowledge of the target composition.

An evaporator, shown in Figure 19, was constructed which would permit evaporation of isotopic lithium--either as metal or as fluoride--with a minimum of waste of the isotope during the evaporation.

The container for the furnace and material to be evaporated is a brass cup (1) with inside dimensions 2 1/2 inches deep and 2 1/2 inches in diameter. This is connected to a short manifold (2), a liquid air trap (3) and a Princeton diffusion pump (4). A roughing-pump by-pass is included in the manifold, which also contains vacuum gauges (5) and a needle-valve (6) permitting one to let air or special gases into the system. The pump may be isolated from the manifold, etc., by a large valve (7). Two filament leads (8) enter the cup through large kovar seals. The wall of the cup is water cooled.

Into the open, upper end of the cup, the target-container is inserted and sealed with a radially-compressed "O"-ring (9). The container is built around a large gate valve which consists of an externally operated steel vane (10) that can be moved across an "O"-ring (11) to seal the aperture. The target blank (12) is supported in a short cylindrical section above this valve in such a way that its face

lies in a horizontal plane, is centered directly above the crucible (13) holding the evaporating material, and is separated from it by about 1 1/2 inches. A cylindrical envelope topped by a 1/2 inch glass plate (14) surrounds the target disk. Several holes (15) in the support for the inner cylinder provide for evacuation of the region surrounding the target blank. With this arrangement, the target disk may be sealed off after the evaporation and the target container may be removed easily from the evaporator.

The material to be evaporated (16) is held in a small crucible of tantalum which is supported in a central position below the top of the cup. This crucible is cylindrical with its mouth flaring out in a large cone. Having a wall thickness of 1/64 inch, the cylindrical section is 1/4 inch outside diameter and 1/2 inch long. The filament (17) serving to heat the crucible by electron bombardment is a single loop of tungsten, partly enclosed by a tantalum shield (18), which is supported in a horizontal plane so that it surrounds the crucible near the middle of its cylindrical section.

Operation of the evaporator is as follows:

1. Target blank cleaned with alcohol and placed in container
2. Material to be evaporated placed in crucible which is in position
3. Target container set in place and enclosed volume evacuated to a pressure of $\sim 2 \times 10^{-5}$ millimeters of mercury

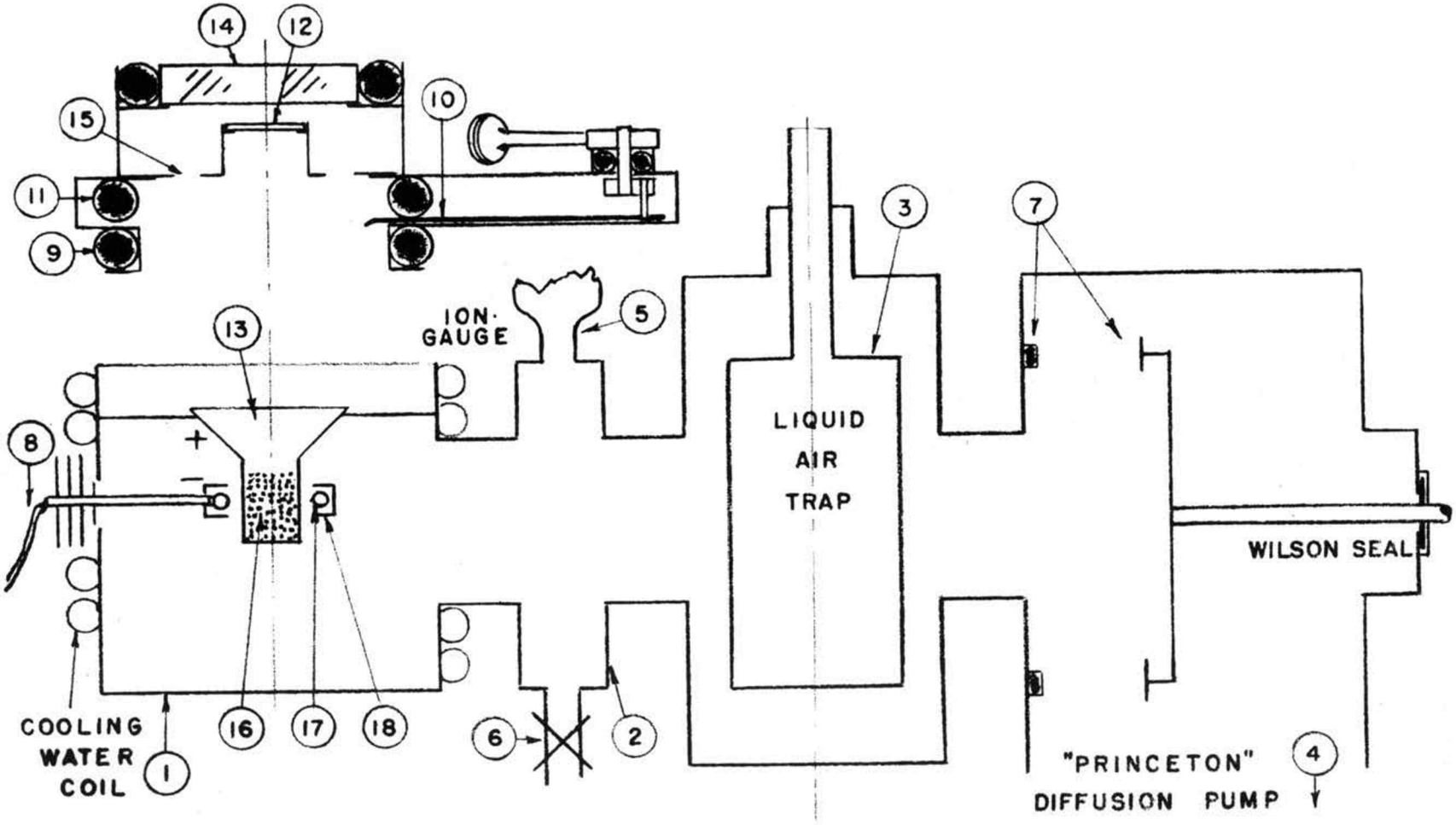

Figure 19. Diagram of the Evaporator

4. Filament heated with a current ~20 amperes at 6 volts
5. Crucible heated by making filament negative to it by ~ 1200 volts (current flow between filament and crucible is ~40 milliamperes at 1200 volts)
6. Desired extent of evaporation is determined by observing deposits upon glass plate of material passing through holes in the target support
7. High voltage and filament current are turned off and target container sealed by closing its valve
8. Diffusion pump valve is closed and air is let into the evaporator
9. Target container is removed from evaporator and placed in a dry box through which helium gas flows continuously
10. Target is removed from container, placed in holder described in connection with the target chamber and is sealed off in the helium atmosphere--ready to be used in the target chamber

Making targets is a process varying in length from about 30 to 90 minutes. Targets which were made in this way are:

1. Normal lithium metal (92.61% Li^7, 7.39% Li^6), (28, p.588)
2. Lithium-7 metal (99.90 $\pm$ 0.01% Li^7)
3. Lithium-7 fluoride (99.6% Li^7F)

4. Lithium-6 fluoride (94.3% Li^6F)
5. Calcium-fluoride (normal CaF_2).

All of these targets were made on aluminum disks 1/2 inch in diameter and 0.030 inch thick. In addition, one "transparent" target of normal lithium metal was made upon an aluminum foil 0.0002 inch thick which had been cemented with Gelva over the 3/16 inch hole in a copper washer.

Other targets which were found useful during the experiment were made of the following:

1. CuO layer on a copper disk
2. a piece of fused quartz
3. dehydrated deposits on aluminum disks of
   a. concentrated NaOH
   b. NH_4NO_3
   c. KNO_3
   d. sodium azide, NaN_3
   e. a mixture of guanidine, $NH{:}C(NH_2)_2$, and NaN_3
   f. thiourea, NH_2CSNH_2
4. ZrN_3 layer on a zirconium disk
5. normal lithium metal.

EXPERIMENTAL PROCEDURE

I. Triton Bombardment - Angles of Observation

When the equipment for the Li + T charged-particle study was in readiness, the target chamber was attached to the target tube of the accelerator. A proton beam was produced and used to align the target and chamber. This was done visually by centering the beam spot on the quartz back plate of the Faraday cage. Small additional adjustments were made to maximize the beam current measured in the cage. The counter was located on the 90° port and a normal lithium metal target was placed in the proton beam, at an angle of 45° to it. For several days, measurements were made of the $Li^{7}(p,\alpha)\alpha$ reaction at 90° for protons having energies from 0.60 to 2.27 Mev. During this period, various counter pressures and voltages were tried and the counter gas purifier was added. Also, different clippers in the amplifier were used to determine the effect of change of decay time upon the pulses entering the pulse height analyzer.

Suitable adjustments and modifications having been made, a beam of tritons was produced with the accelerator. The normal lithium metal target was used for preliminary observations. After making several runs at triton energies between 1 and 2 Mev, the "transparent" lithium metal target was placed in the beam. While it was bombarded, beam currents measured were observed to be much smaller than for the solid target. This appears to have resulted from scattering of too large a fraction of the beam which diverged as it passed through the

target. The current measured by the Faraday cage was thus only a small percent of the beam striking the target. Since modifications in the design of the target electron-barrier and of the Faraday cage were indicated, it was decided to continue with solid targets for the present experiment.

The metallic lithium-7 target was placed in the triton beam and sets of data were taken at triton energy increments of 0.103 Mev from 0.620 to 2.272 Mev with the counter at 90°. Occasionally, a plutonium alpha source was put into the target position with the beam off to provide a pulse height calibration point (plutonium decays by emitting 5.14 Mev alpha particles).

To make a survey of the alpha particles from $Li^7 + T$ at one angle and one triton energy required at least three settings of the analyzer bias. Because of the time required for a complete set of data to be obtained at one angle, the study was limited to two angles, 90° and 165°.

The counter was relocated on the port at 165° and the target was turned normal to the resulting half-angle between beam and counter, $7\ 1/2^{\circ}$ from normal to the beam. An analysis of the alpha groups observed at 165° for a bombarding energy of $\sim$1.7 Mev showed that some contaminant was present in the target. Three alpha groups were indicated by peaks located in the upper half of the pulse heights measured. The outermost of these corresponds to alphas having energies of about 6.5 Mev.

The reaction producing alphas of highest energy from $Li^7 + T$

is $Li^7(T,\alpha)He^6$. At the angle and triton energy mentioned, this alpha should have an energy of about 4.6 Mev. While the data taken at 90° showed the same three alpha groups, only a discrepancy in the energy scale was suspected, until the sets of data taken at 165° were used to check the positions of the peaks. Of the three peaks, the central one was found to agree with the energy of the alpha from Li^7 + T, at both angles. Similarly the lowest energy peak, of those well resolved, corresponds at both angles to one produced by the alpha in the above reaction, when He^6 remains in an excited state about 2 Mev above the ground state. This had been observed by others (23, p.316).

The presence of oxygen or nitrogen contamination of the lithium-7 metal target was suspected, since lithium readily forms Li_3N and Li_2O. To determine this, targets containing oxygen and nitrogen were used. (These have been described in the preceding section.) At higher triton energies, most of these targets gave significant peaks which would coincide with the higher and lower-energy peaks mentioned as coming from Li^7 + T.

An attempt was made to produce a target layer of lithium-7 metal which would have virtually no chance to form the oxide or nitride. This target, likewise gave the same peaks as before, although the higher-energy peak was comparably smaller than was observed when the first lithium-7 metal target was used.

It seemed that further precautions would be necessary to produce metallic lithium targets which were free from contaminants. Hence, the decision was made to use targets made of lithium fluoride for

taking all the data. The fluoride of lithium can be handled in the air with little fear of producing oxides or nitrides. To provide information permitting one to subtract from the data any contributions resulting from F^{19} + T reactions, a CaF_2 target was made as well as Li^7F and Li^6F targets. In discussing the results, it will be pointed out that the probable fluorine content of these three targets is almost identical.

Employing the same energies as indicated before, complete sets of data were obtained at both 165° and 90° for triton bombardment of Li^7F, Li^6F, CaF_2, and CuO targets. Making runs of the order of 100 microcoulombs of tritons with 1/2 microampere of beam current, the data for four targets could be obtained at one triton energy and one angle in about two hours. This required about 15 bias settings on the analyzer, since alphas from Li^6F, CaF_2 and CuO have enough energy to make necessary a fourth bias setting when any one of these three targets is being bombarded.

II. Determination of Absolute Cross Sections

Experimental measurements of nuclear interactions are usually of more value when the differential cross sections can be obtained than when only relative yields can be determined. To permit one to calculate cross sections, one must be able to make measurements which provide the following information: (a) number of bombarding particles per unit time, (b) number of target nuclei, and (c) the combined geometry and efficiency of the detector (permitting one to know the number of reactions which take place per unit time, per unit solid angle).

The differential cross section, $\sigma_{(\theta)}$, is defined as the effective area in square centimeters per unit solid angle per target nucleus. It is given by the relation

$$\sigma_{(\theta)} = N_r/N_b\, N_t,$$

where N_r is the number of reactions observed per unit time per unit solid angle, N_b is the number of bombarding particles per unit time, and N_t is the number of target nuclei per square centimeter.

In the procedure which has been described, the number of accelerated particles per unit time is given by the current integrator. The geometry of the counter has been measured and its efficiency is assumed to be 100% for alpha particles with energies between $\sim$2 and 13 Mev and for deuterons and protons with energies between $\sim$1 and 4 Mev. There are often two or more methods which can be applied to determine the number of target nuclei. If the uniformity of the target layer is known to be good, one may weigh it and measure its area. If

the density of the element is known, the number of target atoms of the element per square centimeter may be calculated directly. A second method is based upon measurements of emitted particles when the target is bombarded. If a calibrated detector is used and the cross sections for the emitted particles are known, the absolute yield from the target may be measured and the number of target atoms which this indicates may be calculated from the expression defining $\sigma_{(\theta)}$. A variation of this method is to obtain a measure of the energy lost by the incident particles in giving a maximum yield from reactions which are known to have very sharp resonances and abrupt thresholds.

The targets which were used contain very thin layers of Li^7F, Li^6F and CaF_2. It was believed that the most accurate way of determining the number of target atoms in these thin targets is by one or both variations of the second method mentioned. The $Li^7(p,n)Be^7$ reaction has a very abrupt threshold, when observed at 0°, which occurs at 1.882 Mev bombarding energy (10, p.308). As the proton energy is increased from just below the threshold, the neutron yield passes through a high value at the threshold, drops to a minimum at about 2 Mev then rises to a maximum in a resonance at about 2.3 Mev. The high neutron yield occurring at the threshold results from a geometrical effect.

As the threshold for the reaction is reached, the neutrons which are emitted from the compound nucleus, Be^8, have the velocity of the center-of-mass and are emitted in the forward (0°) direction. As the bombarding energy is increased, the additional energy supplied by the protons appears in the reaction products so that the neutrons

may have velocity components in directions other than forward. While the actual cross section for the reaction is increasing modestly with increasing proton energy, the neutron detector intercepts nearly all of the neutrons emitted at the threshold, then intercepts fewer of them as the cone within which the neutrons emerge widens out with increasing bombarding energy.

One may utilize the threshold of this reaction to indicate the energy loss for protons, with $\sim$ 2 Mev energy, in passing through a layer of Li^7. If the layer is extremely thin, one would expect lithium atoms throughout the target depth to interact with the incident protons at the threshold bombarding energy. This would be detected as an abrupt increase in yield at the threshold which would drop off with a small increase of bombarding energy. Similarly, if the target depth is such as to dissipate, say, 50 Kev of the incident proton energy before the deepest layer of nuclei are bombarded with protons of threshold energy, one would expect the threshold yield to increase more gradually with proton energy and reach a maximum at a bombarding energy $\sim$50 Kev above the threshold.

The number of Li^7 atoms per square centimeter in the Li^7F target was obtained by the two variations of the second method just described. Accurate weighings of the target were not obtained.

Protons were produced by the accelerator and observations were made of the $Li^7(p,n)Be^7$ reaction. The Li^7F target was placed at 45° to the proton beam so that the proportional counter, located at 90°, could be used concurrently to observe the $Li^7(p,\alpha)\alpha$

reaction. The neutron yield at 0° was measured for proton energies ranging from 1.869 to 2.127 Mev. Throughout the proton bombardment, the neutron detector, a long counter (11, p.673-677), was located about 1 1/2 meters from the target at 0°.

The curve indicating data obtained for the $Li^7(p,n)Be^7$ reaction is presented in Figure 20. The Li^7F target indicates an effective thickness of $\sim$ 70 Kev for 2 Mev protons. The actual calculations which are used to obtain a value for the number of Li^7 atoms per square centimeter from this curve are shown in APPENDIX IIIC. The apparent number of Li^7 atoms in the Li^7F target (placed at 45° to the beam) determined to $\pm$ 12% by this method is 1.21×10^{19} atoms/cm^2.

An alternate determination of this number can be made from the threshold curve and a measurement of the counter geometry-efficiency factor. If one makes the reasonably good assumption that the long counter is equally sensitive to neutrons produced by a RaBe source and those arising from the $Li^7(p,n)Be^7$ reaction, the geometry-efficiency factor can be obtained. To do this, a RaBe source whose flux is known to $\pm$ 5% is placed in the target chamber where the target had been located. The number of counts per unit time which this source produces in the long counter is recorded. With this information, one obtains a value for the counts per emitted neutron. The 0° differential cross section for $Li^7(p,n)Be^7$ has been reported as 2.5×10^{-26} cm^2, $\pm$ 12%, at a proton energy of 2 Mev (29, p.380). The method of determining the number of target atoms from these values is shown in APPENDIX IIIC. The value obtained for the apparent number of target atoms

(target at 45°) is 1.4×10^{19} atoms/cm^2, $\pm$ 15%.

The number which was used in cross section calculations is an average of the two values obtained. It is 1.31×10^{19} atoms/cm^2, with an error of $\pm$ 14%, for the target at 45° to the beam.

The method of obtaining the number of Li^6 atoms in the Li^6F target and the number of F^{19} atoms in the CaF_2 target is described in the section following RESULTS and illustrated in APPENDIX IIIC. The differential cross sections for reactions resulting from triton bombardment of each of these targets are given to $\pm$ 15% by the product of number of counts per microcoulomb and the following corresponding factor:

	90°	165°
Li^6 --	2.71×10^{-29} cm^2/steradian	3.80×10^{-29} cm^2/steradian
Li^7 --	2.78 " " "	3.92 " " "
$(CaF_2)F^{19}$ --	2.62 " " "	3.68 " " "

RESULTS

I. Li^7 + T Yields

Curves shown in Figures 22 through 29 depict the data obtained from Li^7 + T. The charged particle yield is plotted for counts per microcoulomb as a function of pulse height. The pulse height scale, originally recorded as pulse height analyzer volts, has been converted to indicate particle energy loss in the counter, in Mev. A linear scale has been assumed in making this conversion. Actually, particles indicating less than $\sim$1.5 Mev in the counter have distorted energy values. The actual energies lost by these particles is $\sim$5 to 30% less than is indicated. No energy distortion was detected for pulses greater than 1.5 Mev.

The abscissa scale is not constant in these figures while that for the ordinate values is. The latter may be interpreted as differential cross section having units of cm^2/steradian by obtaining the product of counts per microcoulomb and the corresponding factors indicated in the preceding section. Particle energy values outside and inside the counter are related by curves included in APPENDIX I.

Detailed curves of data obtained at 90° and at 165° are shown for only three bombarding energies. Small scale curves of all data are indicated to show trends with changing triton energy. In the detailed curves, statistical errors are indicated by vertical lines. Absolute and relative errors in energy are estimated to be less than 0.150 Mev and 0.050 Mev, respectively.

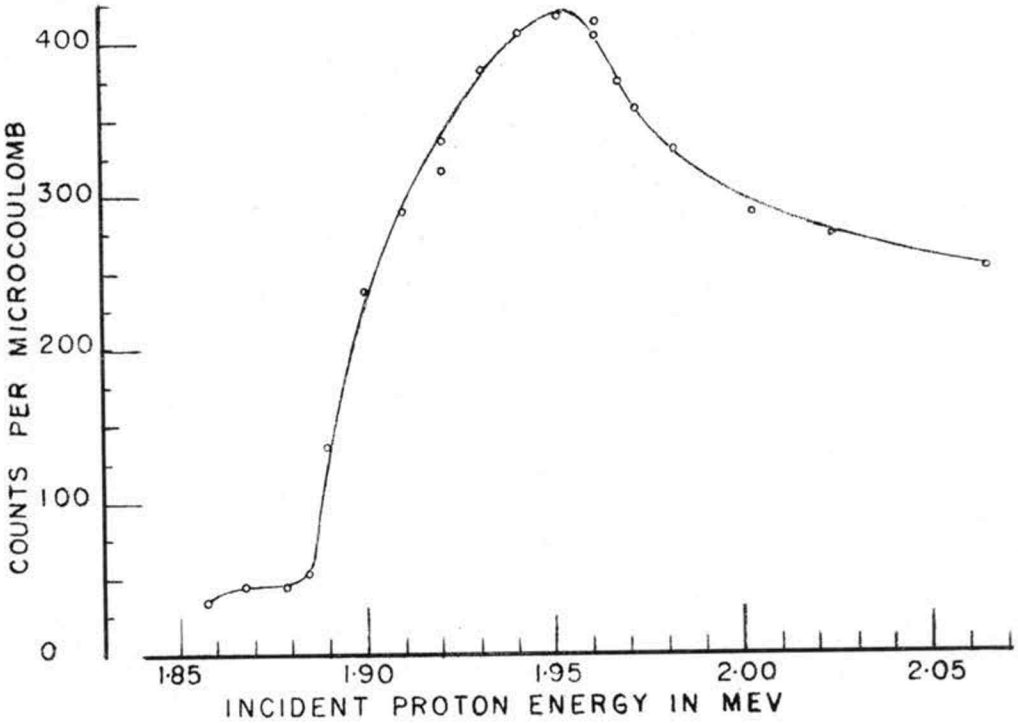

Figure 20. Yield Near Threshold of the $Li^7(p,n)Be^7$ Reaction

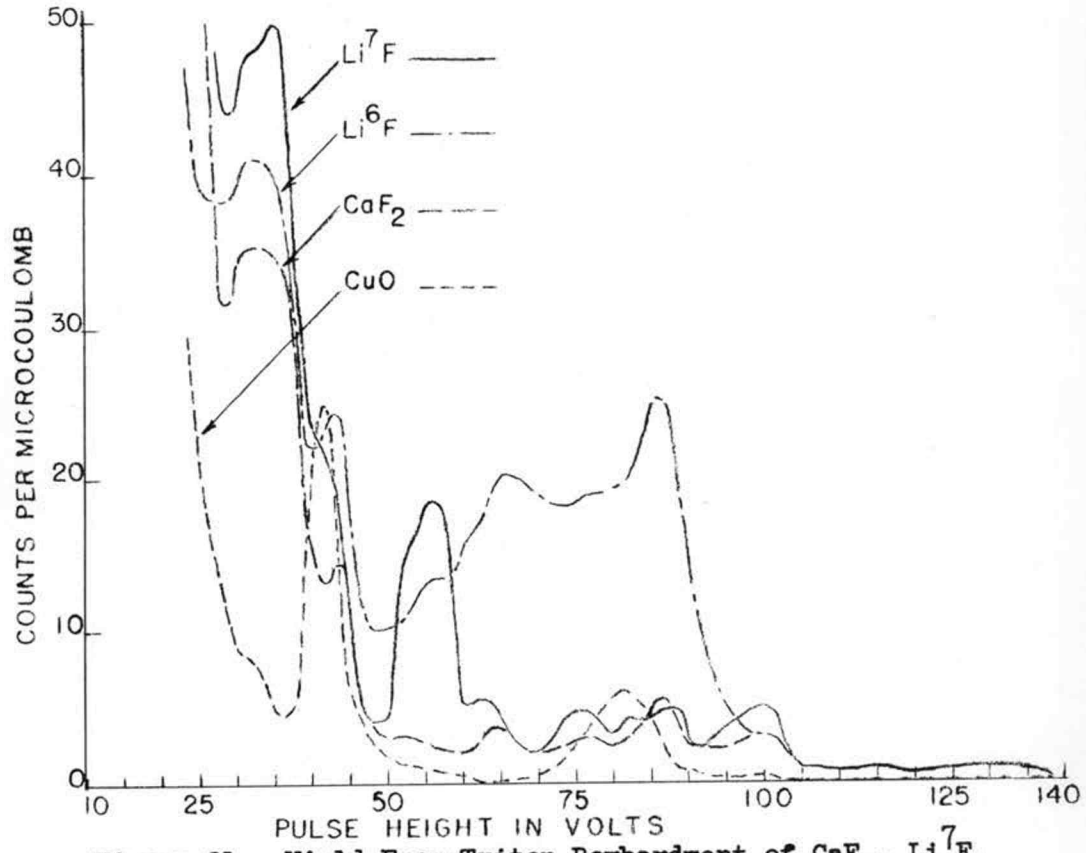

Figure 21. Yield From Triton Bombardment of CaF_2, Li^7F, Li^6F, and CuO at 165°, for E_t = 2.065 MeV

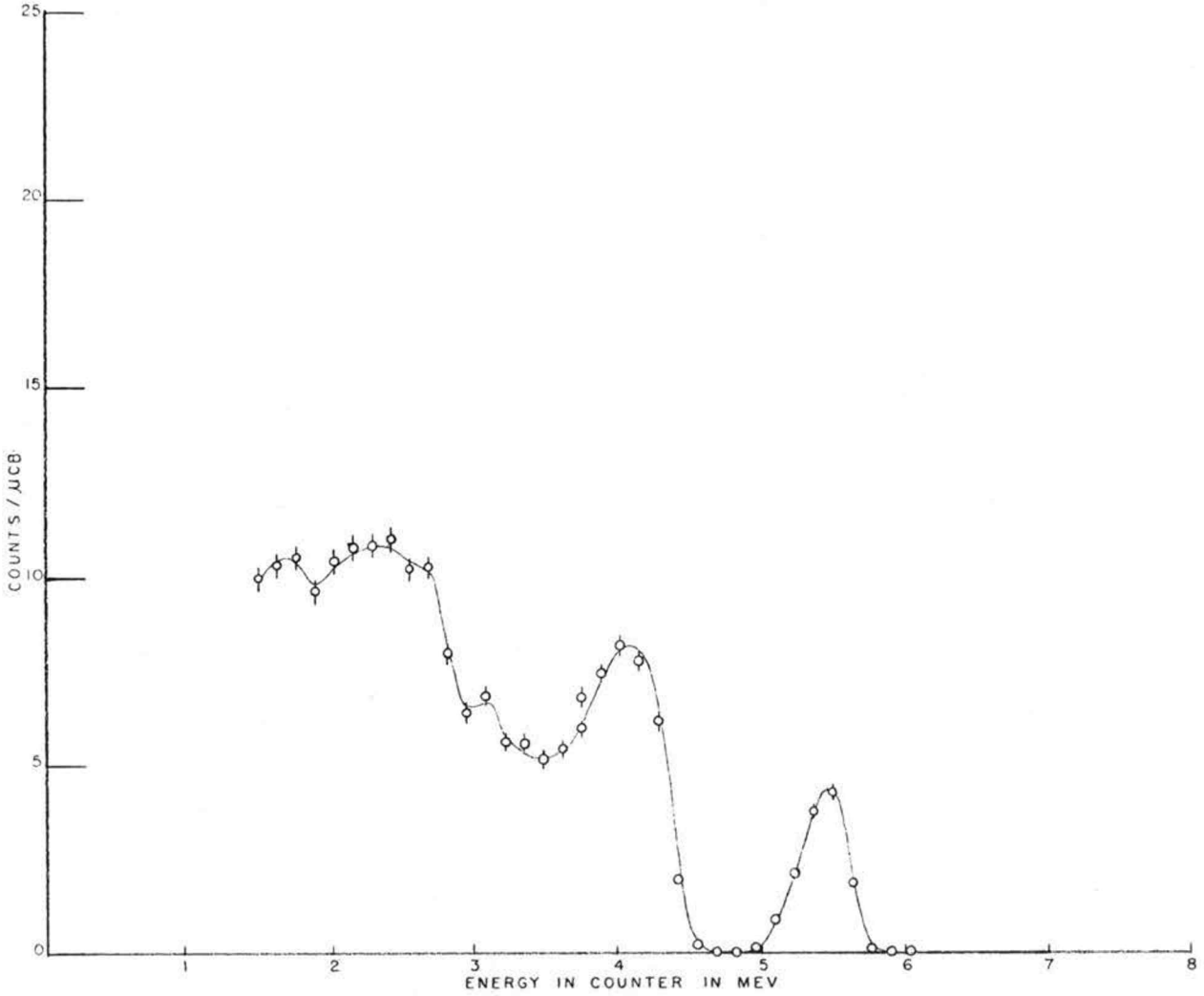

Figure 22. Yield From Li^7 + T, 90°, E_t = 0.620 Mev

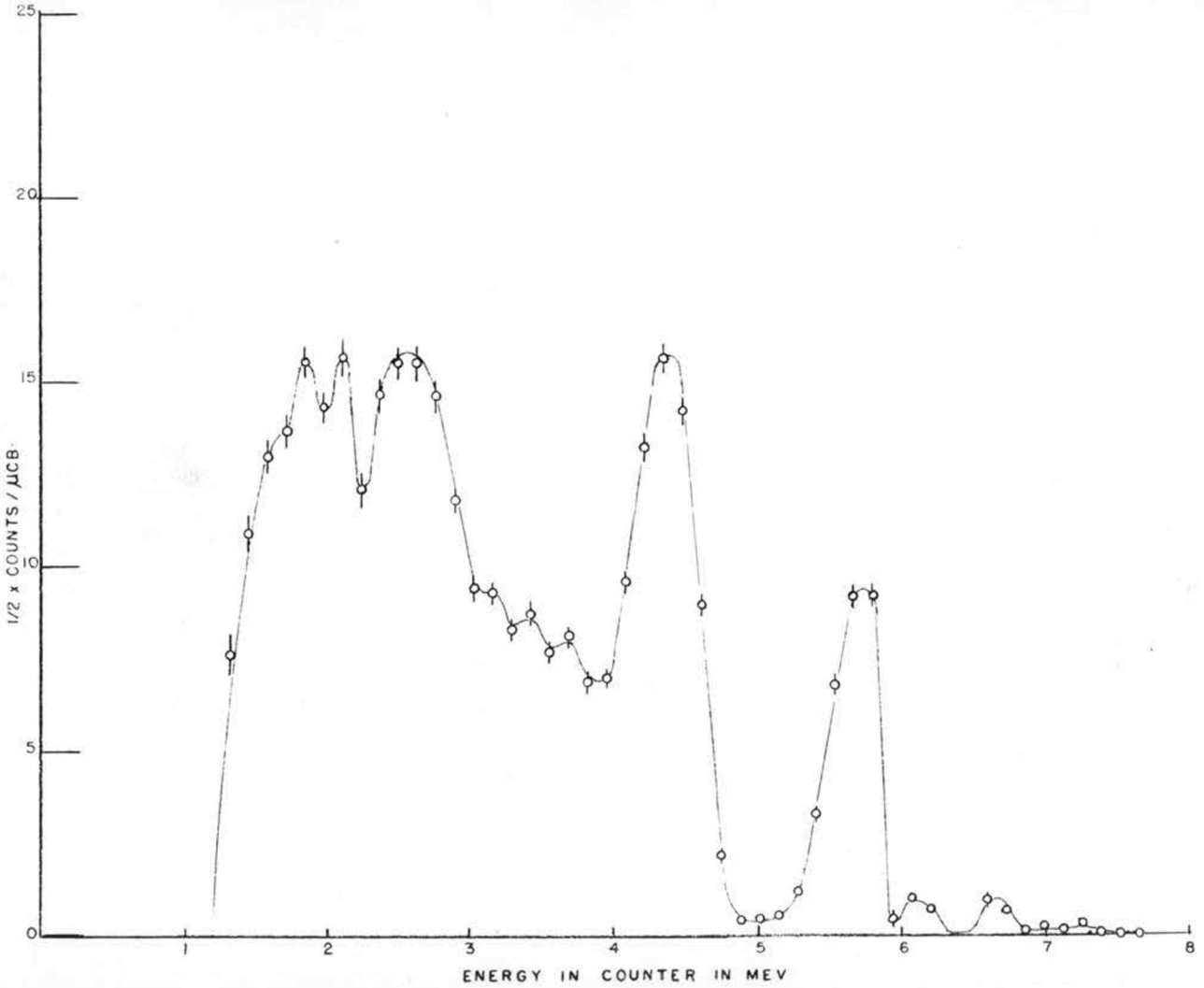

Figure 23. Yield From Li^7 + T, 90°, E_t = 1.446 Mev

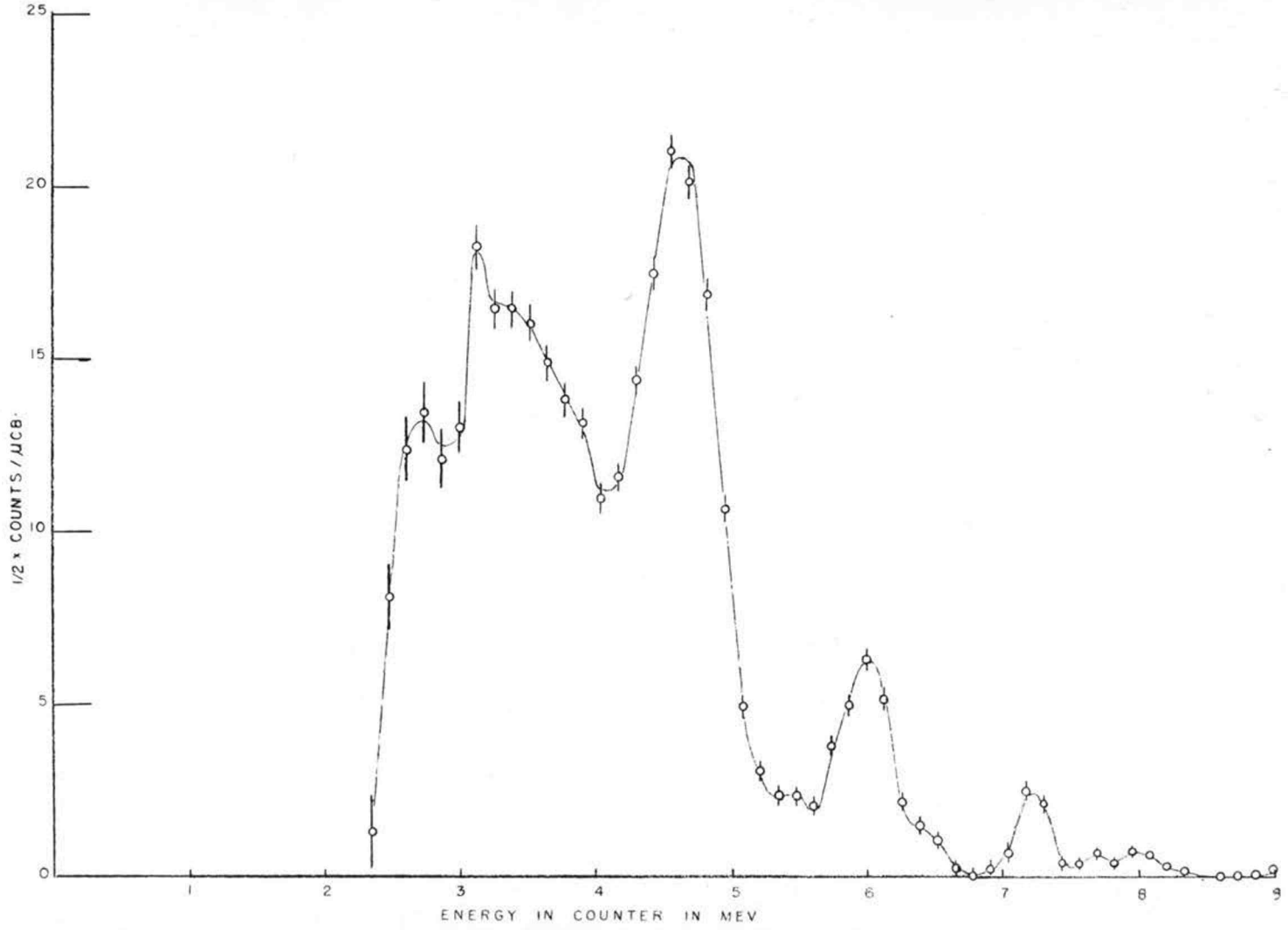

Figure 24. Yield From Li^7 + T, 90°, E_t = 2.272 Mev

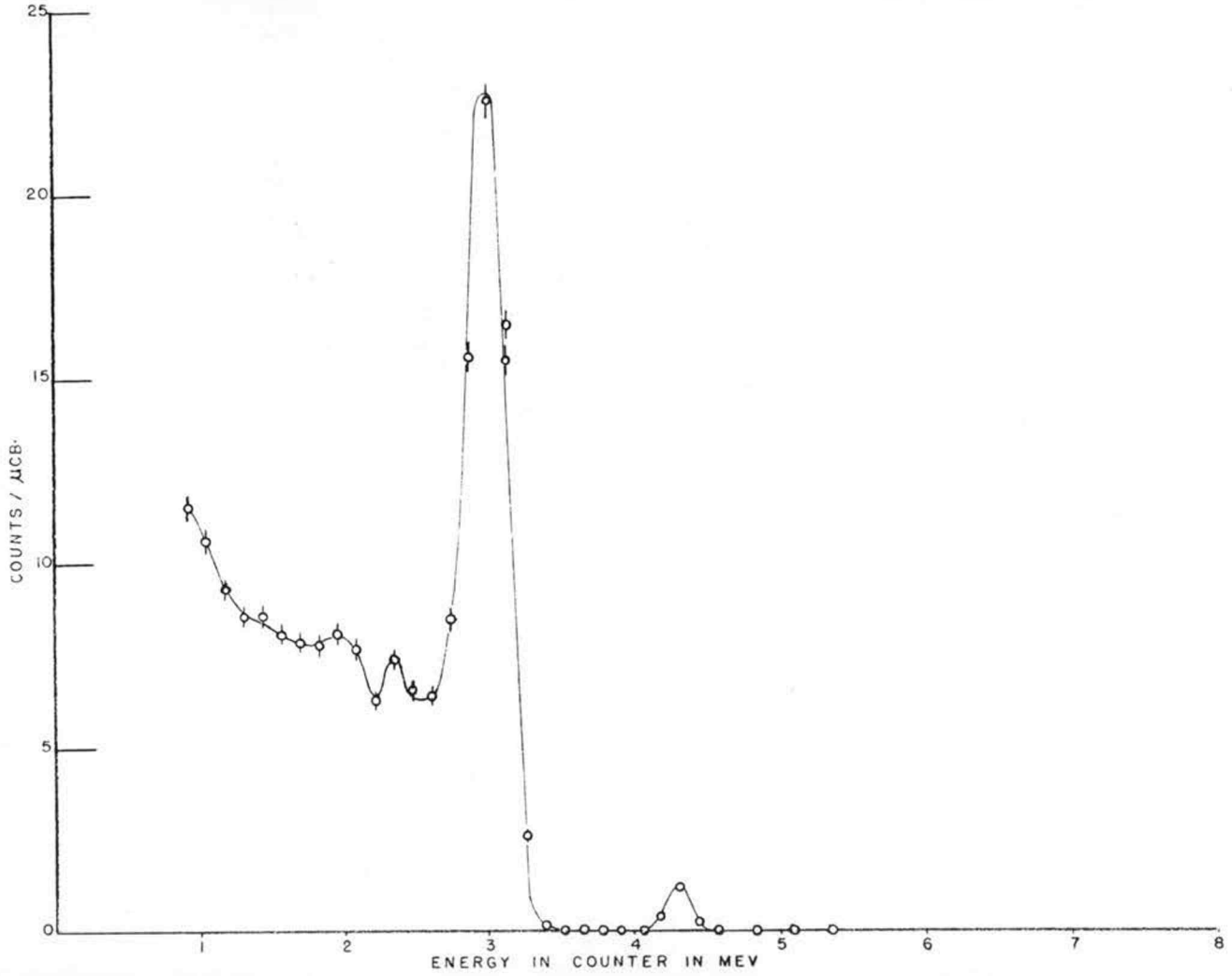

Figure 25. Yield From Li^7 + T, 165°, E_t = 0.620 Mev

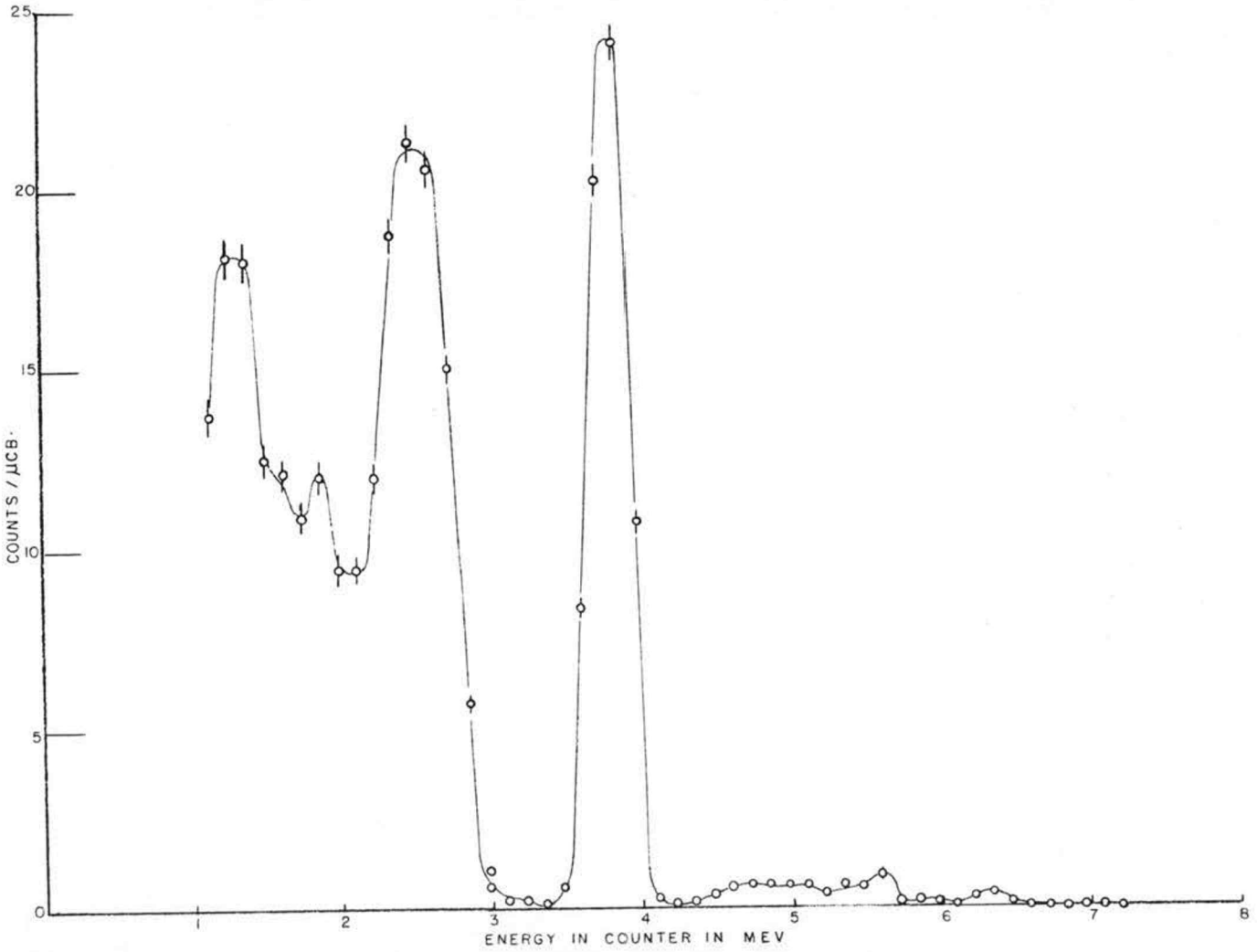

Figure 26. Yield From Li^7 + T, 165°, E_t = 1.446 Mev

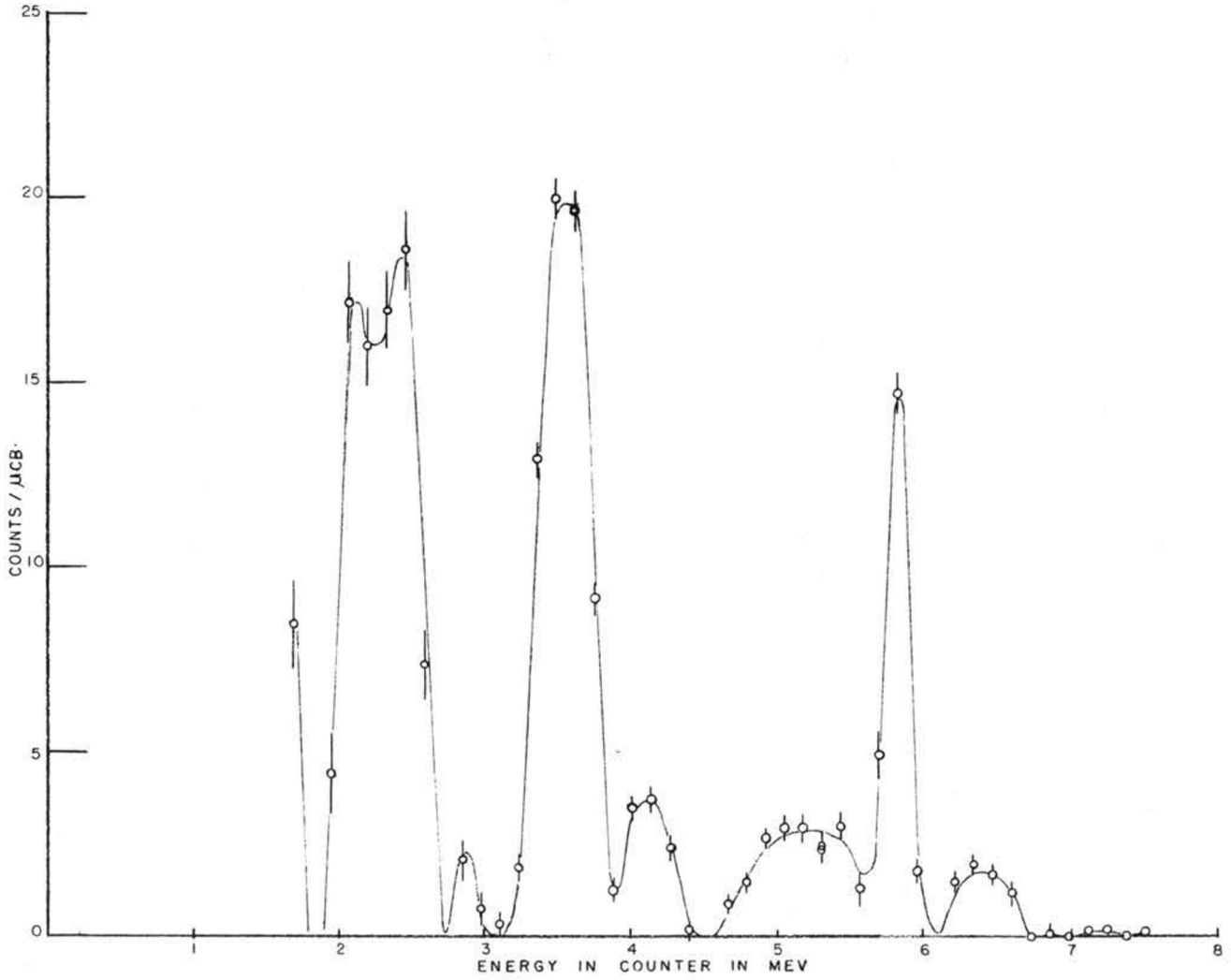

Figure 27. Yield From Li^7 + T, 165°, E_t = 2.272 Mev

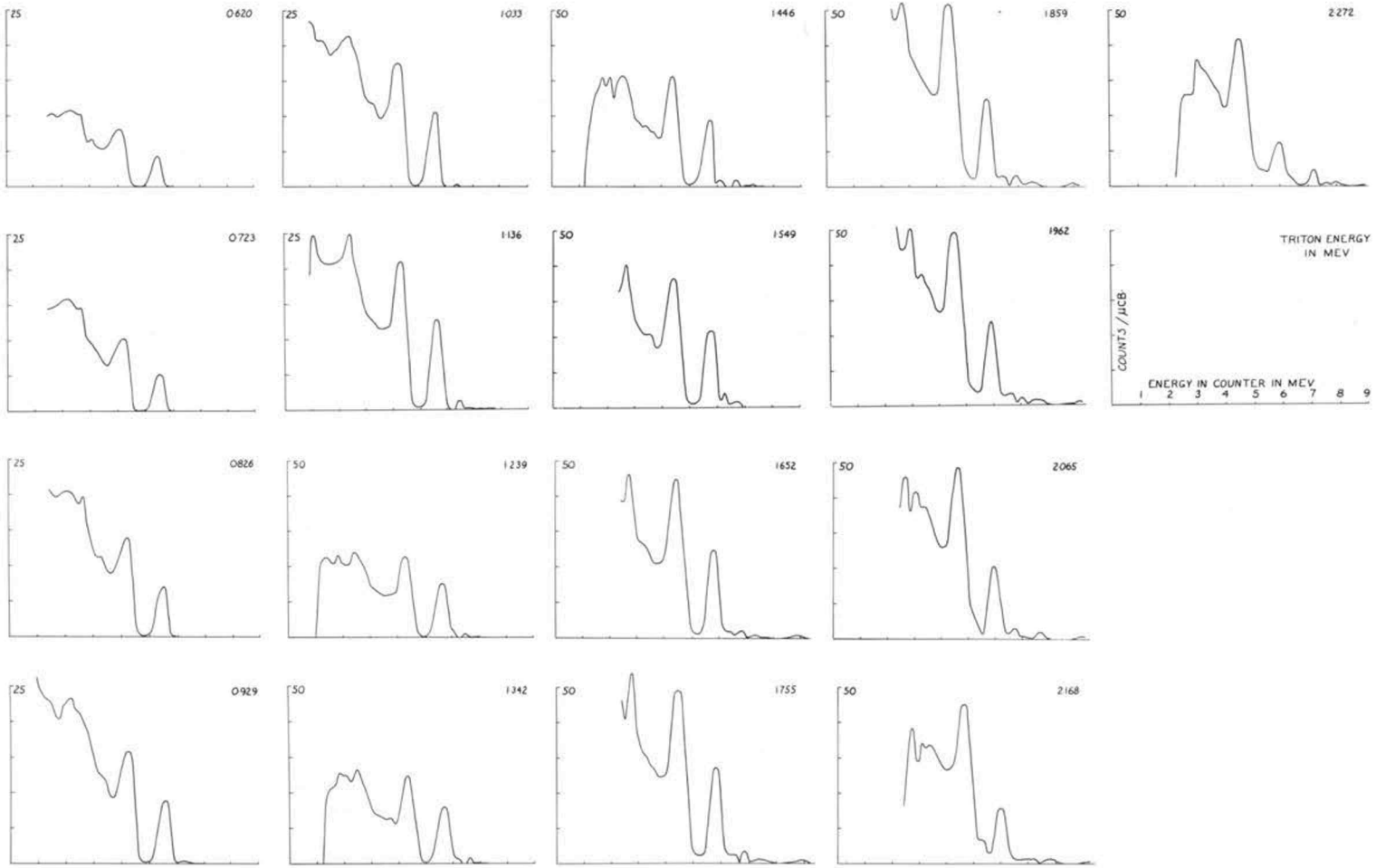

Figure 28. All Data Obtained at 90° From Li^7 + T

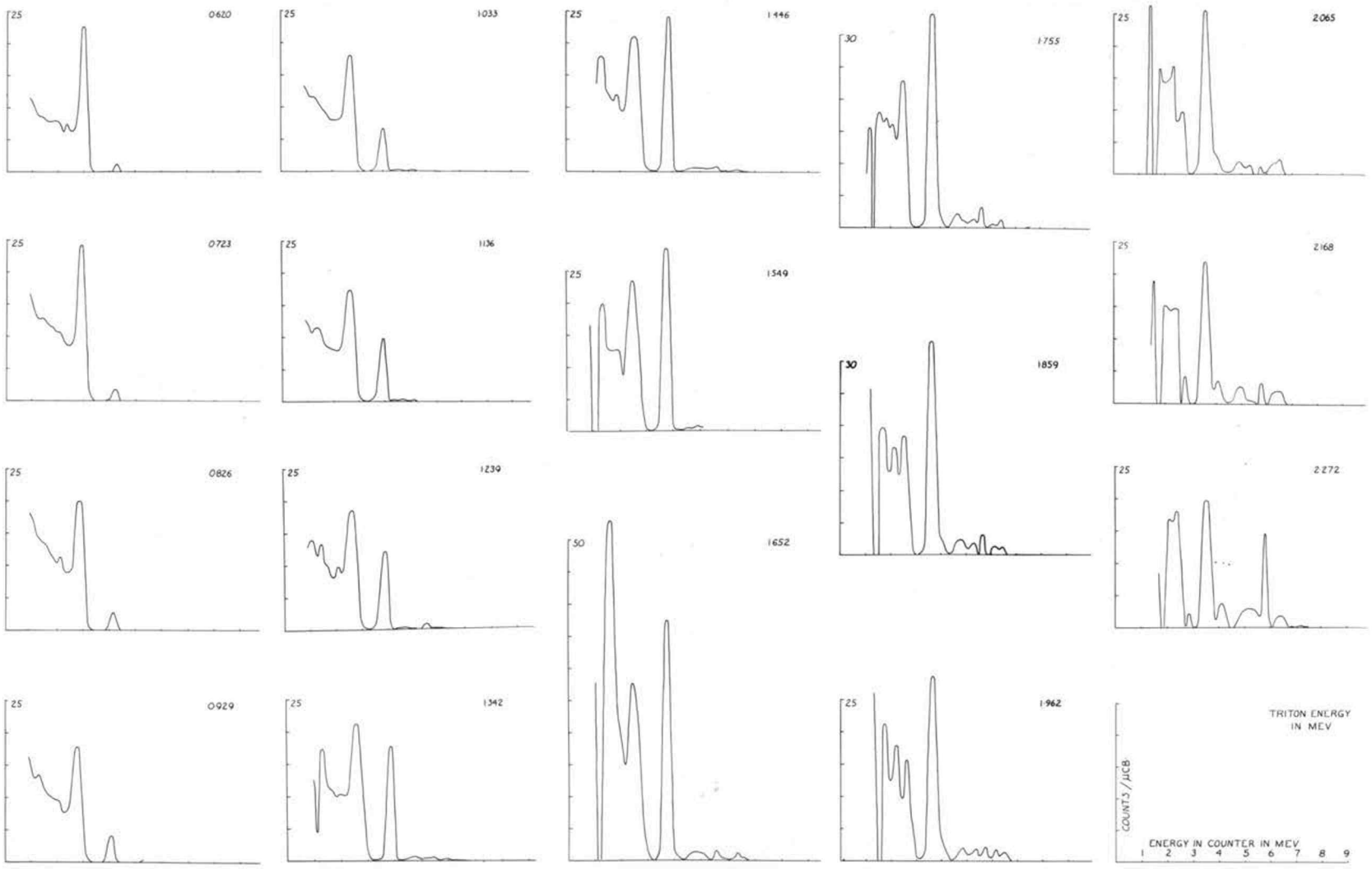

Figure 29. All Data Obtained at 165° From Li^7 + T

II. Li^6 + T Yields

Charged particle measurements of the reactions produced by Li^6 + T were used in plotting the curves shown in Figures 30 through 38. These figures have the same properties as those just described for Li^7 + T. Figure 38 contains the information that was obtained in observing the $Li^6(t,d)Li^7$ reaction at 90° and low bombarding energies.

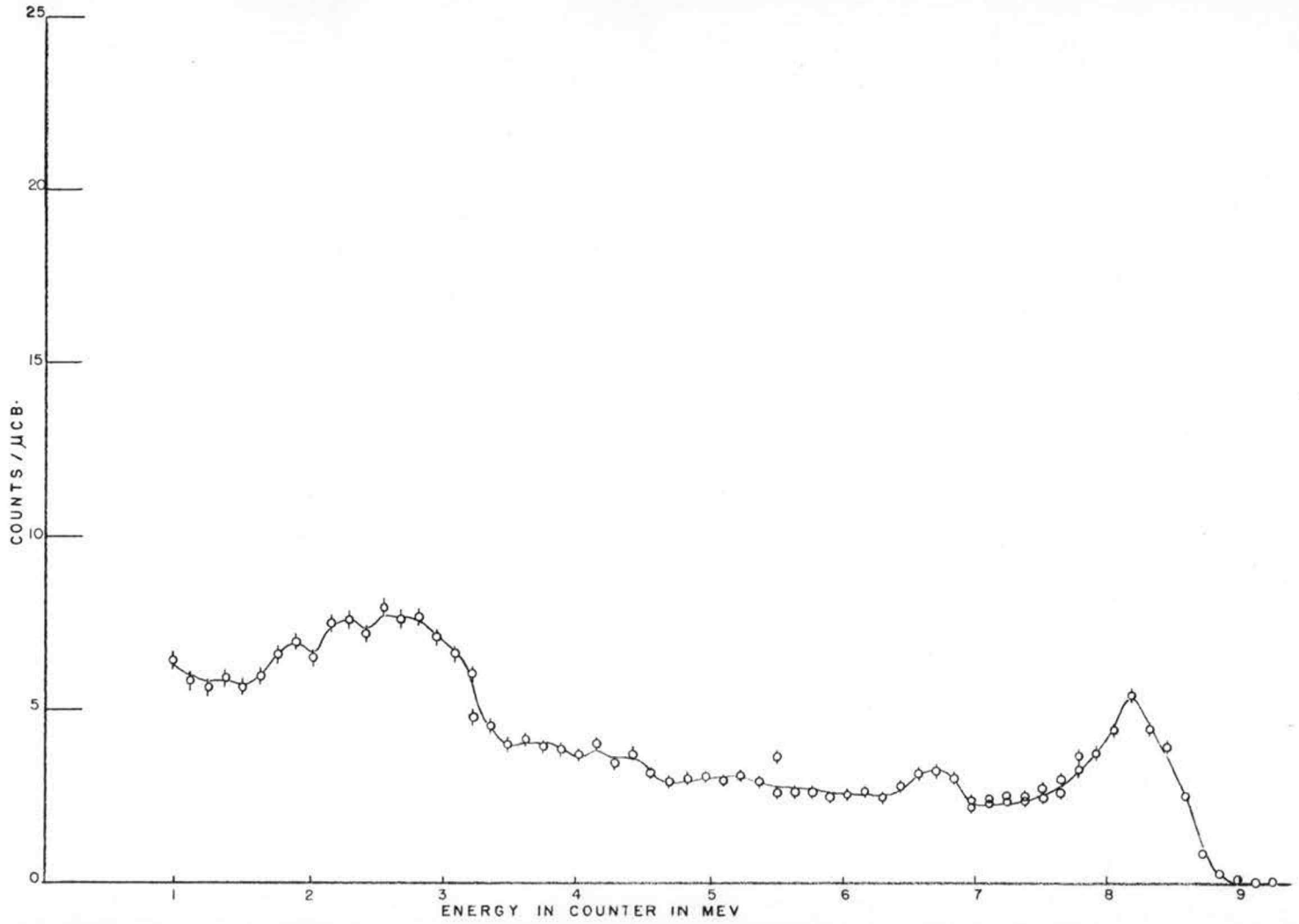

Figure 30. Yield From Li^6 + T, 90°, E_t = 0.620 Mev

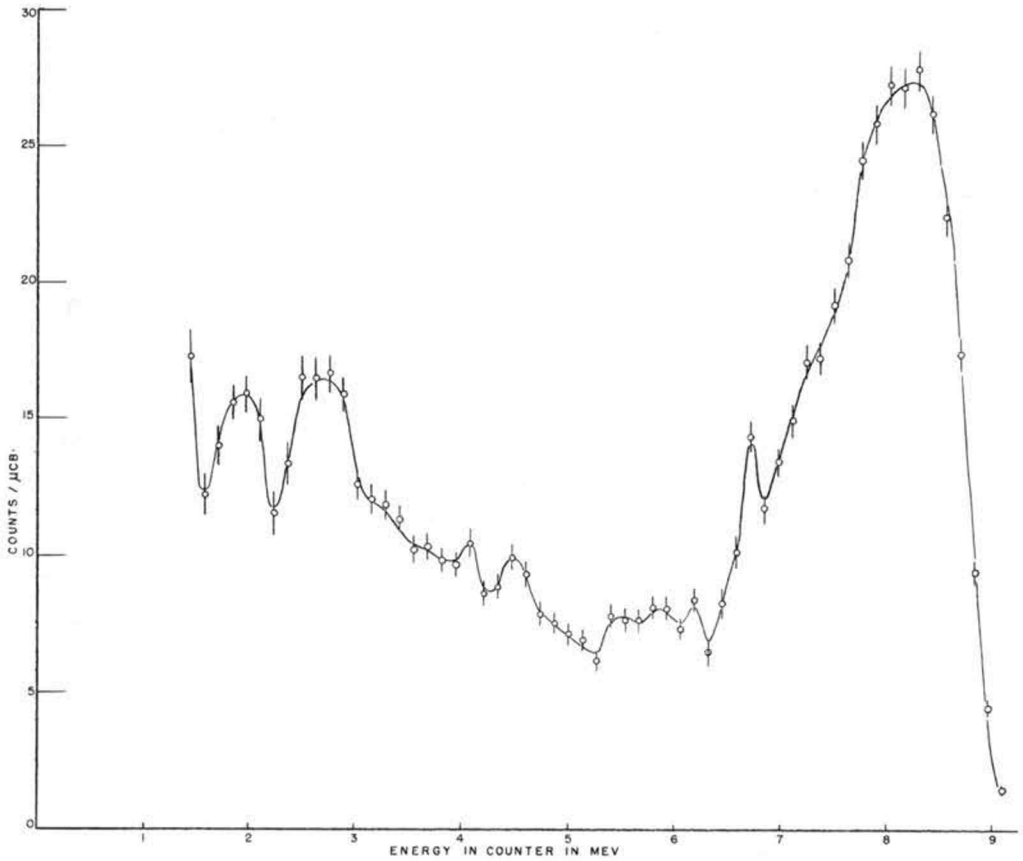

Figure 31. Yield From Li^6 + T, 90°, E_t = 1.446 Mev

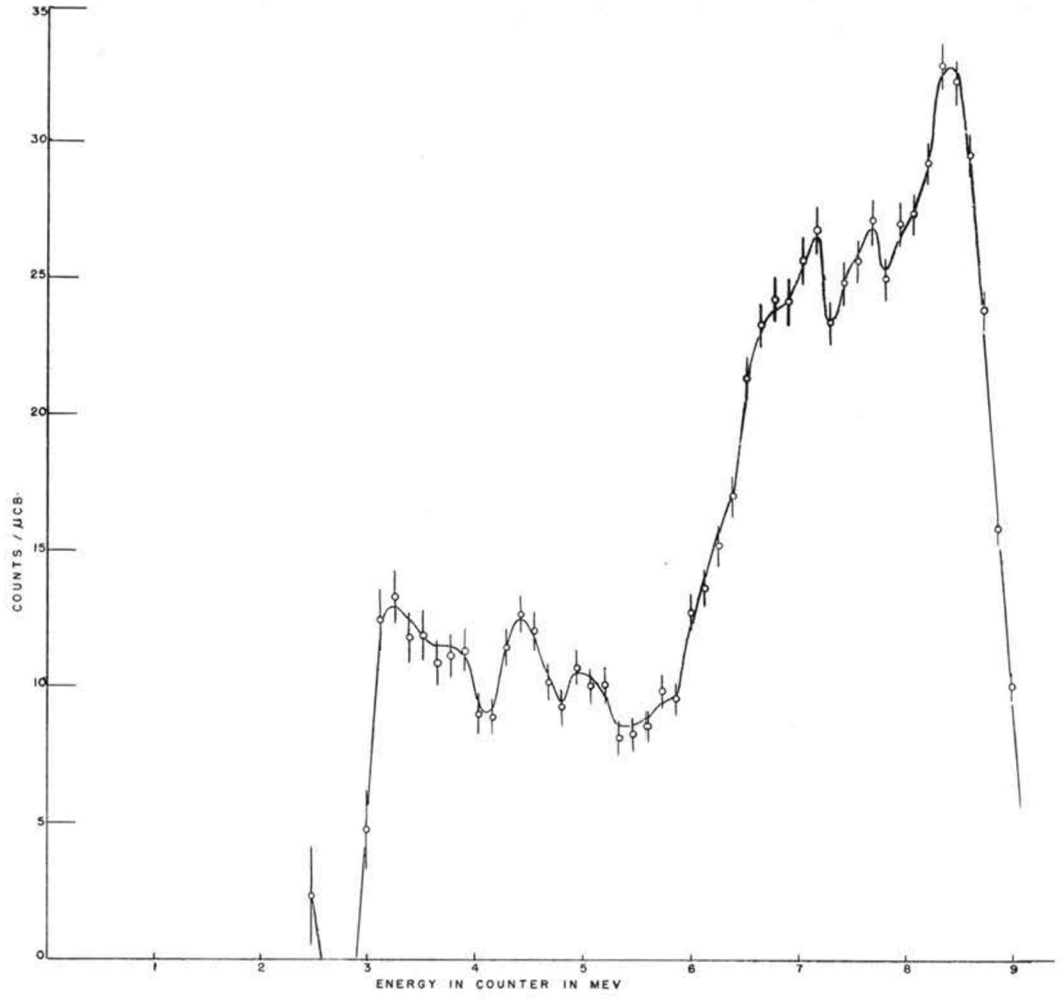

Figure 32. Yield From Li^6 + T, 90°, E_t = 2.272 Mev

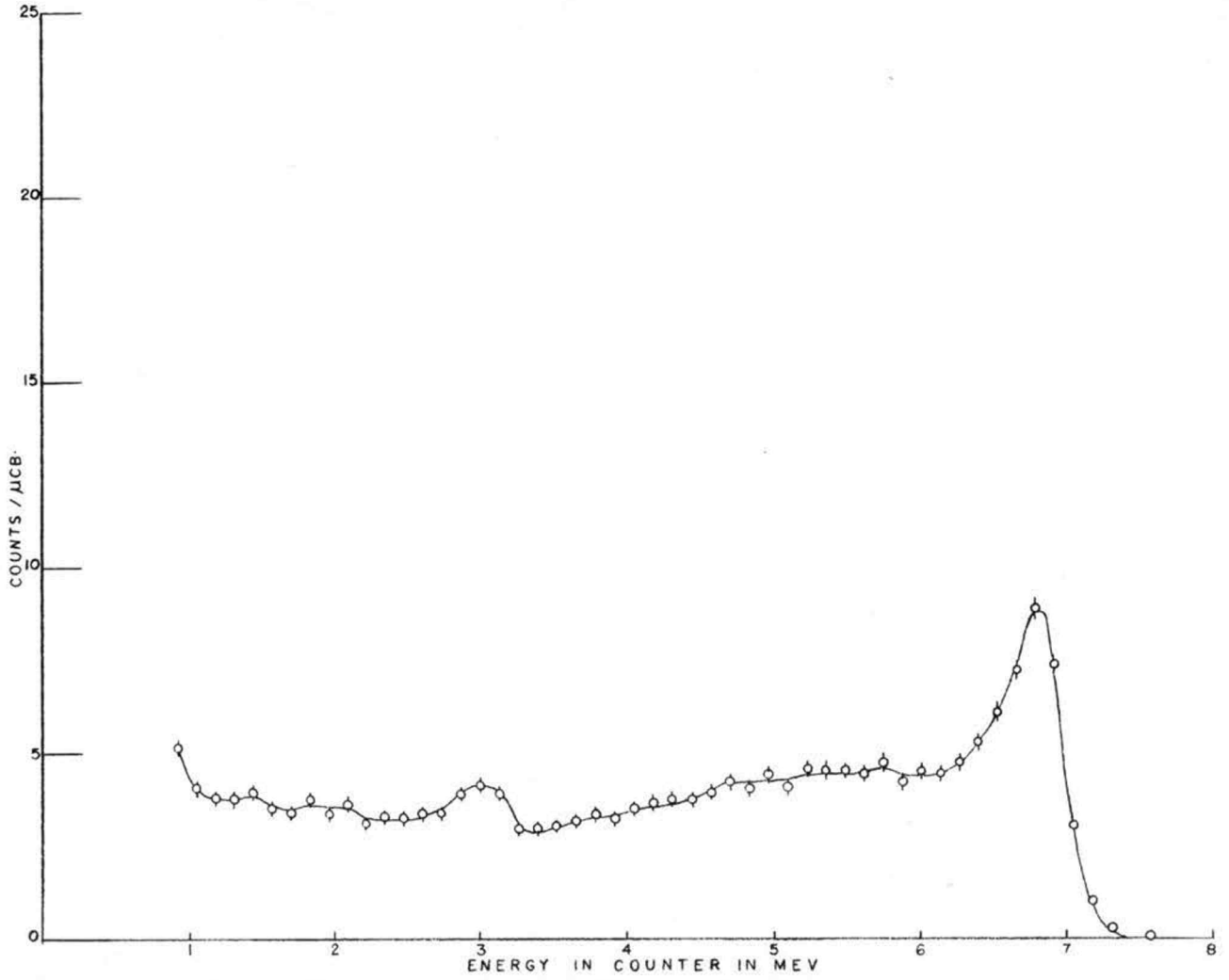

Figure 33. Yield From Li^6 + T, 165°, E_t = 0.620 Mev

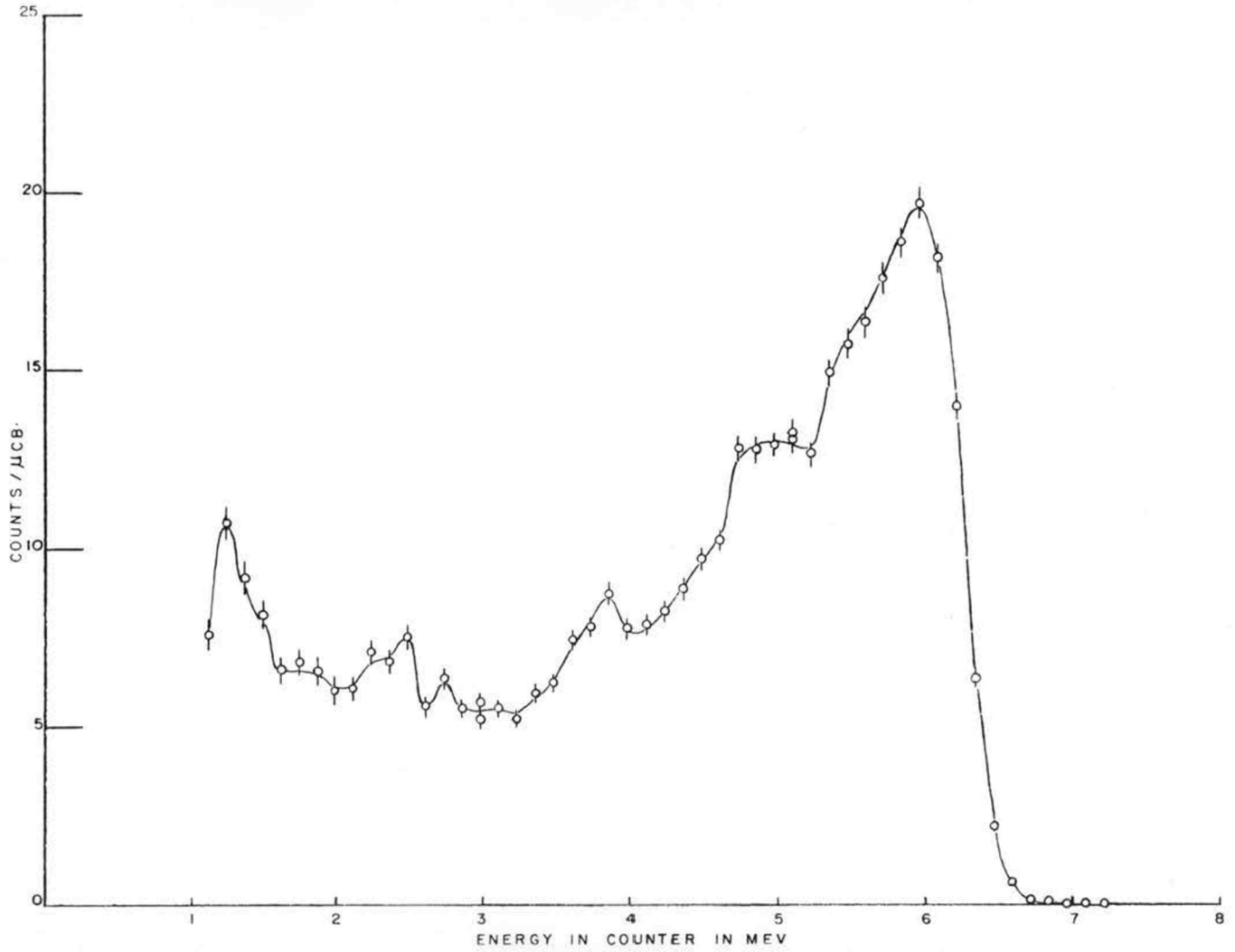

Figure 34. Yield From Li^6 + T, 165°, E_t = 1.446 Mev

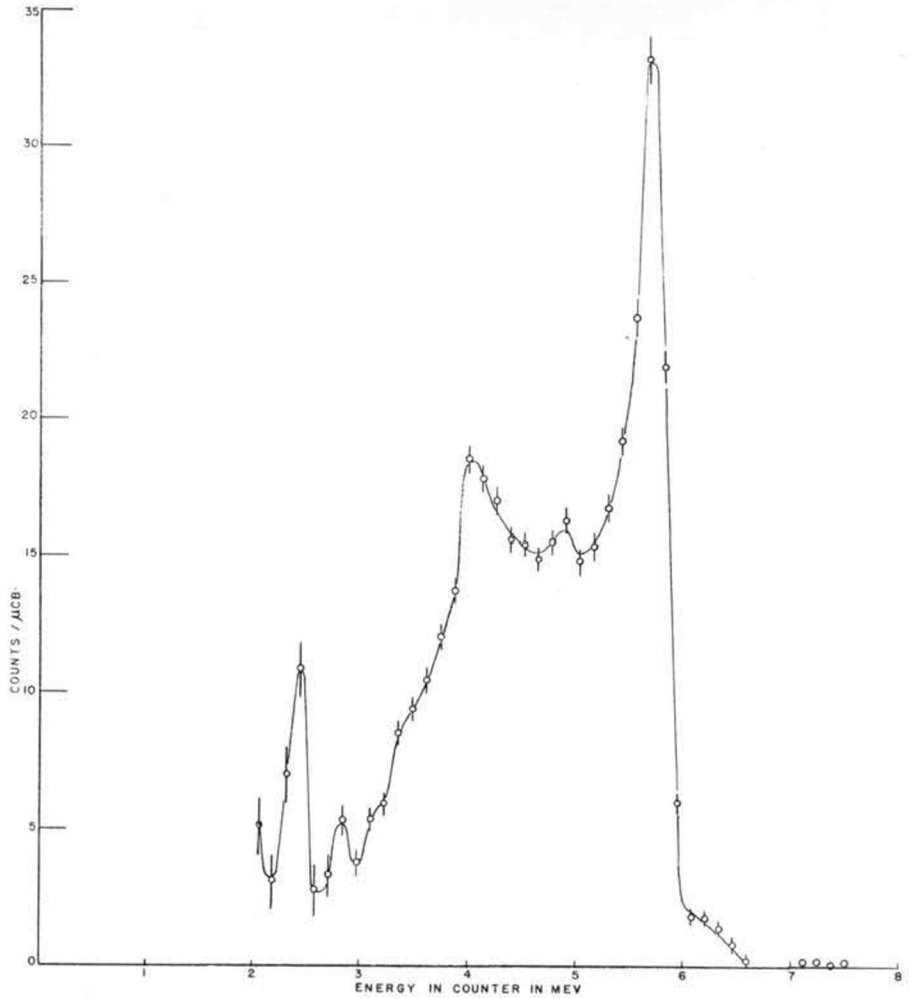

Figure 35. Yield From Li^6 + T, 165°, E_t = 2.272 Mev

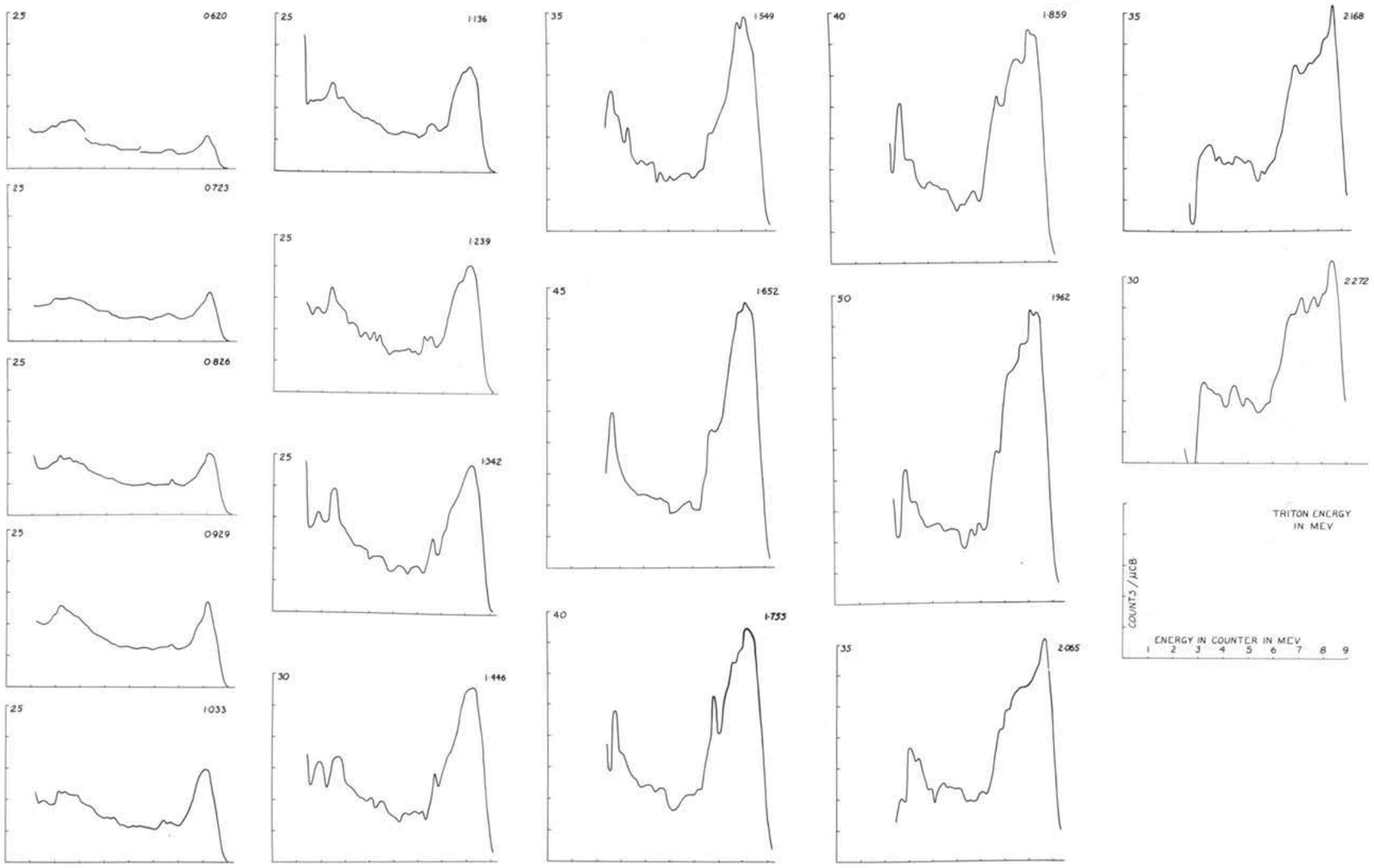

Figure 36. All Data Obtained at 90° From Li^6 + T

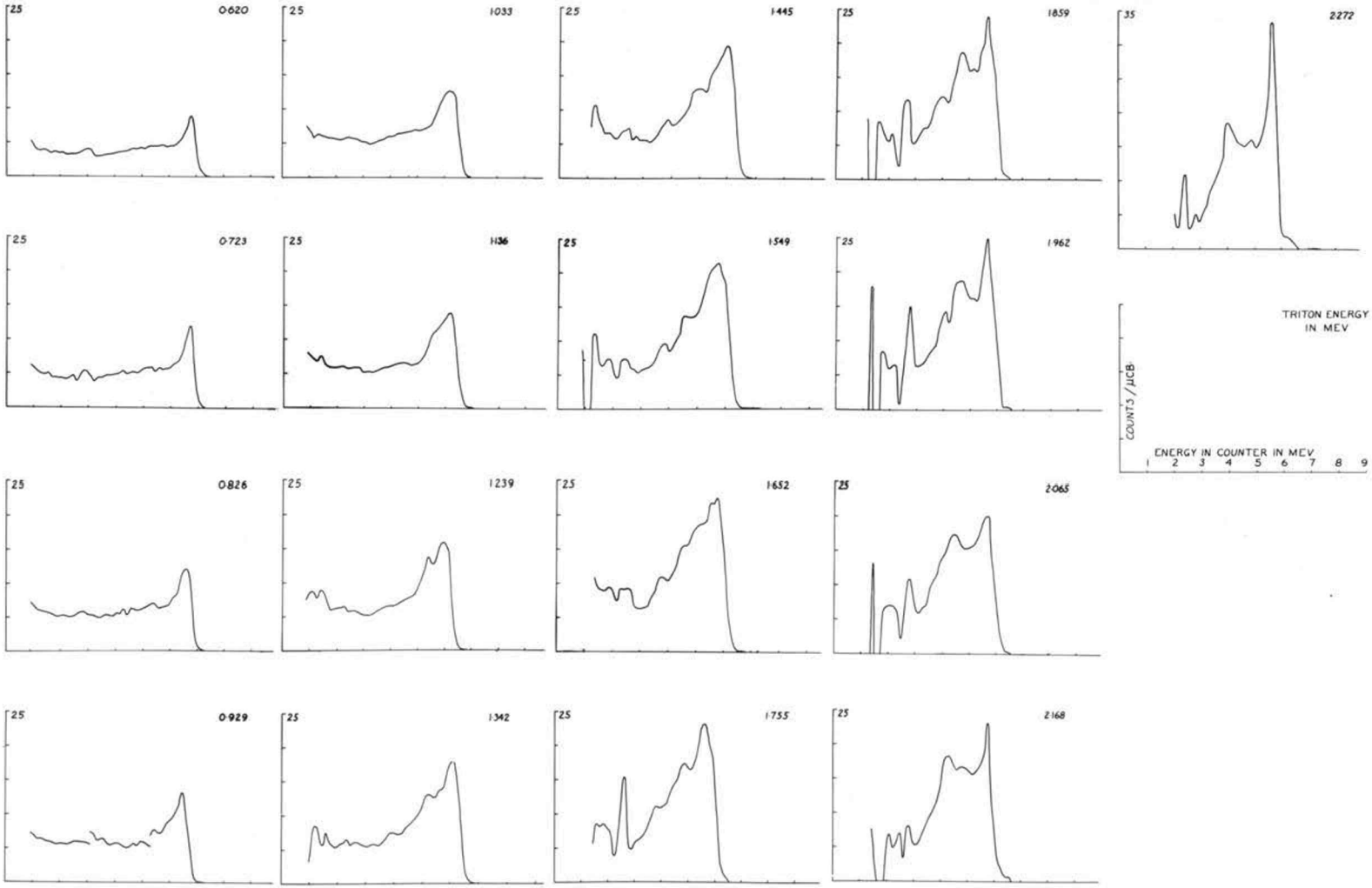

Figure 37. All Data Obtained at 165° From Li^6 + T

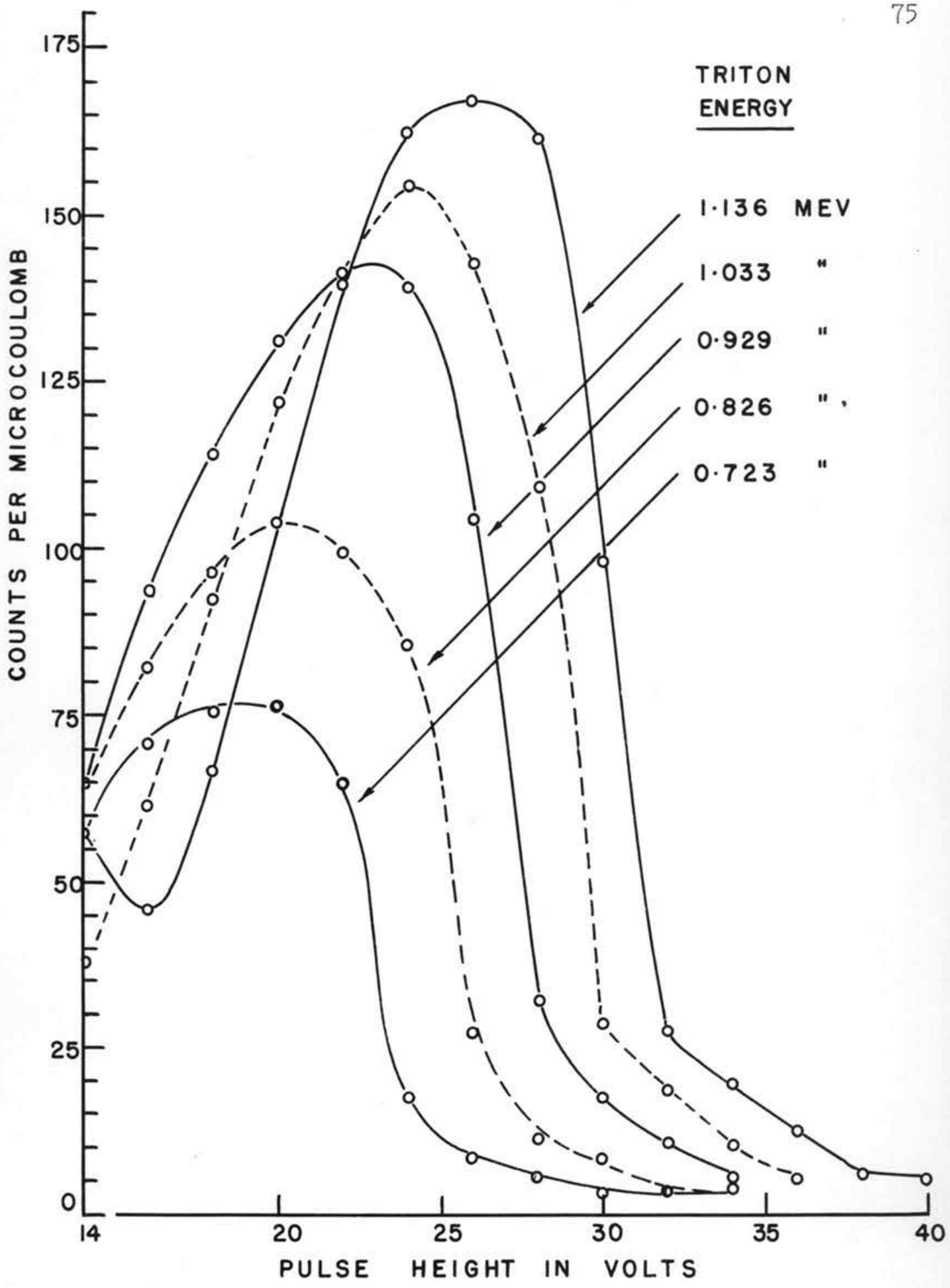

Figure 38. Yield From $Li^6(t,d)Li^7$ at 90°

III. T + N,O, and F Yields

The curves shown in Figures 39 through 46, which follow, are taken from raw data obtained from triton bombardment of the targets indicated. Except for that obtained from the CaF_2 target, the data was not extensive and much of it was taken at only one bombarding energy and one angle.

Errors in the energy values indicated are the same as was stated for Li^7 + T data. Statistical errors are shown, also.

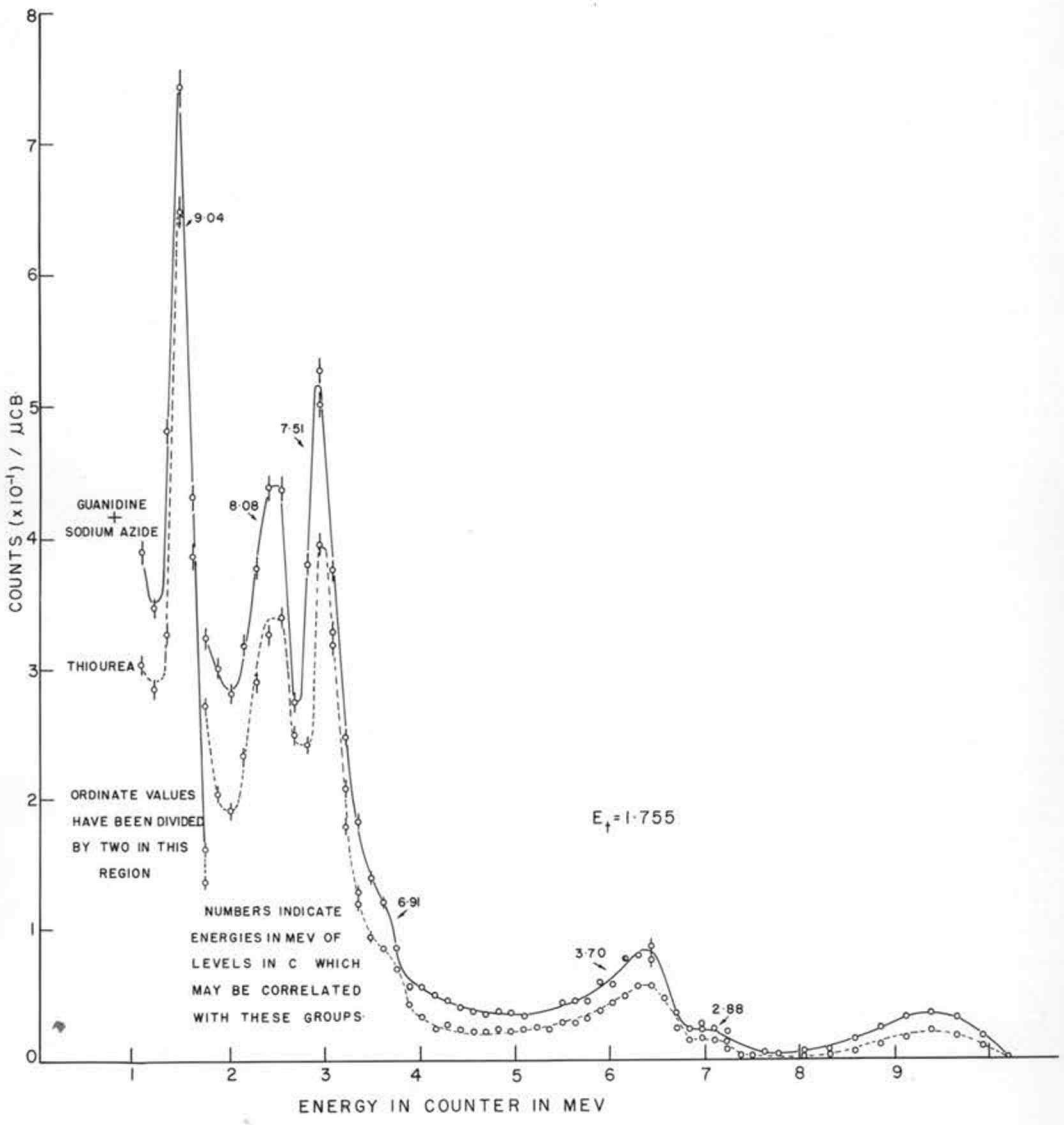

Figure 39. Yield From N + T at 165°

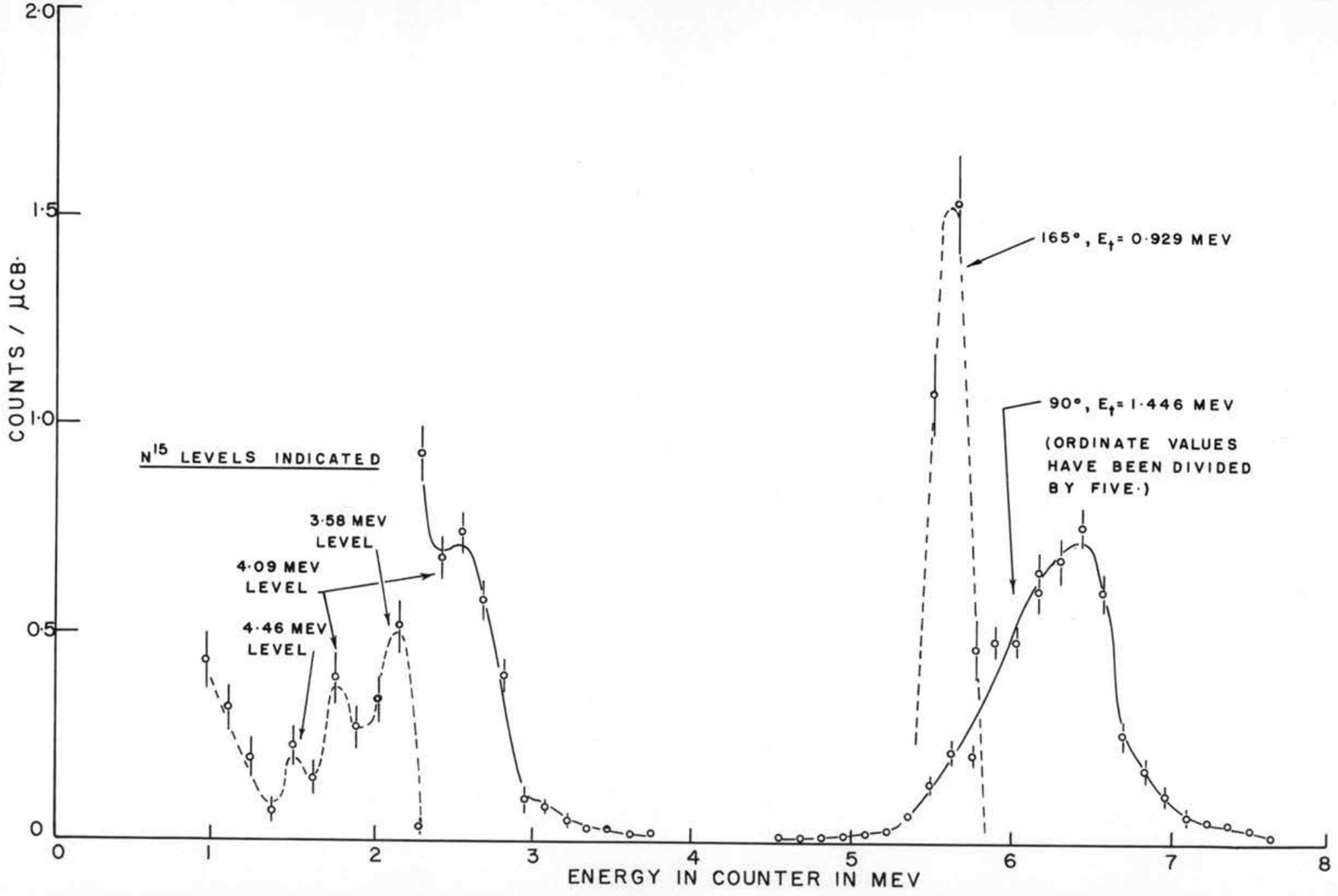

Figure 40. Yield From O + T at 90° and 165°

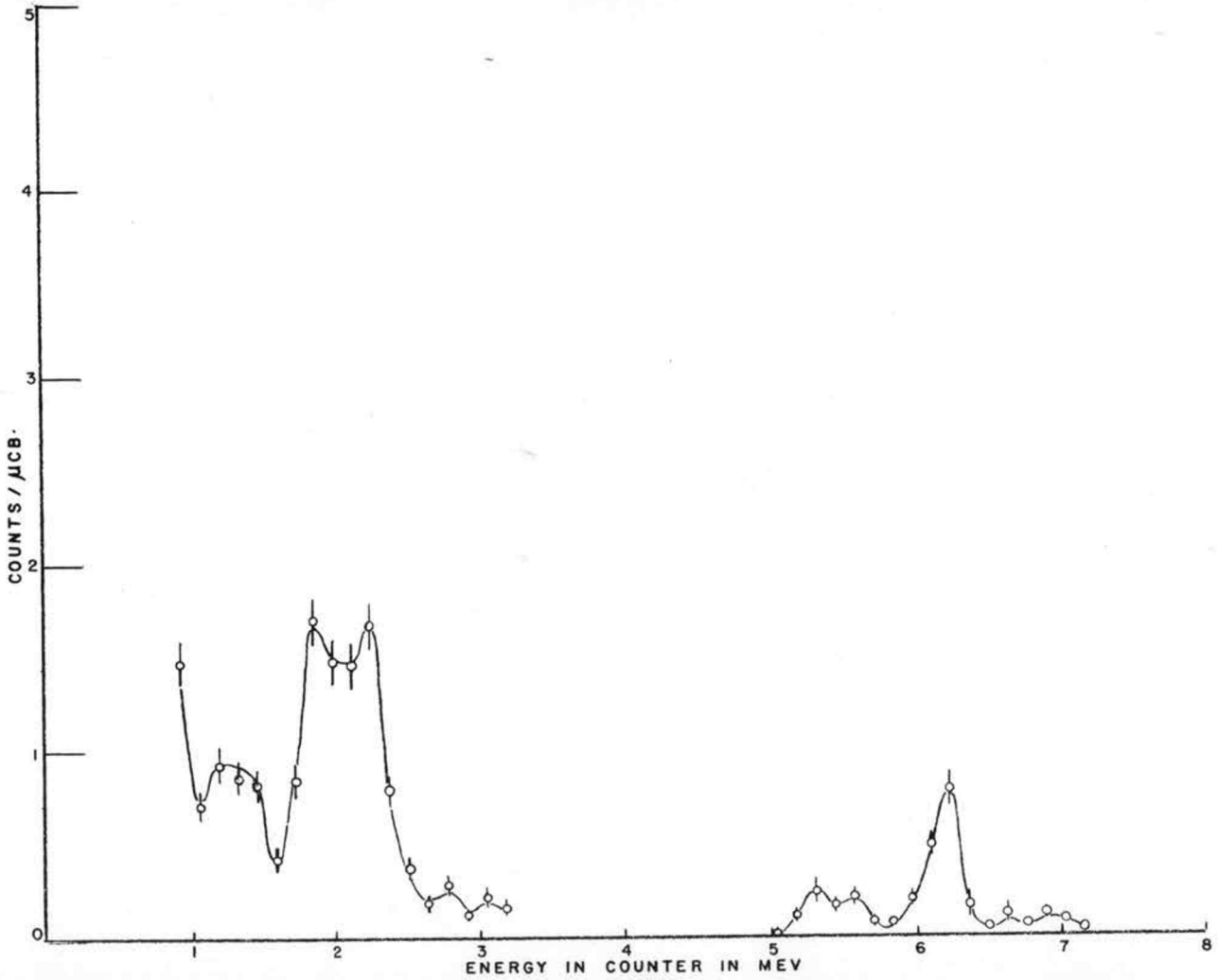

Figure 41. Yield From Triton Bombardment of CaF_2 at 90°, E_t = 1.033 Mev

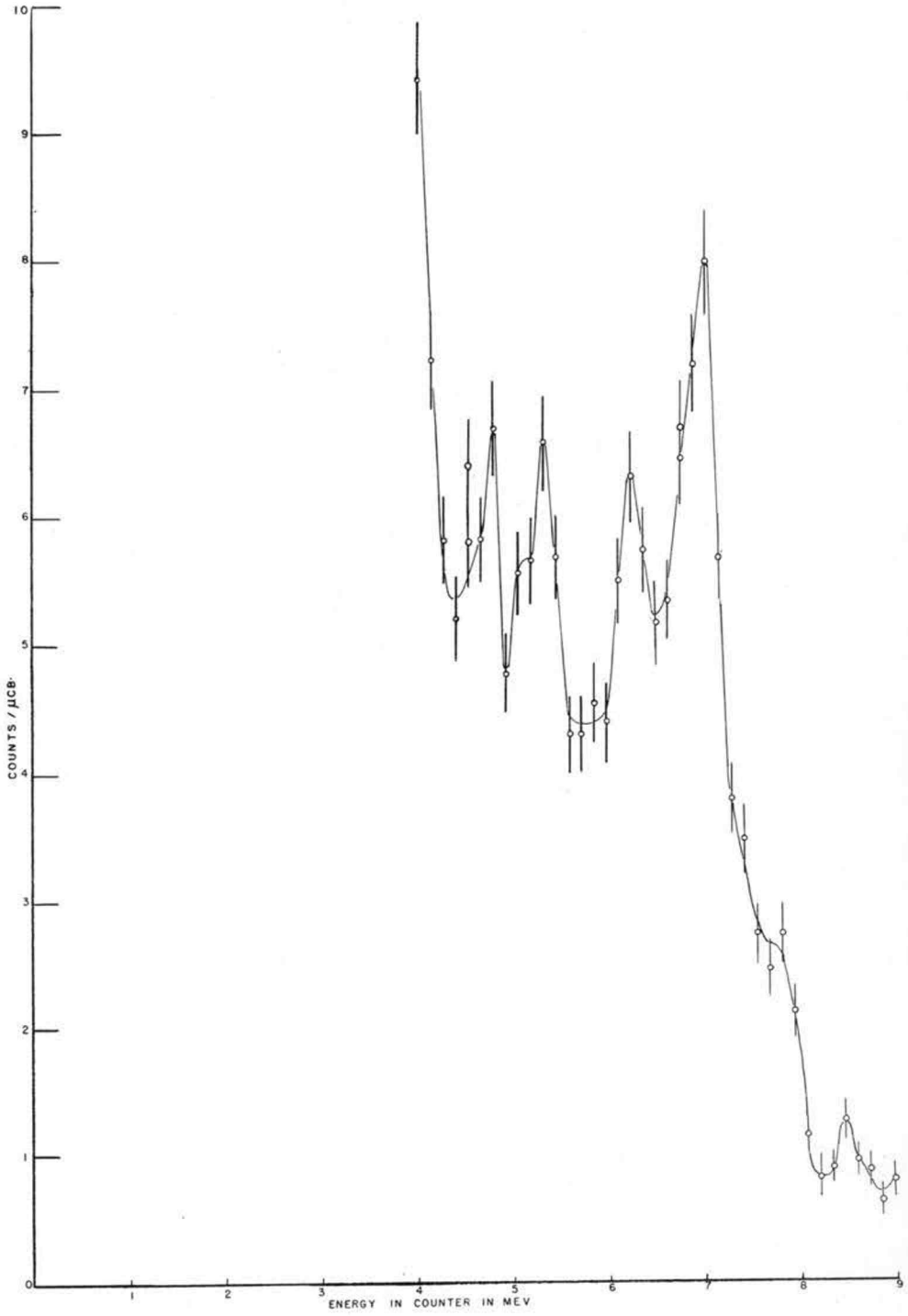

Figure 42. Yield From Triton Bombardment of CaF_2 at 90°, E_t = 2.272 Mev

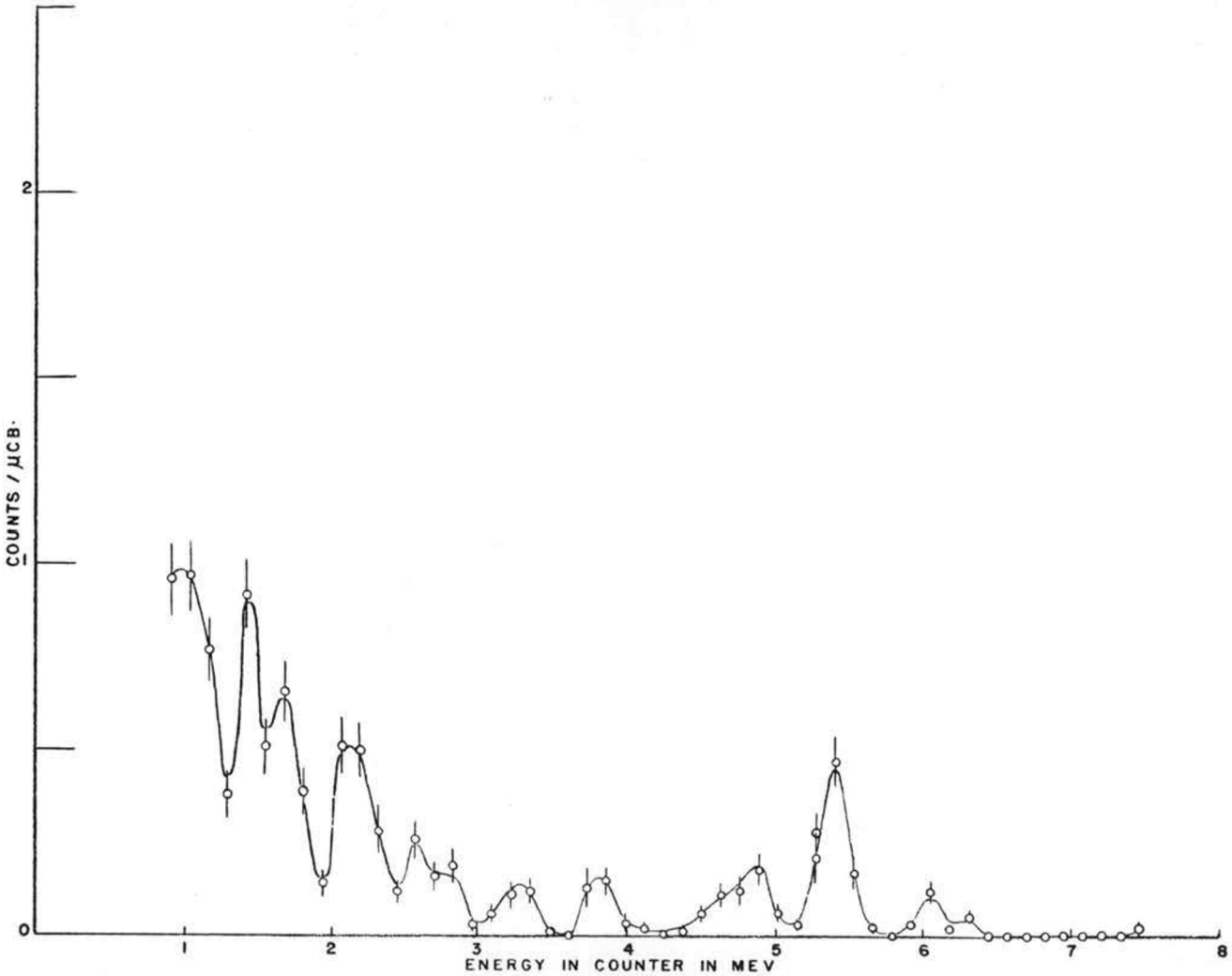

Figure 43. Yield From Triton Bombardment of CaF_2 at 165°, E_t = 1.033 Mev

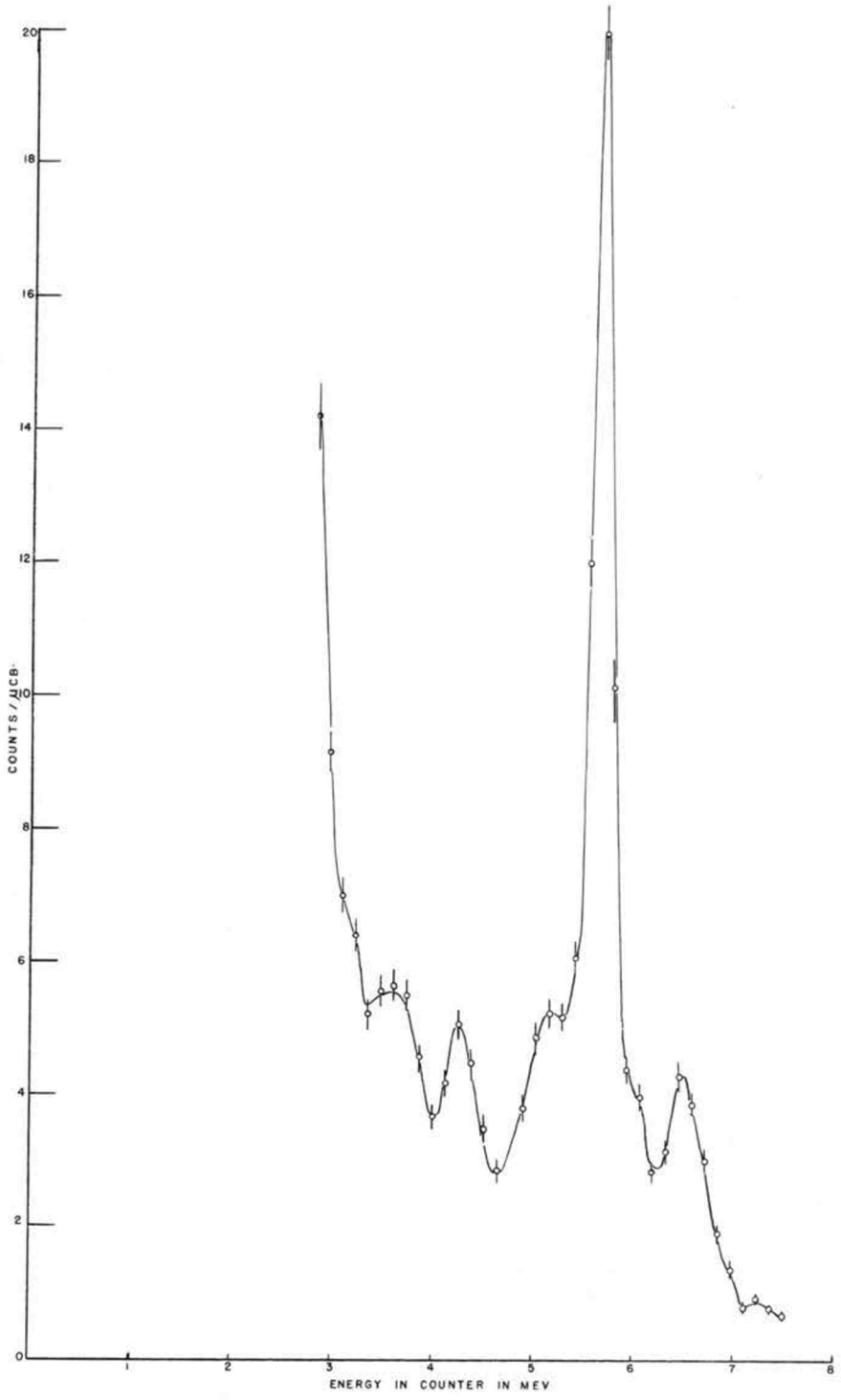

Figure 44. Yield From Triton Bombardment of CaF_2 at 165°, E_t = 2.272 Mev

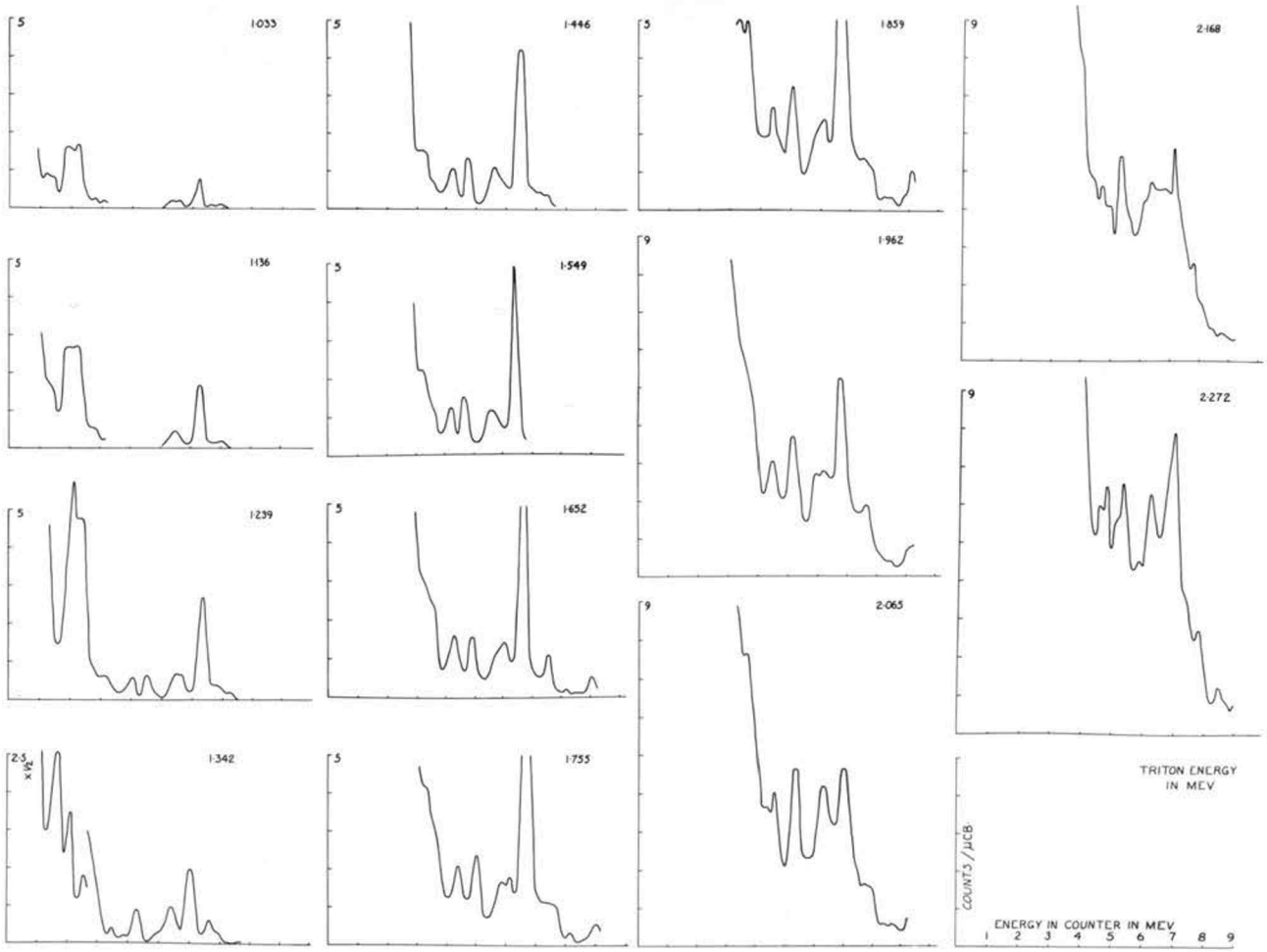

Figure 45. All Data Obtained at 90° From CaF_2 Target

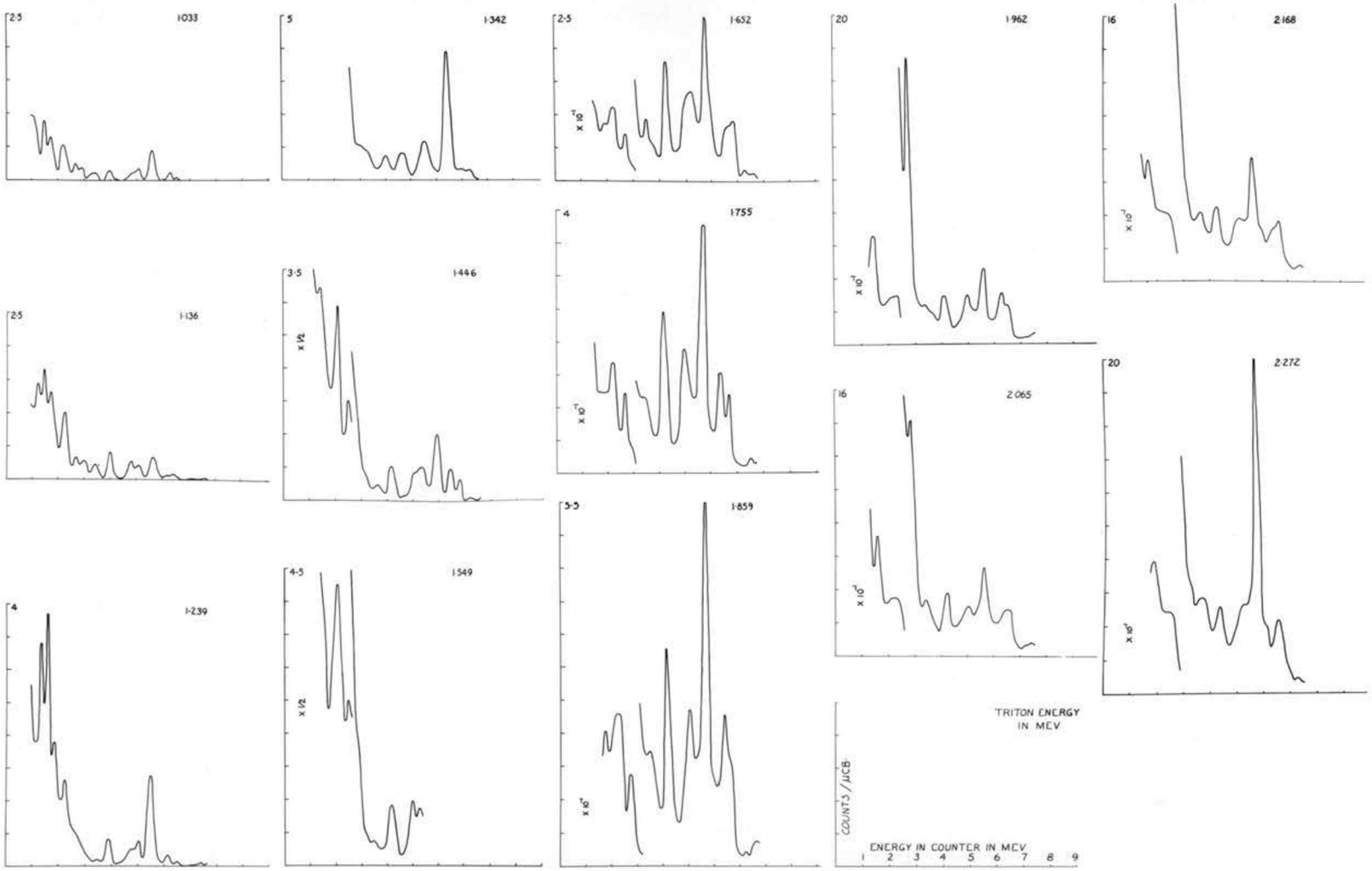

Figure 46. All Data Obtained at 165° From CaF_2 Target

DETERMINATION OF BACKGROUNDS AND PARTICLE ENERGIES

I. Use of Data Obtained From CaF_2 + T

In the section preceding the results, the method was outlined for obtaining the number of target atoms per square centimeter of Li^7 in the Li^7F target. This is also the number of F^{19} atoms in the Li^7F target.

The approximate numbers of target atoms in the Li^6F target and the CaF_2 target are obtained by comparing the charged particle yields of these two with the Li^7F target. The yields actually compared are those assumed to be alphas from $F^{19}(t,\alpha)O^{18}$ in the pulse height region of 107 to 139 volts. This region is beyond the maximum pulse heights one observes for alphas from tritons on Li^7 and on Li^6. The yield from tritons on F^{19} in this region appears to be great enough that one may compare the three different targets with respect to fluorine content.

One set of curves for triton bombardment of Li^6F, Li^7F, and CaF_2, (CuO, also) was obtained at 165° and a bombarding energy of 2.065 Mev. These curves are shown in Figure 21. The total counts recorded in the region specified indicate that the actual numbers of fluorine nuclei per square centimeter contained in the Li^6F, Li^7F, and CaF_2 targets have ratios of 1.037, 1.000, and 1.067, respectively.

These values permit one to calculate cross sections for reactions involving Li^7, Li^6, and F^{19}. They also make it possible to subtract fluorine-contributed yields from the data obtained with the

Li^6F and Li^7F targets. The presence of high Coulomb barriers (11, p. 369) associated with the heavier nuclei makes it reasonable to assume that calcium (Z=20) would probably not interact with tritons having energies less than $\sim$ 2.3 Mev. However, no measurements were made to verify this assumption, experimentally. Yields from Li^7 + T and Li^6 + T were obtained by subtracting appropriate fractions of the corresponding CaF_2 yields from the Li^7F and Li^6F data. The values used are:

$$Li^7 \text{ yield} = Li^7F \text{ yield} - (0.937)\ CaF_2 \text{ yield}$$
$$Li^6 \text{ yield} = Li^6F \text{ yield} - (0.972)\ CaF_2 \text{ yield}.$$

These corrections for background seem to remove fluorine contributions from most of the original data. However, for bombarding energies of about 1.6 Mev, and higher, fluorine contributions in the high-energy pulse region are still observed in the data obtained from Li^7F after the corrections are made. The data obtained from Li^7F and Li^6F targets, plotted without making corrections for fluorine content, are illustrated in Figure 21.

In corrected data obtained for the higher bombarding energies, "holes" appear near the low energy end of the pulse height range. These result from subtracting CaF_2 data from that obtained with the lithium fluoride targets. When the CaF_2 target was used, data obtained indicates a high yield for a well resolved group in this pulse height region. Calculations indicate that the peak is caused by tritons scattered from the calcium nuclei in the CaF_2 target.

II. Method of Determining Energies of Counter Pulses

Interpretation of the pulse height data depends upon a reasonably precise determination of the energy scale for such data. In discussing the experimental procedure, the occasional use of a plutonium source was mentioned. This source, a thin deposit of plutonium oxide, PuO_2, on an aluminum target blank, was inserted in the chamber facing the counter, in place of a target. The group of alpha pulses was observed and used to provide an energy reference point for the pulse heights recorded when the lithium targets were bombarded by tritons. From the counter window energy loss curve (APPENDIX I) one sees that the 5.14 Mev plutonium alphas would produce a pulse height representing 4.63 Mev in the counter.

Actually, small shifts, with time, of the effective gain of the counter and amplifier combination were observed for various time intervals by noting the average pulse height value for alphas from the plutonium source. Because of the time lapse between taking pulse height data from targets and from the plutonium source, use of the source as an energy reference point is probably not uniformly accurate for all the data.

This difficulty was avoided, for data obtained from $Li^7 + T$, by using the alpha peak from $Li^7(t,\alpha)He^6$ to establish an energy reference point, at corresponding angles and bombarding energies, for all the data. This peak was well resolved and the energy it represented was accurately calculated. References given by the plutonium alphas were used only to verify the positions of this alpha group at both

angles and various energies. The calculated values for alphas from $Li^7(t,\alpha)He^6$ were within $\pm$ 0.050 Mev of values measured with reference to the plutonium alpha group.

In using the alphas from $Li^7(t,\alpha)He^6$ as energy standards for pulses recorded when targets other than Li^7F were bombarded, the errors resulting from gain shifts with time are to be expected. The energies in the counter for this alpha group were made by assuming that the actual peak was produced by alphas originating about half-way through the effective layer of Li^7F on the target blank. APPENDIX II outlines the assumptions and calculations pertaining to target energy losses of the incident tritons and the emitted alpha particles.

A factor, consisting of calculated energy in the counter, for the alphas from $Li^7(t,\alpha)He^6$, divided by pulse height position in volts, was obtained for each bombarding energy at each of the two angles. The product of this factor and the pulse height position of another peak, is the average energy lost in the counter by particles producing the peak. This method was applied to all peaks (having significance) in the pulse height curves.

Once the energies were determined, an examination of the possible reactions was made by calculating particle energies which would be produced in the counter and comparing these calculated values with those actually observed.

DISCUSSION AND CONCLUSIONS

I. General Considerations of Nuclear Interactions

When two nuclei are caused to interact, it is convenient to think of the reaction as occurring in at least two stages. First, the two nuclei combine to form a compound nucleus (5, p.344). This is likely to exist for a short time in some excited state while the surplus energy, a combination of energies resulting from mass defect and from the kinetic energy of the bombarding particle, is distributed among all the nuclear particles. Next, depending upon the distribution of this energy, the compound nucleus usually breaks up into two or more particles. Subsequent break-up or decay of these secondary particles may occur.

Rules which predict what may happen in any nuclear interaction require that "charge, mass number, energy, and momentum must [each] be conserved" (3, p.186). For special cases, then, one may calculate how the energy released in a reaction will be distributed. Methods for calculating particle energies as a function of bombarding energy and of observing angle have been discussed by many workers in this field (19, pp.276-281), (10, pp.369-381). One version of these methods, which is based upon the assumption that the compound nucleus breaks up into two particles, is outlined in APPENDIX III. If three, or more, particles are produced in the break-up, the possible energies which one of these may have will be given by all values between zero and a maximum. The maximum value can be calculated by assuming

that, in effect, a two-body break-up occurs. The masses of all other particles produced in the reaction are lumped together, as one, in making this calculation.

In discussing reactions from which two particles evolve, it is convenient to refer to the particle detected (usually the lighter of the two) as the emitted particle and the other as the residual or recoil nucleus (19, p.276).

Most nuclei may exist in several energy states. The lowest of these is called the ground state, others are called excited states. If the excited states represent small additional amounts of kinetic energy above the ground state, the nucleus usually decays to some lower state, or to the ground state, by emitting the energy equivalent to this change in the form of a γ-ray. These excited states are called bound states. If the nucleus exists in a higher state, for which the kinetic energy is sufficient to permit particles to be emitted in the decay process, it is said to be in a virtual state.

Bound states are most often observed in residual nuclei. The energy equivalent to that required to raise the residual nucleus to such a state is obtained from the mass defect energy, or Q. A corresponding reduction in the energy of the emitted particle is what one observes when this happens.

Virtual states may be observed in compound nuclei. Resonances in the energy dependence of yields of emitted particles give evidence of virtual states. The energy available to a compound nucleus at one of these resonances is the corresponding value of the

state. Procedures used to calculate bound and virtual states in nuclei are developed in APPENDIX III. Some nuclei have virtual ground states (i.e. they exist as such for finite periods of time and decay by particle emission). Light nuclei which have very brief mean life-times are He^5 and Be^8. When these are emitted from a compound nucleus, one observes only their decay products.

If the direction of emission of the decay products is not independent of the direction of motion of the parent nucleus, it is likely that these secondary particles will be emitted forward or backward along the path traveled by the parent nucleus. It is probable that this happens when He^5 decays into $\alpha + n$ from its ground state and when Be^8 decays into two alpha particles from some of its well known virtual levels (13, p.310). If the He^5 emitted particle leaves its compound nucleus in the direction of a counter, the alpha particle produced by its decay should be observed to have one of two possible energies, depending upon whether its velocity adds to or subtracts from that of the parent He^5 nucleus. Actually, it is unlikely that the direction of break-up of the decay products will be completely restricted to the forward and backward directions. Consequently, from a large number of monoenergetic He^5 nuclei, one would expect to see alpha particles with all possible energies between some maximum and minimum values at which these alpha particles would be concentrated.

A similar effect would be observed for Be^8 break-up if the same assumptions are made. In this case, however, the low energy

alpha group consists of alphas emitted toward the counter from parent Be^8 nuclei which have been moving away from the counter.

Data resulting from charged particle observations of nuclear reactions will, in general, have certain characteristics. It is convenient to describe these in the form which is most commonly used, plots of number of particles as a function of particle energy.

1. In a two-particle disintegration, the observed particle will have one definite energy at one angle and bombarding energy. If the residual nucleus is reasonably stable, such a reaction gives rise to a well defined group of observed particles. Definition of this group suffers if residual nuclei are very unstable.

2. Decay products from highly unstable emitted particles will produce a band of pulses covering the energies between some maximum and minimum values. These particles will tend to peak at the maximum and minimum energies if an asymmetric distribution of the secondary particles occurs.

3. Disintegration into three, or more, particles will give rise to a band of energies for the same type of observed particle. These energies extend from zero to a maximum value given for the observed particle when all other particles are emitted together in the opposite direction.

4. Additional, lower energy groups of emitted particles from the same reaction give evidence of excited states in the residual nucleus.

5. Virtual levels in the compound nucleus produce

resonances in emitted particle yield. These would be observed in data for which yield is a function of bombarding energy.

These characteristics will be recognized in data which is discussed in the following sections.

II. Discussion and Summary of the Reactions from Li^7 + T

The Li^7 + T reactions which have positive Q-values are listed on page 2. Of these, one expects to be able to identify only

9. $Li^7(t,\alpha)He^6$

and 13. $Li^7(t,He^5)He^5$.

A third reaction is 9a. $Li^7(t,\alpha)He^{6*}$, where He^6 remains in an excited state $\sim$ 2 Mev above the ground state (22, p.55).

Reactions producing particles having a wide range of energies are 13, above, and

10. $Li^7(t,2\alpha)2n$.

According to Pepper, et al.(23, p.316) the cross section for reaction 10 is much larger than those for 9 and 9a.

Figures 22 through 29 show the charged particle distributions from Li^7 + T taken at 90° and at 165° for bombarding energies from about 0.6 to 2.3 Mev.

In all of these figures, reactions 9 and 9a are observed. The alpha group representing reaction 9 gives pulses between $\sim$ 5.4 and 6.0 Mev at 90° and $\sim$4.3 and 3.5 Mev at 165°. Alphas from reaction 9a appear as a group located from 1.2 to 1.5 Mev lower than those from reaction 9. A level in He^6 at 2.11 $\pm$ 0.05 Mev is responsible for this group.

The He^6 ions produced in reaction 9 may help to form the group appearing at energies between 2.5 and 2.7 Mev in the 90° data. They are probably not observed at 165° where they would be indicated by pulses of less than 1 Mev.

Reaction 13 would produce pulses between 0.2 and 4.3 Mev at 90° and ~ 0 and 2.6 Mev at 165°. If grouping at the highest and lowest energies occurs, only the high energy alphas would be observed. These would appear between 3.8 and 4.3 Mev at 90° and between 2.1 and 2.6 Mev at 165°. These groups, if they exist will appear with energies slightly less than the alphas from reaction 9a. The peak attributed to alphas from reaction 9a has an asymmetric shift toward the low energy side. This may be caused by alphas from break-up of He^{5} nuclei produced from reaction 13.

Most of the pulses produced by alpha particles from reaction 10 would lie in the region between 1.5 and 3.0 Mev. The few alpha particles having the maximum energy available with this reaction would give pulses with about 0.5 Mev more energy than the corresponding alpha groups from reaction 9a. The relatively large number of alphas having intermediate energies which one would expect to observe from this reaction may help to explain the numerous pulses generally observed in the 2 Mev region.

The energy dependence of differential cross sections for reactions 9 and 9a are shown in Figure 47. The resonances appearing in these curves are not well defined. The bombarding energies corresponding to these resonances give indications of virtual states in Be^{10}. From the $Li^{7}(t,\alpha)He^{6}$ reaction, evidence is given for levels at $\sim$18.6 and 19.0 Mev. Values of 18.0, 18.5, and 19.0 Mev result from the data for $Li^{7}(t,\alpha)He^{6*}$. The estimated errors in these values is less than 0.15 Mev. Similar levels indicated by an earlier

measurement of neutron yield from Li + T reactions (7, pp.100-101) were observed at 18.07 and 18.93 Mev. (These values, calculated on the basis of current mass values, differ from those stated in the reference.)

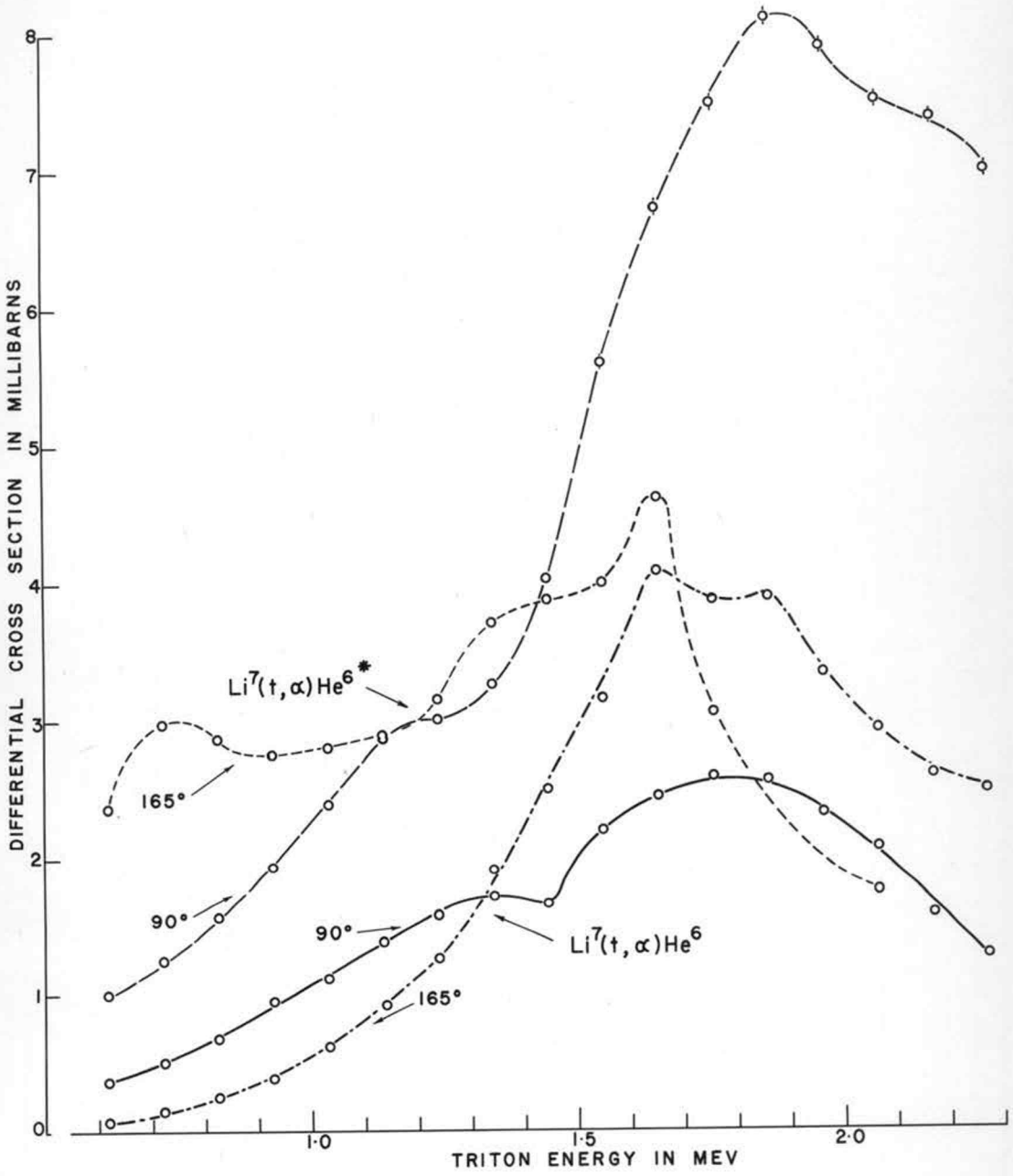

Figure 47. Excitation Curves of $Li^7(t,\alpha)He^6$ and $Li^7(t,\alpha)He^{6*}$ at 90° and 165°

III. Discussion and Summary of the Reactions from Li^6 + T

The reactions from Li^6 + T which have positive Q-values are listed on page 1. Some Li^6 + T reactions have been observed by others at a lower bombarding energy (24, pp.155-156). It is likely that one could identify clearly

4. $Li^6(t,\alpha)He^5$

and

5. $Li^6(t,d)Li^7$.

The protons from reaction 6, $Li^6(t,p)Li^8$, have energies too low to be observed. A third reaction, 4a, $Li^6(t,\alpha)He^{5*}$ is possible, in which He^5 remains momentarily in a level $\sim$2.6 Mev (17, pp.559-560).

Other reactions which may contribute alpha particles that would be observed are:

2. $Li^6(t,2\alpha)n$

and

3. $Li^6(t,Be^8)n$.

Each of these would probably produce alpha particles having a band of energies. Reaction 3 would give rise to alpha particles having energies $\sim$2 Mev or more only if Be^8 remained in one of its virtual levels.

The group of alpha particles representing reaction 4 is observed in all the data plotted in Figures 30 through 37. At 90°, the group has values varying from about 8.1 to 8.6 Mev. Corresponding energies at 165° are about 6.8 to 5.7 Mev. This group is not always well defined, particularly in data taken at 90°. It is to be expected that the short mean lifetime of He^5 would be reflected in the energy spread of these alphas.

The alpha particles produced by break-up of He^5 nuclei

(reaction 4), those resulting from possible break-up of Be^8 (reaction 3), and those produced in the three-particle break-up (reaction 2) will all give rise to pulses having energies very near to the pulses resulting directly from the major group of alphas from $Li^6(t,\alpha)He^5$. These may help to obscure the main group.

Alphas from reaction 2 will have mean energies between 2.0 and 5.5 Mev. The maximum energies they may have is about 0.5 Mev higher than corresponding values for the major group of alphas from reaction 4.

The He^5 nuclei from reaction 4 will produce groups of alphas giving pulses between 2.7 and 7.7 Mev at 90° and between 0.8 and 5.7 Mev at 165°. If these show tendencies to form peaks at the maximum and minimum values, at 90°, the maximum peak would occur between 7.0 and 7.7 Mev and the minimum peak would appear between 2.7 and 3.2 Mev. At 165°, corresponding values would be 5.7 to 4.8 Mev and 1.6 to 0.8 Mev. The high energy groups would help to explain pulses filling in a region with about 1.5 Mev width just below the main alpha group. This is particularly noticeable at the higher bombarding energies. The low energy groups are probably present to the same degree. However, neither low nor high energy groups are clearly defined.

Levels in Be^8 which would provide sufficient energy that alphas from it would be observed vary between 2.9 and 14.7 Mev (13, p.310). Levels at which Be^8 is known to decay to two alphas are at 9.8, 7.5, and 2.9 Mev. Alphas producing pulses as high as 9 Mev could

arise from this reaction if Be^8 decays to alphas directly from the higher levels, also.

A level in He^5 at 2.52 ± 0.16 Mev would explain a pulse group at 6.6 to 6.7 Mev appearing in the 90° data (Figures 30, 31, 32, and 36). Data taken between 1.5 and 2.1 Mev, at 165°, has a suggestion of this group at 4.3 to 4.5 Mev (Figure 37).

Deuterons from reaction 5 could be detected with the counter. However, deuteron energies are so low that these particles are not observed at 165°. The rapid increase in numbers of low-energy pulses (probably elastically scattered tritons) with increasing bombarding energy made it necessary to raise the bias setting of the 18-channel analyzer as bombarding energy was increased. Consequently, the deuteron group could be observed only at the lower bombarding energies, at 90°. This group is shown in Figure 38. From the data obtained, the yield appears to increase uniformly with increasing bombarding energy. At a bombarding energy of 1.136 Mev, the estimated differential cross section for deuteron production at 90° is 21 ± 2 millibarns per steradian.

In Figure 48, an attempt has been made to graph the approximate yield of $Li^6(t,\alpha)He^5$ by plotting the energy dependence of the magnitude of the alpha peak from this reaction. Virtual levels in Be^9 given by faint resonances in these curves are at 18.8 ± 0.15 and 19.0 ± 0.15 Mev. At the highest bombarding energies (Figures 32 and 35) the areas under the alpha peaks at the two angles have been estimated with probable errors less then ± 10%. Differential cross sections

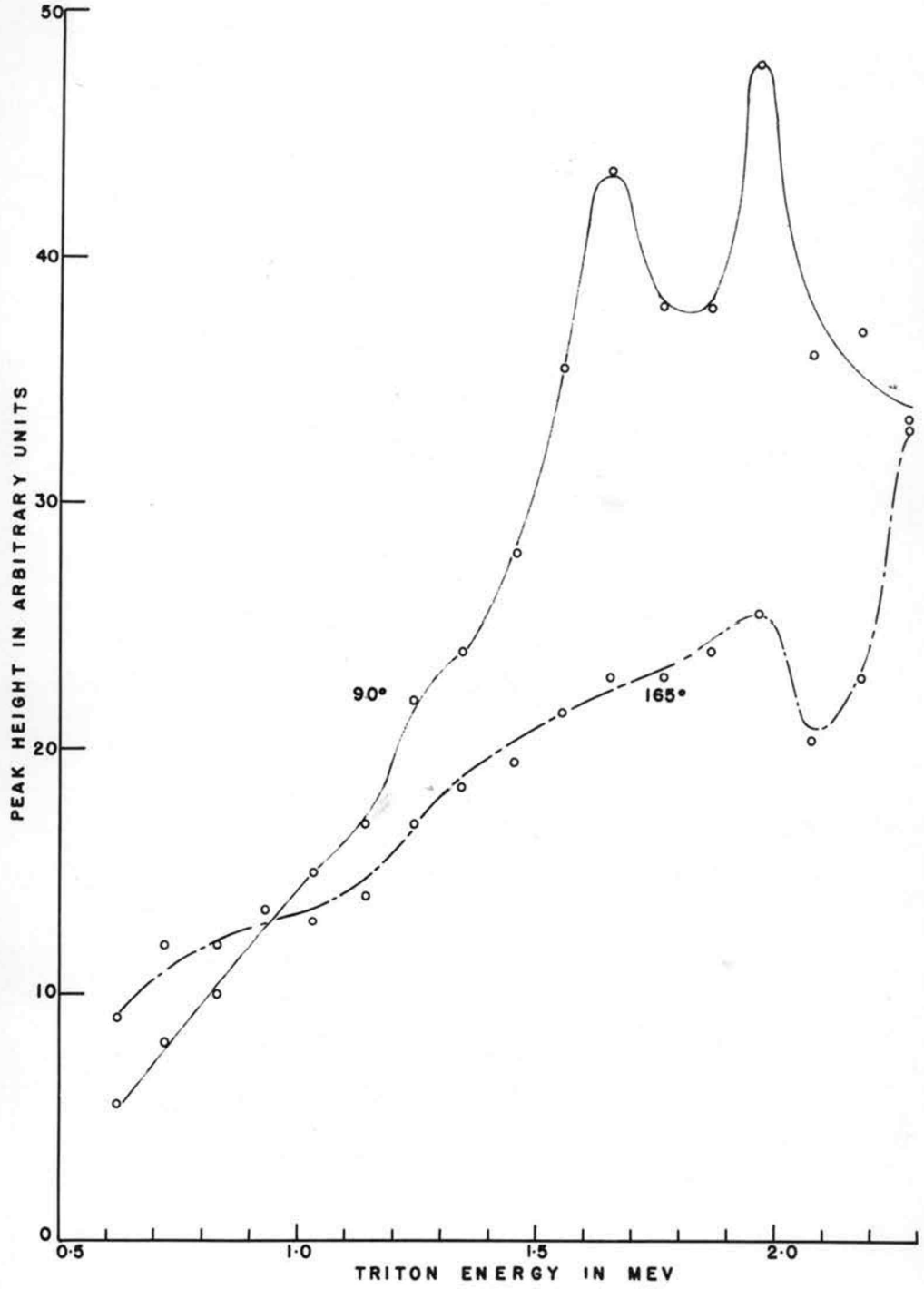

Figure 48. "Excitation Curves" of $Li^6(t,\alpha)He^5$ at 90° and 165°

given by these values are 5.5 and 3.4 millibarns per steradian at 90° and 165°, respectively, for E_t = 2.272 Mev.

IV. Discussion and Summary of Yields from Triton Bombardment of N, O, and F.

IVA. The $N^{14}(t,\alpha)C^{13}$ Reaction -- Levels in C^{13}

The data shown in Figure 39 illustrates the yield one obtains from the triton bombardment of nitrogen. Only three runs were made which provided useful information. All of these were observed at 165°. The guanidine plus sodium azide target was bombarded with tritons having 1.652 and 1.755 Mev incident energy. The target consisting of thiourea was also bombarded at the higher energy.

Levels in C^{13} which are indicated by these groups have been labeled. Additional possible levels which might account for the irregularities of the data have been calculated. All of the levels in C^{13} for which there is definite indication, as well as those for which slight evidence exists, are listed in Table I along with approximate values and references for levels which have been observed by others.

While making calculations for the levels assigned to C^{13}, several possibilities were explored. All of these proved to be inadequate to explain the groups observed. Charged particles from the following reactions involving nuclei known or suspected to be in the targets would not produce groups where these were observed. Reactions are: $C^{12}(t,\alpha)B^{11}$, $C^{12}(t,p)C^{14}$, $Na^{23}(t,\alpha)Ne^{22}$, $S^{32}(t,\alpha)P^{31}$, $N^{14}(t,p)N^{16}$, and $N^{14}(t,d)N^{15}$. Several others were considered which have negative Q-values. Tritons scattered from target nuclei did not produce pulses comparable with those detected.

TABLE I

Levels in C^{13}, based on α-groups from the reaction $N^{14}(t,\alpha)C^{13}$ observed at 165° for E_t = 1.652 and 1.755 Mev. Absolute errors are $\sim\pm$ 0.150 Mev.

Effective Q (Mev)	Observed Level (Mev)	Observations used	Relative Intensity	Published Level** (Mev)
12.259	0	2	1.0	--
9.38	2.88	3	0.1	3.11*
8.56	3.70	3	1.1	3.77*
8.0	4.3	1	-	4.29***
7.0	5.25	1	-	5.15*
6.4	5.9	1	-	5.87*
6.1	6.2	1	-	6.34*
5.35	6.91	2	0.1	6.91*
4.75	7.51	3	2.9	7.58*
4.18	8.08	3	2.0	8.02*
3.22	9.04	3	5.7	8.84*

Note: Those Q-values indicated as being approximate are for levels implied by doubtful evidence.

*(27, p.34) The value for 3.77 Mev is described as a doublet combined with a level at 3.90 Mev.

** Most of these levels are reported in the review article on levels of light nuclei (13, pp.321-331).

*** This value results from the proton group giving a Q = -0.22 Mev for the B(α,p)C reaction reported by Frye and Wiedenbeck (8, p.961).

The table and curves illustrating the results of triton bombardment of nitrogen are self-explanatory. It may be instructive to point out, however, that a much discussed low intensity level in C^{13} at $\sim$0.8 Mev is not detectable in this data. A group responsible for this level would be found joining the ground state peak on its low-energy side. The poor resolution of the ground state peak would obscure such a group if its intensity is low.

IVB. The $O^{16}(T,\alpha)N^{15}$ Reaction -- Levels in N^{15} and F^{19}

The curves shown in Figure 40 are results from the triton bombardment of the CuO target. The high Z-value of copper makes it unlikely that a reaction with copper was observed. However, the pile-up of tritons scattered from the copper nuclei made it impossible to observe the low pulse height region when this target was used. As a result, the known levels in N^{15} were not responsible for groups of pulses shown in the data. The lowest known level in N^{15} is at 5.28 Mev (13, pp.338-340). In general, the peaks noted when the copper oxide target was used were also observed with the same relative intensities when all other targets containing oxygen were used. To avoid confusion with other reactions resulting from different nuclei in the target, however, the CuO target was considered to be the best.

Four main groups of pulses appear to result from O^{16} + T. The highest energy pulse group is the one given by alpha particles from $O^{16}(t,\alpha)N^{15}$, where N^{15} is in its ground state. This peak is the

one first observed in the metallic lithium targets. Three other peaks may be seen near the low energy end of the pulse height curves. As labeled in Figure 40, these may indicate levels in N^{15} at ~ 3.6, 4.2, and 4.5 Mev, respectively. The lowest of these is adequately explained by assuming that the pulses are produced by protons from $O^{16}(t,p)O^{18*}$, where O^{18} remains in a 2 Mev excited state to be mentioned in connection with triton bombardment of fluorine.

Two levels thus attributed to N^{15} are at 4.15 ± 0.03 and 4.46 ± 0.07 Mev. The lower of these appears in only four observations and at 165° only. The higher level appears in four observations at 165° and five at 90°. Both are visible in some of the data from other "oxygen" targets. No other observers report levels in N^{15} below ~ 5.28 Mev except for one instance (15, pp.723-724) in which a γ-ray from $N^{14}(n,\gamma)N^{15}$ was observed to have an energy of 4.49 Mev. This γ-ray was adequately interpreted, however, as resulting from a two-step decay of N^{15} from an excitation energy of 10.82 Mev to a level at 6.32 Mev in N^{15}. Some indication has been reported of a level ~ 4 Mev in the mirror nucleus, O^{15}(13, p.341).

An excitation curve for $O^{16}(t,\alpha)N^{15}$ is shown in Figure 49. The resonances which appear are for the compound nucleus, F^{19}. From the data, virtual states of F^{19} are indicated at the energies 12.6, 12.9, and 13.25 Mev with estimated errors less than ± 0.15 Mev. Published values (13, pp.353-354) of 12.4 and 13.2 Mev are given. The 12.9 Mev level has not been reported, thus far.

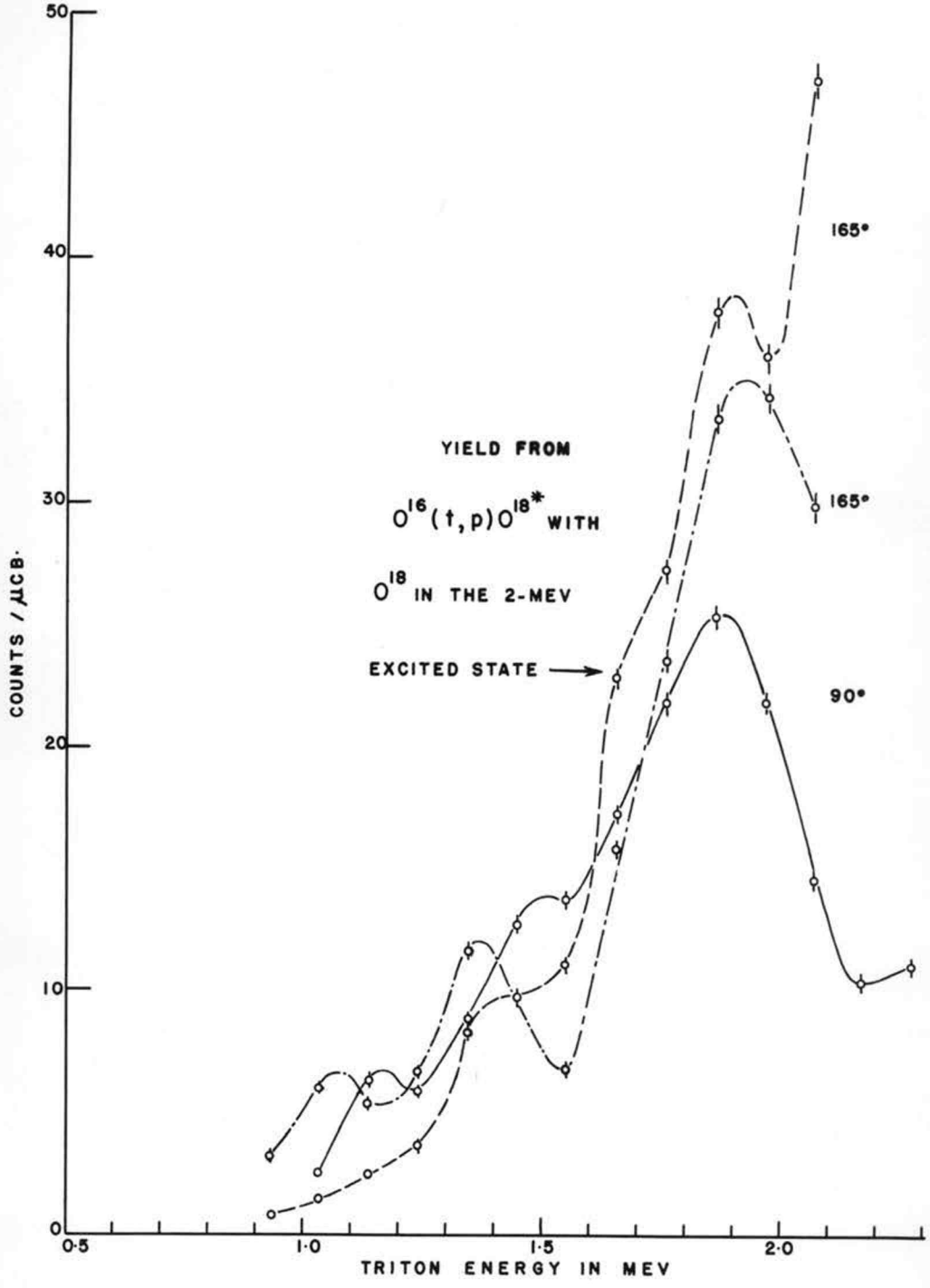

Figure 49. Excitation Curves of $O^{16}(t,\alpha)N^{15}$ at 90° and 165°

IVC. The Reactions $F^{19}(t,\alpha)O^{18}$ and $O^{16}(t,p)O^{18*}$ - Levels in O^{18} and Ne^{22}

The triton bombardment of a CaF_2 target between triton energies of 1.032 and 2.272 Mev gave 90° and 165° observations, shown in Figures 41 through 46, of the charged particles resulting from F^{19} + T.

The possibility that pulses were produced by protons, deuterons, scattered tritons, etc., was investigated. Reactions which have positive Q-values are $F^{19}(t,He^6)O^{16}$, $F^{19}(t,d)F^{20}$, and $F^{19}(t,p)F^{21}$. Of these, only the reaction yielding protons could produce charged particles in the counter with energies which may have been recorded. All the protons from this reaction would have energies higher than they could dissipate in the counter gas. (The highest proton pulse the counter would indicate is $\sim$3.2 Mev.) No groups appear having energies $\sim$3 Mev, as one might expect from $F^{19}(t,p)F^{21}$. The energy groups which appear are attributed to $F^{19}(t,\alpha)O^{18}$, indicating numerous excited states in O^{18}. No levels in O^{18} have been reported heretofore. These levels are listed in Table II. Energies indicated are believed to be in error by less than $\pm$ 0.150 Mev. The relative certainty of each level is indicated by listing the number of sets of data curves that show the group attributed to it. Those observed in $\sim$10 or fewer sets of data are probably very weak or transitory. The group which is most obvious is that which appears to result from a 4.42 Mev level in O^{18}. The peak representing this group is well resolved in nearly all the data. The approximate area under this peak has been interpreted as the differential cross section and plotted to give the

TABLE II

Levels in O^{18}, based on α-groups from the reaction $F^{19}(t,\alpha)O^{18}$ observed at 90° and 165° for ΔE_t = 0.103 Mev from 1.033 to 2.272 Mev.

Q (Mev)	Energy Level (Mev)	Number of Observations	Q (Mev)	Energy Level (Mev)	Number of Observations
11.81	0	-	6.43	5.58	24
10.11	1.70	3	5.95	5.86	4
9.82	1.99	4	5.44	6.37	24
9.57	2.30	9	5.02	6.79	5
9.08	2.73	14	4.77	7.04	24
8.83	2.98	2	4.53	7.28	10
8.49	3.32	19	3.97	7.84	19
8.22	3.59	21	3.67	8.14	24
7.96	3.85	12	3.24	8.57	16
7.39	4.42	25	2.86	8.95	16
7.13	4.68	1	2.58	9.23	8
6.70	5.11	18	2.20	9.61	1

excitation curves shown in Figure 50.

Resonances which appear were averaged to give values of 22.6, 23.0, and 23.2 Mev for virtual states in Ne^{22}, which is produced by F^{19} + T with a Q-value of 21.426 Mev. No previously published values for levels in Ne^{22} have energies as high as these.

The ground state for O^{18} does not appear in the data. Since the Q for this reaction is 11.81 Mev, the alpha particles resulting in the break-up have sufficient energy to produce a pulse just beyond the region recorded. None of the data was taken with reduced gain settings on the amplifier, hence, one has an indication of this ground state group only from the pulses recorded in the surplus channel. These indicate a relatively low intensity group for the bombarding energies used.

In the foregoing section (IVB), the pulse group which one could interpret as a level of ~ 3.6 Mev in N^{15} may have been produced by protons instead of alpha particles. If one assumes that the level at 1.99 Mev in O^{18} is responsible for the proton group from $O^{16}(t,p)O^{18*}$, with a Q-value of 1.69 Mev, this group is well explained. The standard deviation of experimental energy values from those calculated is $\pm$ 0.076 Mev, if one assumes that the pulse-group observed is from protons, whereas a standard deviation of $\pm$ 0.125 Mev results from the assumption that the group is alpha particles from $O^{16}(t,\alpha)N^{15*}$. It is tempting to believe that the 3.6 Mev level in N^{15} is not indicated but that the 1.99 Mev level in O^{18} is substantiated by this data.

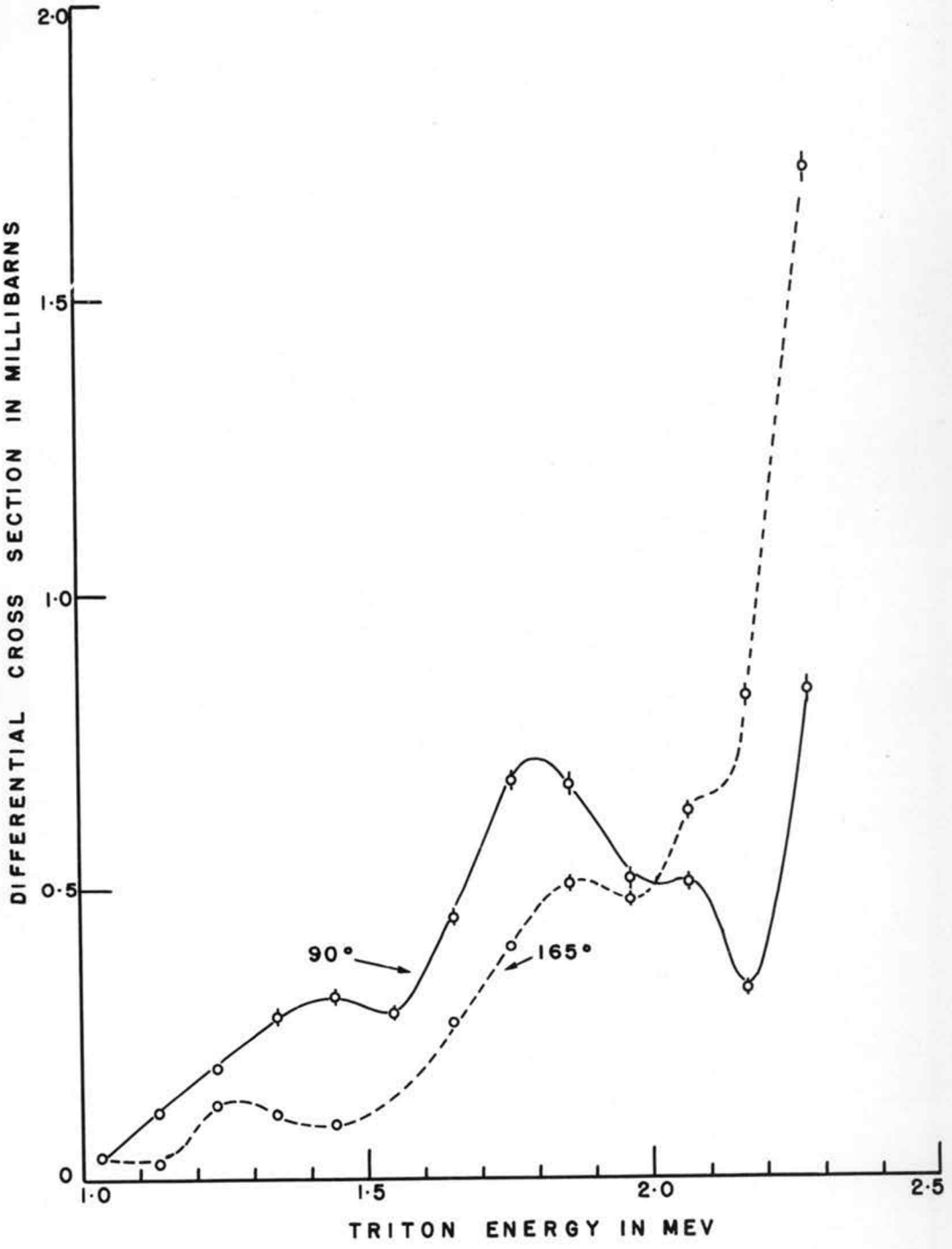

Figure 50. Excitation Curves of $F^{19}(t,\alpha)O^{18}$ at 90° and 165°

BIBLIOGRAPHY

1. Bennett, W. E. The stopping power of mica for α-particles. Proceedings of the royal society, 155: 419-434. 1936.

2. Bethe, H. A. Elementary nuclear theory. New York, Wiley, 1947. 147p.

3. Bethe, H. A. Nuclear physics. B. Nuclear dynamics, theoretical. Reviews of modern physics, 9: 69-244. 1937.

4. Bethe, Hans A. The properties of atomic nuclei, II-Range-energy curves. Brookhaven national laboratory technical bulletin (BNL-T-7). 1949. 39 figures.

5. Bohr, Niels. Neutron capture and nuclear constitution. Nature 137: 344-348. 1936.

6. Cockroft, A. L. and S. C. Curran. The elimination of the end effects in counters. Review of scientific instruments 22: 37-42. 1951.

7. Crews, R. W. Neutron yield for the Li + T reactions. Physical review 82: 100-101. 1951.

8. Frye, G. M. and M. L. Wiedenbeck. Magnetic analysis of the B(α,p)C reaction. Physical review 82: 960-961. 1951.

9. Gittings, H. T. A current integrator. Review of scientific instruments 20: 325-326. 1949.

10. Halliday, David. Introductory nuclear physics. New York, Wiley, 1950. 558p.

11. Hanson, A. O. and J. L. McKibben. A neutron detector having uniform sensitivity from 10 kev to 3 mev. Physical review 72: 673-677. 1947.

12. Herb, R. G.; D. B. Parkinson and D. W. Kerst. The development and performance of an electrostatic generator operating under high air pressure. Physical review 51: 75-83. 1937.

13. Hornyak, W. F., et al. Energy levels of light nuclei. III. Reviews of modern physics 22: 291-372. 1950.

14. Jorgensen, Theodore. A study of adjustments of a Zinn-type ion source. Review of scientific instruments 19: 28-30. 1948.

15. Kinsey, B. B., G. A. Bartholomew, and W. H. Walker. Neutron capture gamma-rays from Be^9, C^{12}, and N^{14}. Physical review 77: 723-724. 1950.

16. Korff, Serge A. Electron and nuclear counters. New York, Van Nostrand, 1946. 212p.

17. Leland, Wallace T. and Harold M. Agnew. Evidence for an excited state of He^5. Physical review 82: 559-560. 1951.

18. Li, C. W., et al. Masses of light nuclei from nuclear disintegration energies. Physical review 83: 512-518. 1951.

19. Livingston, M. Stanley and H. A. Bethe. Nuclear physics. C. Nuclear dynamics, experimental. Reviews of modern physics 9: 245-390. 1937.

20. McKibben, J. L.; D. H. Frisch, and J. M. Hush. Control equipment for 2.5 Mev Van de Graaff giving an ion beam constant to $\pm$ 1.5 kev. MDDC-222: 1-5. 1946. (Unclassified document).

21. Margenau, Henry and George Moseley Murphy. The mathematics of physics and chemistry. New York, Van Nostrand, 1943. 581p.

22. Pepper, T. P., E. Almquist, and P. Lorrain. Angular Distribution of α-particles from $Li^7(t,\alpha)He^6$. Bulletin of the American physical society 27: 55. Jan. 31, 1952. (Paper ZB 10).

23. Pepper, T. P., et al. Disintegration of lithium by tritons. Physical review 81: 315-316. 1951.

24. Pepper, T. P., et al. Protons and deuterons from Li^6 + T reactions. Physical review 85: 155-156. 1952.

25. Rosenfeld, L. Nuclear forces. New York, Interscience, 1948. 543p.

26. Rossi, Bruno B. and Hans H. Staub. Ionization chambers and counters. New York, McGraw-Hill, 1949. 243p.

27. Rotblat, J. Report on energy levels in C^{13} and O^{17}. Proceedings of the Harwell nuclear physics conference, September 1950. A.E.R.E. G/M 68. 1950. 115p.

28. Seaborg, G. T. and I. Perlman. Table of isotopes. Reviews of modern physics 20: 585-667. 1948.

29. Taschek, Richard and Arthur Hemmendinger. Reaction constants for $Li^7(p,n)Be^7$. Physical review 74: 373-385. 1948.

APPENDIXES

APPENDIX I

Relation of Particle Energies Inside and Outside the Counter

From Bennett's work on the stopping power of mica (1, p.426) one may obtain an approximate stopping power value for various α energies. A sample of mica used for the counter window measured 3.718 $\pm$ 0.054 cm^2 and weighed 3.930 $\pm$ 0.020 milligrams. This gives a value of 1.057 $\pm$ 0.016 mg/cm^2. A nominal value of 1.06 mg/cm^2 was used in the calculations.

By dividing the thickness of the mica window by the stopping power values from the curve mentioned above, one obtains the centimeters air equivalent for the mica window as a function of α-particles energy. Values obtained are:

$E\alpha$ (Mev)	Air Equivalent (cm)	$E\alpha$ (Mev)	Air Equivalent (cm)
1.0	.67	5.0	.73
1.5	.69	6.0	.74
2.0	.70	7.0	.74
2.5	.71	8.0	.74
3.0	.72	9.0	.74
3.5	.72	10.0	.75
4.0	.73	11.0	.75
4.5	.73	12.0	.75

Using Bethe's range-energy curves (4, Figs. 1-2), one may subtract the corresponding air equivalent from the range of α's for each of these energies. The new energies are obtained from the

resulting range values.

The energies of α-particles inside the counter which correspond to α-energies outside the counter have been plotted in Figure 51.

A similar curve for protons was prepared from Bethe's range-energy curves (4, Fig. 3) by assuming that the same window stopping power values were applicable to protons having velocities corresponding to those of the α-particles. This curve is shown in Figure 52.

The triton window-correction curve (Figure 53) was made from the same data as was used for protons. In this case one uses Bethe's curves in conjunction with the following relation:

The range of a triton having energy E_t will be three times the range of a proton having energy $E_t/3$, (19, p.271).

Curves were not drawn for deuterons and for He^6-particles. In calculations where these particles were considered, the energies in the counter were determined, in similar fashion as for tritons, for the individual particle energies which were computed. (For deuterons, the range of a deuteron with energy E_d, will be twice the range of a proton with energy $E_d/2$. For He^6-particles with energy E, their range will be 1.5 times the range of α's having energy 0.67 E.)

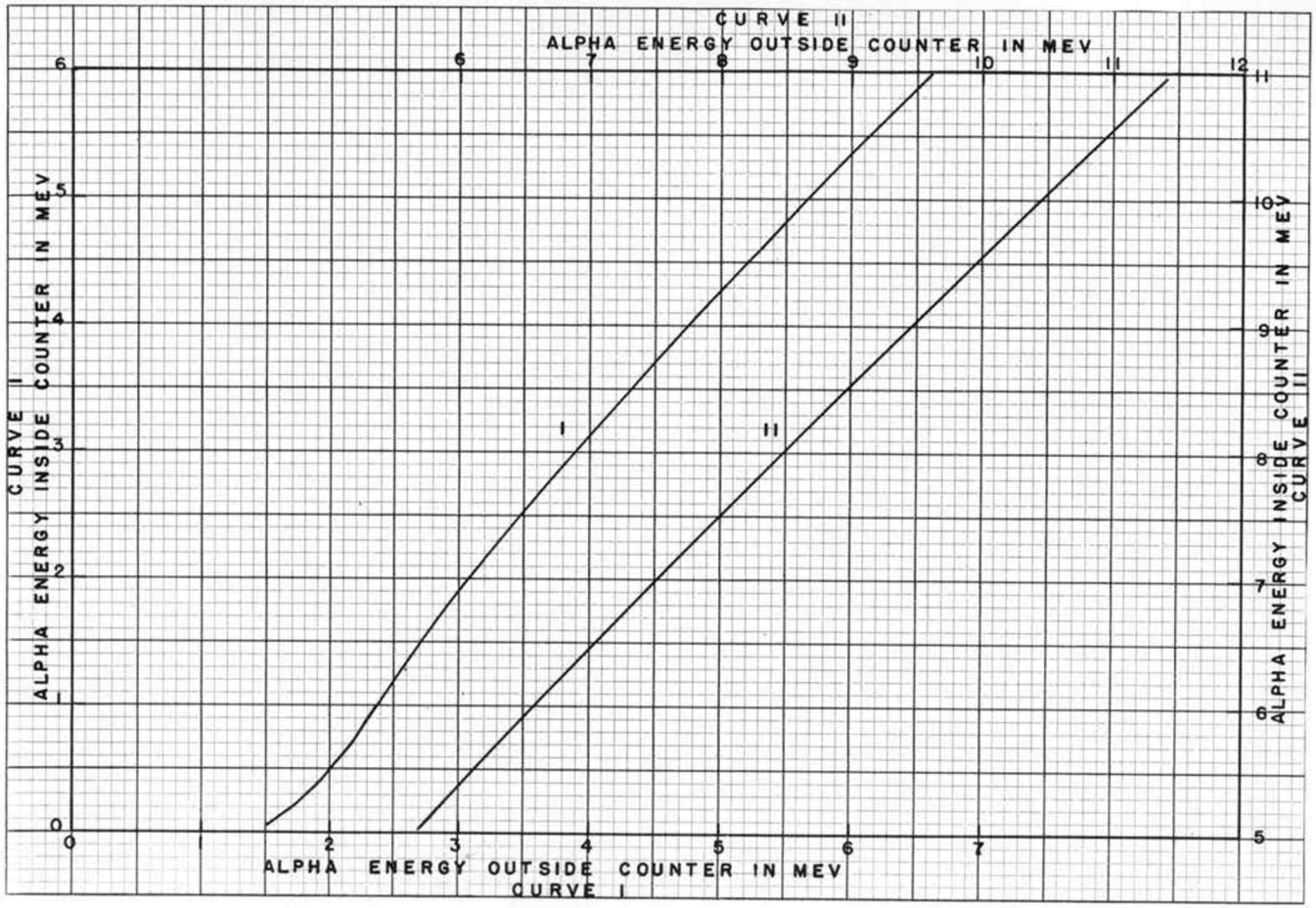

Figure 51. E_α Inside Counter as a Function of E_α Outside Counter

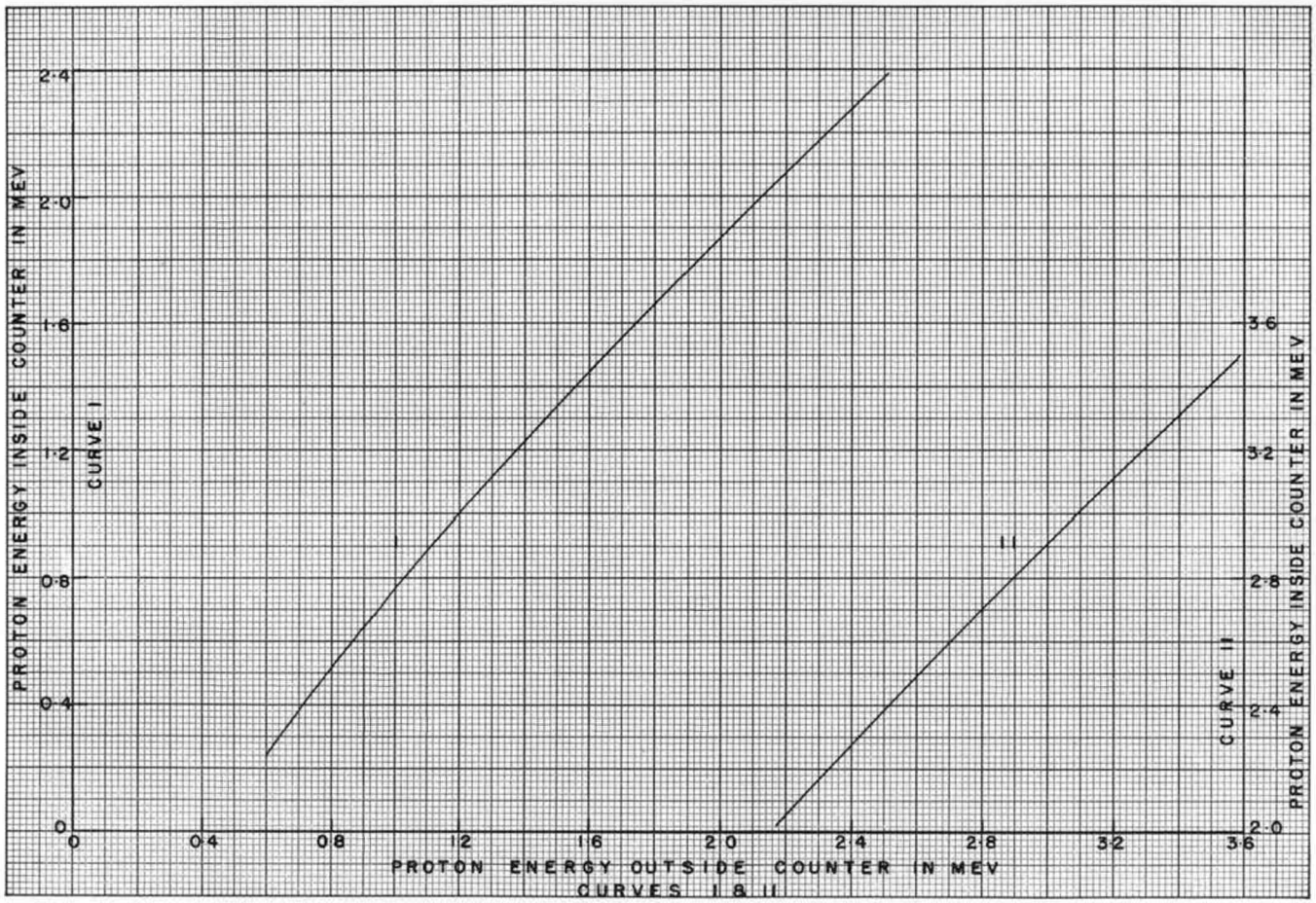

Figure 52. E_p Inside Counter as a Function of E_p Outside Counter

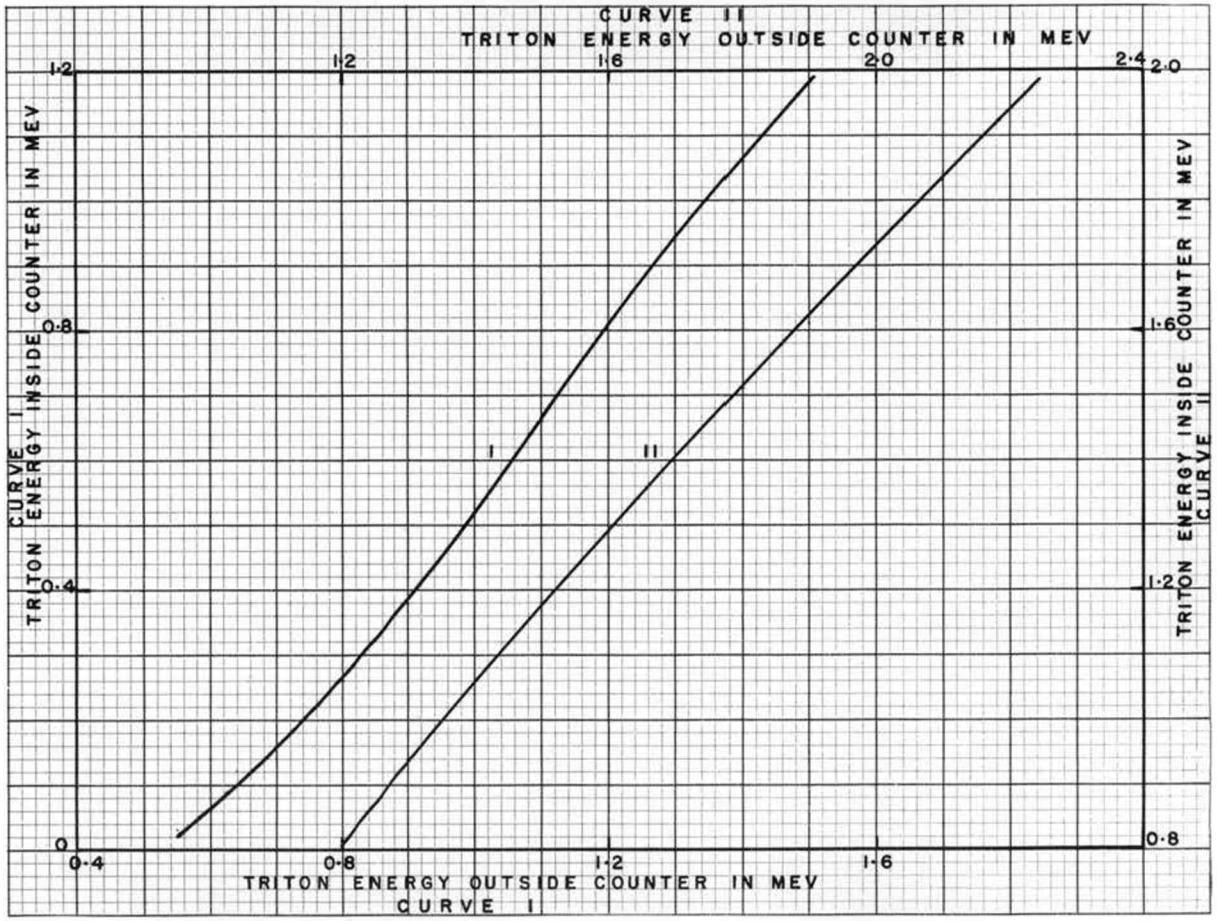

Figure 53. E_t Inside Counter as a Function of E_t Outside Counter

APPENDIX II

Energy Losses of Particles in the Targets

A. Appearance of Beam Spot

With reference to Figure 54 (a), one sees that

$T = d/\sin \alpha$

$a = T \sin (\theta-\alpha) = (d/\sin \alpha) \sin (\theta-\alpha)$.

Thus, if $\theta = 2\alpha$, $a = d$. By setting the counter at an angle to the beam which is always twice the angle made by the plane of the target to the beam, the target spot will appear to the counter as a circular disk with the same diameter as the incident beam.

In taking data, when the counter was placed at 90° to the beam, the target plane was placed at 45° to the beam. With the counter at 165°, the plane of the target was placed at 82.5°.

B. Angle of Divergence, ϕ

Again, from Figure 54 (a), one obtains the following relations:

$a/\ell = f/(L-\ell)$, so that

$\ell = aL/(a + f)$, and

$L-\ell = fL/(a + f)$.

Then $\phi = 2 \tan^{-1} [\, f/2(L-\ell)] = 2 \tan^{-1} [(a + f)/2L]$.

for the geometry indicated,

$\phi = 2 \tan^{-1} [0.250/16] = 2 \tan^{-1} 0.0156$

$= 2 (0.895^{\circ})$

$= 1.79^{\circ}$.

C. Relations Between Actual and Apparent Target Thicknesses

By imposing the condition that $\theta = 2\alpha$, one observes from Figure 54 (b), that

$$t/t' = \sin \alpha, \text{ or}$$

$$t = t' \sin \alpha.$$

The only measurement of the apparent thickness of the Li^7F target was made for $\alpha = 45^\circ$. Hence,

$$t = 0.707\ t'_{(45^\circ)}.$$

The apparent target thickness for $\alpha = 82.5^\circ$ is given by

$$t'(82.5^\circ) = t'(45^\circ) \sin 45^\circ / \sin 82.5^\circ$$

$$= 0.713\ t'_{(45^\circ)}.$$

D. Method of Determining the Air Equivalent of the Apparent Half-thickness of the Li^7F Target

Making use of Bethe's proton range-energy curves (4, Fig. 3) and the curve for the $Li^7(p,n)Be^7$ threshold (Figure 20) one may say that the Li^7F target produces an energy loss of $(1.9514 \pm 0.0015) - (1.8838 \pm 0.0002)$ Mev $= 0.0676 \pm 0.0016$ Mev for protons having a mean energy of 1.917 Mev. These protons have a range of 6.67 cm in air.

When the target is 45° to the beam, the apparent air equivalent of half its thickness will be given as follows:

Half energy loss = 0.0338 Mev

Thus, residual energy = 1.917 - 0.034 = 1.883 Mev

Range corresponding = 6.50 cm

Loss in range = 6.67 - 6.50 = 0.17 cm, air equivalent.

When the target is placed 82.5° to the beam, the half-energy loss will be about 0.713 times 0.0338, or 0.024 Mev.

Residual energy = 1.917 - 0.024 = 1.893 Mev

Range corresponding = 6.53 cm

Loss in range = 6.67 - 6.53 = 0.14 cm, air equivalent.

E. Relation of Incident Triton Energy to Triton Energy at Apparent Half-thickness of Li^7F Target

Table III shows the values for triton energies at the apparent half-thickness of the target as compared with the incident triton energy. The values are obtained by subtracting the air equivalent values (above) from the range corresponding to each incident triton energy - and obtaining the triton energy equivalent to the resulting range. The range of tritons in air was obtained from Bethe's proton energy-range curves after multiplying the units of both coordinates by three.

F. Relation of Emitted Particle Energy Outside Target to Emitted Particle Energy at Apparent Target Half-thickness

This information is obtained in the same manner as described in Section E. In this case, the alpha particle range-energy curves may be used directly. For each alpha particle energy value obtained as described in APPENDIX III, the energy may be determined for the particle after it has passed through the half-thickness of the target.

TABLE III

Incident Triton Energy (Mev)	Triton Energy at Apparent Target Half-thickness (Mev)	
	45°	82.5°
0.620	0.476	0.504
.723	.595	.620
.826	.700	.726
.929	.824	.842
1.033	.932	.951
1.136	1.041	1.059
1.239	1.153	1.170
1.342	1.263	1.277
1.446	1.366	1.380
1.549	1.473	1.486
1.652	1.580	1.592
1.755	1.684	1.698
1.859	1.791	1.802
1.962	1.896	1.920
2.065	2.001	2.012
2.168	2.105	2.116
2.272	2.215	2.225

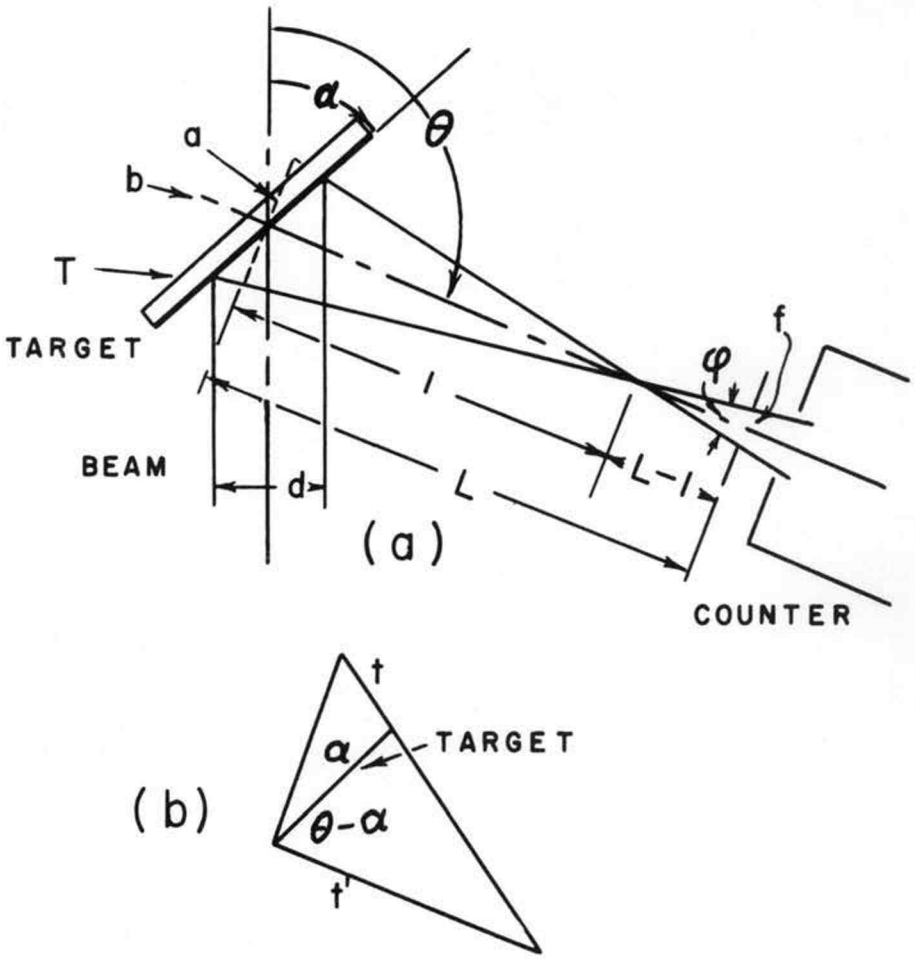

a = diameter of target spot as it is defined for the counter (a b)
b = axis of counter collimating system
d = diameter of collimated beam = 0.125 inch
f = diameter of defining aperture to the counter = 0.125 inch
L = radial distance from center of target to f = 8.000 inches
l = distance from center of target to focal point
T = major axis of elliptical beam spot on target
t = actual thickness of target material
t' = apparent thickness of target material
α = angle of plane of target to the axis of the beam
θ = angle of b to the axis of the beam
φ = maximum angle of divergence of particles entering the counter from the target spot

Figure 54. Target-Counter Geometry Diagram

APPENDIX III

Expressions Used in Making Calculations

A. Energies of Particles

Masses of all nuclei considered are in the literature: (a) masses of neutron and all light nuclei, except He^5, up through F^{20} (18, p.517); (b) mass of He^5 (10, p.299); and (c) all other masses (2, pp.125-126). The energy equivalence of an atomic mass unit is also published (18, p.517).

The Q-value, or energy released in a nuclear reaction, is obtainable from the above information. It is given as the energy equivalent to the difference in total mass of the initial and final nuclei involved in the reaction. For example, the reaction

$$Li^7 + H^3 \rightarrow He^6 + He^4 + Q.$$

Masses are: $Li^7 = 7.018223$ $\quad He^6 = 6.020474$

$H^3 = \underline{3.016997}$ $\quad He^4 = \underline{4.003873}$

Sums are: 10.035220 $\quad$ 10.024347

Difference (Initial-Final) = + 0.010873 mass units

(0.010873 mass units)(931.152 Mev/mass unit) = 10.124 Mev.

This method was used to obtain Q-values for all the reactions discussed in this thesis.

Next, one may obtain the energy for an emitted particle in the case of two-body break-up if the following considerations are made (references are to the diagrams in Figure 55):

(a) Obtain velocity of the center-of-mass (v):

$E_o = 1/2\ m_o v_o^2$; $v_o = \sqrt{2\ E_o/m_o}$. Because momentum is conserved, $m_o v_o = (m_o + M_o)V$.

Thus, $v = (m_o\sqrt{2\ E_o/m_o})/(m_o + M_o)$

$= \sqrt{2\ m_o\ E_o}/(m_o + M_o)$ (1)

(b) Obtain energy available in the center-of-mass system (E_r). $E_r = Q + E_o - 1/2\ (m_o + M_o)v^2$, since the energy available is given by the total energy diminished by the amount used to move the center-of-mass. By substituting for v from (1), one obtains

$$E_r = Q + E_o - m_o\ E_o\ /(m_o + M_o)$$
$$= Q + M_o E_o/(m_o + M_o) \quad (2)$$

(c) Obtain energy of emitted particle in the center-of-mass system (E_2').

Conservation of energy provides that

$$E_r = 1/2\ M_1 v_1'^2 + 1/2\ M_2 v_2'^2$$

Conservation of momentum provides that

$M_1 v_1' = M_2 v_2'$; or $v_1'^2 = M_2^2 v_2'^2/M_1^2$.

In the energy equation, substituting for $v_1'^2$ gives

$E_r = 1/2\ (M_2^2 v_2'^2)/M_1 + 1/2\ M_2 v_2'^2$. Then

$v_2'^2 = 2\ M_1 E_r/M_2(M_1 + M_2)$.

Since $E_2' = 1/2\ M_2 v_2'^2$,

$$E_2' = M_1 E_r/(M_1 + M_2)$$
$$= \left[M_1/(M_1 + M_2)\right]\left[Q + M_o\ E_o\ /(m_o + M_o)\right] \quad (3)$$

(d) Obtain energy of emitted particle in the laboratory system (E_2).

The law of cosines states that $v_2'^2 = v_2^2 + v^2 - 2v\ v_2 \cos\theta_2$,

where reference is made to Figure 55b. Rearranging,

$$v_2^2 - 2\, v\, v_2 \cos\theta_2 - (v_2'^2 - v^2) = 0.$$

The quadratic formula gives for a solution,

$$v_2 = 1/2\left[2\, v \cos\theta_2 \pm \sqrt{4\, v^2 \cos^2\theta_2 + 4\,(v_2'^2 - v^2)}\,\right].$$

By removing a factor of 2 and substituting $1 - \sin^2\theta_2$ for $\cos^2\theta_2$, one obtains

$v_2 = v\cos\theta_2 \pm \sqrt{v_2'^2 - v^2\sin^2\theta_2}$. The negative root gives results which violate physical laws, hence only the positive root is to be used.

$$v_2^2 = (v\cos\theta_2 + \sqrt{v_2'^2 - v^2\sin^2\theta_2})^2, \text{ and}$$

$$E_2 = 1/2\, M_2(v\cos\theta_2 + \sqrt{v_2'^2 - v^2\sin^2\theta_2})^2 \qquad (4)$$

In equation (4), the value of v is given by equation (1) and

$$v_2'^2 = 2\, M_1\, Q/(M_2\, M_1 + M_2^2) + 2\, M_o M_1 E_o/\left[M_2(m_o + M_o)(M_1 + M_2)\right].$$

(e) For the special case $\theta_2 = 90^\circ$, the value of E_2 is simpler. Substitution of expressions for v and $v_2'^2$ in equation (4) gives

$$E_2 = \frac{M_2\, v_2^2}{2} = \frac{M_1\, Q}{M_1 + M_2} + \left[\frac{M_o M_1(m_o + M_o) - m_o M_2(M_1 + M_2)}{(M_1 + M_2)(m_o + M_o)^2}\right] E_o \qquad (5)$$

This is a linear equation of the form $E_2 = A\, Q + B\, E_o$.

For computation purposes, both equations (4) and (5) were found to be simple expressions to use.

(f) The energy of a secondary particle produced in the break-up of the emitted particle may easily be found for the limiting cases in which the observed secondary particle continues in the direction of the primary emitted particle, or in the opposite direction. Using the symbols defined in Figure 55 (b),

$$E_4 = M_4/2 \left[v \cos \theta_2 + \sqrt{v_4'^2 - v^2 \sin^2 \theta_2} \right]^2, \qquad (6)$$

where v is defined by equation (1),

$$v_4' = v_2' \pm V_4',$$

$$v_2' = \sqrt{2 E_2'/M_2},$$

where E_2' is given by equation (4),

and $V_4' = \sqrt{(2 M_3 q)/M_4(M_3 + M_4)}$. A simplification of equation (6), for $\theta_2 = 90^\circ$, is

$$E_4 = (M_4/2)(v_4'^2 - v^2). \qquad (7)$$

Expressions (6) and (7) are used in calculating maximum and minimum energies of alpha particles produced by break-up of He^5 and Be^8 nuclei.

B. The Expression Used in Solving for Excited State Energies, E_x

Reference is made to the notation and relationships used in the preceding Section, A.

Since

$$1/2\, M_2 v_2'^2 = 1/2\, M_2 v_2^2 + 1/2\, M_2 v^2 - M_2 v v_2 \cos \theta_2, \text{ and}$$

$$E_2' = M_1 Q/(M_1 + M_2) + M_o M_1 E_o/(M_1 + M_2)(m_o + M_o),$$

and since $1/2\, M_2 v_2^2 = E_2$ and $v_2 = \sqrt{2 E_2/M_2}$, a solution for Q is

$$Q = \frac{(M_1 + M_2)E_2}{M_1} + \frac{(M_1 + M_2)M_2 v^2}{2 M_1} - \frac{M_2(M_1 + M_2 \cos \theta_2\, v \sqrt{2 E_2/M_2})}{M_1}$$

$$- M_o/(m_o + M_o).$$

For an excited state, one would obtain the same expression where $Q^* < Q$ and $E_2^* < E_2$. By subtracting the expression for Q^* from that given for Q, one obtains

$$Q-Q^* = E_x = (M_1 + M_2)/M_1 \left[(E_2 - E_2^*) - M_2 \, v \cos\theta_2 \left(\sqrt{2\,E_2/M_2} - \sqrt{2E_2^*/M_2}\right)\right],$$

or

$$E_x = (M_1 + M_2)/M_1 \left[(E_2 - E^*_2) - \sqrt{2\,M_2}\, v \cos\theta_2 \left(\sqrt{E_2} - \sqrt{E_2^*}\right)\right] \qquad (8)$$

For the special case that $\theta_2 = 90^\circ$,

$$E_x = (M_1 + M_2)/M_1 (E_2 - E_2^*). \qquad (9)$$

C. Determination of Cross Section

In the discussion of proton bombardment of the Li^7F target, the expression for the differential cross section is given as

$$\sigma_{(\theta)} = N_r/N_b N_t.$$

For the charged particle measurements, N_r is given by the proportional counter, which is assumed to be 100% efficient for those particles passing through its window. The solid angle indicated in Figure 13 is $4.36 \pm 0.25 \times 10^{-4}$ steradians.

N_b is given directly in microcoulombs by the current integrator.

N_t must be obtained from other measurements. As indicated in the text, the value for N_t was obtained for the Li^7F target by measuring threshold rise and by measuring yield of the $Li^7(p,n)Be^7$ threshold. With reference to the curve represented in Figure 20, one may obtain the number of Li^7 atoms per square centimeter in the Li^7F target (placed at 45° to the proton beam) in the two ways which follow.

(a) From the threshold rise -

1. Variation in E_p between threshold and the first maximum is 1.9514 - 1.8838 = 0.0676 Mev.

2. Mean value for E_p is 1.917. Range of protons with this energy is (4, Fig. 3) 6.67 centimeters of air.

3. Range for protons having energy 1.917 - 0.0676 = 1.849 Mev is 6.30.

4. Difference in range corresponding to average energy loss in the target is 6.67 - 6.30 = 0.37 centimeters of air, $\pm$ 3%.

5. Number of "molecules of air" per cm^3 of air is $(6.023 \times 10^{23}$ molecules/mole)/$(2.24 \times 10^4$ cm^3/mole) = 2.689×10^{20} molecules/cm^3. In the "air equivalent target" one would find 9.95×10^{18} molecules of air/cm^3.

6. Stopping power (19, p.272) of Li^7F is about 1/2 (0.50 + 1.15) = 0.825 times that of air, $\pm$ 5%. The number of Li^7F molecules in the target is$(9.95 \times 10^{18}$ molecules/$cm^2)/0.825 = 2.41 \times 10^{19}$ molecules/cm^2.

7. The apparent number of atoms of Li^7(or of F^{19}) in this target is, therefore, 1.21×10^{19} atoms/cm^2, $\pm$ 12% (for the target placed at 45° to the beam). The <u>actual</u> number is 0.86×10^{19} atoms/cm^2.

(b) From neutron yield at E_p = 2 Mev -

1. Definition of $\sigma_{(\theta)}$ may be used to obtain the number of target nuclei per cm^2, for

$$N_t = N_r/\sigma_{(\theta)}N_b.$$

2. Since the RaBe source used has a total flux of 6.02×10^6 neutrons/second, it may be assumed to emit 4.75×10^5 neutrons/sec/steradian. The long counter calibration indicated 42.22

counts/second. Therefore, the long counter gave 8.81×10^{-5} counts/neutron/steradian.

3. $Li^7(p,n)Be^7$ yield at 2 Mev indicates $\sim$193 counts/μcb. Therefore, $193/8.81 \times 10^{-5} = 2.19 \times 10^6$ neutrons/μcb/steradian, $\pm$ 10%, is the value for N_r.

4. N_b is 6.25×10^{12} proton/μcb.

5. $\sigma_{(0^\circ)} = 2.5 \times 10^{-26}$ cm^2/steradian, $\pm$ 12%, (29, p.390).

6. Solving for N_t, then, one obtains

$$N_t = 1.40 \times 10^{19} \text{ atoms/cm}^2, \pm 15\%.$$

An average value of 1.31×10^{19} atoms/cm^2 of Li^7, $\pm$ 14%, is used to determine the values for cross section of charged particle reactions from Li^7 + T.

From the curves indicated in Figure 21, one obtains the total number of counts/100μcb from each target in the pulse height region 107-139 volts. These are:

CaF_2	1014 counts
Li^6F	986 "
Li^7F	951 "
CuO	17 "

By considering CuO to give a background yield which is subtracted from the other three, one obtains the relative fluorine content of the three targets:

$$Li^7F/1.000 = Li^6F/1.037 = CaF_2/1.067.$$

The fluorine content of Li^7F is taken to be $(0.707)\ 1.31 \times 10^{19} = 0.93 \times 10^{19}$ atoms/cm^2. Therefore, the other targets contain 0.96×10^{19}

and 0.99×10^{19} atoms/cm^2 for Li^6F and CaF_2, respectively. In the case of Li^6F, this number represents either Li^6 or F^{19} atoms.

For subtracting CaF_2 yields from those of Li^6F and Li^7F, one finds that approximate "background" corrections will be given as follows:

$$Li^6 \text{ yield} = Li^6F \text{ yield} - 0.972\ CaF_2 \text{ yield}$$

$$Li^7 \text{ yield} = Li^7F \text{ yield} - 0.937\ CaF_2 \text{ yield}.$$

This must be done point-by-point.

At 45°, the effective number of target atoms/cm^2, ± 14%, is

$$Li^6 = 1.36 \times 10^{19}$$

$$Li^7 = 1.31 \times 10^{19}$$

$$CaF_2 = 1.40 \times 10^{19} \text{ (fluorine atoms)}.$$

At 82.5°, the effective number of target atoms/cm^2, ± 14%, is

$$Li^6 = 0.968 \times 10^{19}$$

$$Li^7 = 0.938 \times 10^{19}$$

$$CaF_2 = 0.999 \times 10^{19} \text{ (fluorine atoms)}.$$

Since total counts/μcb = $\sigma(\theta)$ (atoms/cm^2)(tritons/μcb) (4.355×10^{-4} steradians), and since there are 6.25×10^{12} tritons/μcb, the differential cross section for reactions with Li^6, Li^7, or F^{19} observed at 90° or at 165° will be given by substituting the appropriate values in this expression:

$$\sigma(\theta) = (\text{total counts}/\mu\text{cb})(1/\text{no. of target atoms} \times \text{cm}^{-2})(3.67 \times 10^{-10}\ \mu\text{cb/steradian} \times \text{tritons}).$$

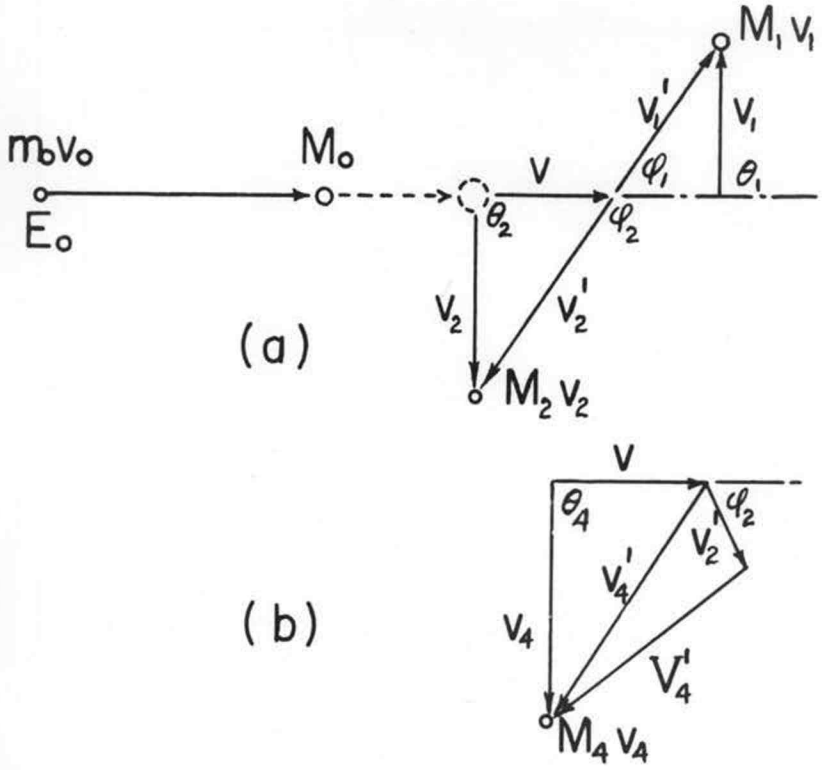

Notation:

m_o = mass of bombarding particle

M_o = " " target nucleus

M_1 = " " recoil nucleus

M_2 = " " emitted particle

M_3 and M_4 are masses of secondary particles resulting from break-up of the emitted particle

θ is angle measured in the laboratory system

φ is angle measured in the center-of-mass system

v = velocity of the center-of-mass

V_4' = velocity of the secondary emitted particle as measured with reference to its parent nucleus

Velocities and energies measured in the center-of-mass system are primed. Velocities and energies measured in the laboratory system are unprimed.

Figure 55. Diagram of Reaction Mechanics